UNIVERSIDADE FEDERAL DE SÃO CARLOS
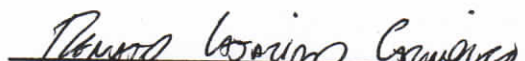
CENTRO DE CIÊNCIAS EXATAS E DE TECNOLOGIA

DEPARTAMENTO DE QUÍMICA

PROGRAMA DE PÓS-GRADUAÇÃO EM QUÍMICA

SYNTHESIS OF NEW COCRYSTAL SOLID FORM OF FLUCONAZOLE-FUMARIC ACID

Bolaji Charles Dayo Owoyemi*

Dissertation presented as part of the requirements to obtain the title of master in chemistry area of concentration: ANALYTICAL CHEMISTRY.

Supervisor: Prof. Dr. Renato Lajarim Carneiro

*scholarship CAPES

São Carlos – SP

2015

Folha de Aprovação

Assinaturas dos membros da comissão examinadora que avaliou e aprovou a Defesa de Dissertação de Mestrado do candidato Bolaji Charles Dayo Owoyemi, realizada em 29/09/2015:

Prof. Dr. Renato Lajarim Carneiro
UFSCar

Prof. Dr. Javier Alcides Ellena
IFSC/USP

Prof. Dr. Alejandro Lopez Castillo
UFSCar

I dedicate this work to the Glory of

GOD and the benefit of mankind.

ACKNOWLEDGEMENT

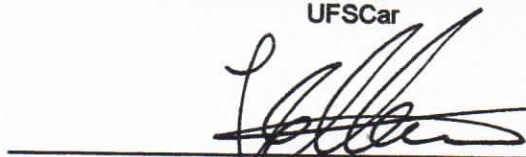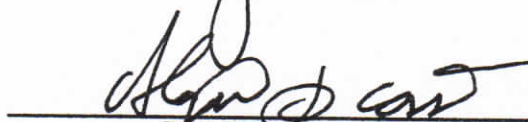My most appreciation goes to the Almighty God for giving me the gift of life, without Him nothing would have been possible.

My warmth appreciation goes to my parents Victor Adedayo and Philomena for their love, support, and the guidance through life. To my sisters Dr.Ifeloju and Omolola, and their spouses Dr. Segun Folarin and Mr Olalekan and my nephews Afolabi, Samuel and Paulo. I thank you all for your affection and unconditional love. To Jane and her mum for the affections, care and love towards me.. I appreciate you all.

Special thanks to my supervisor Prof. Dr. Renato Lajarim Carneiro, for all the knowledge and teachings that I received during these two years. I would like to thank him for the patience endured in bearing with me. Special thanks to my co-supervisor, Prof. Dr. Caio Marcio Paranhos da Silva, for the assistances rendered during the course of my programme. Also, to Profs. Drs. Ernesto Chaves Pereira de Souza; Orlando Fatibello-Filho; Antonio Aparecido Mozeto; Edenir Rodrigues Pereira Filho; Pedro S. Fadini for training me towards attaining important life lessons during the Graduate in Chemistry program classes. To Prof. Dr. Ernesto Chaves Pereira de Souza and Prof. Dr. Julio Zukerman Schpector, I am grateful for your assistance, advice and scientific discussions that have helped me in learning. Special thanks to Egnr Adeleke Adegbemile, for his support, his fatherly advice and importantly for his role in my academic pursuits. To my mentor, Dr Shayo Olubosede for his contributions towards my academics right from my undergraduate days.

I appreciate Frederico, Jorge and Francisco (LIEC) my good friends, who help and advice on the development of my master's work. Without them, I don't know! Thank you so much. My best friends Banky AmuwaOlorun and Sunday A. Ojo, for their friendship and assistance at all time and especially affections I received during this period of my life. All my colleagues in the lab for their friendship and assistance provided at the beginning of this experience. To my friends in Brazil, UK (London), Nigeria especially, Murphy, Aguda Segun, Olumide Taiwo, Pat , Deji , Oye, Seun and people who have always been with open arms to talk, vent and laugh at everything I do. God bless you all.

Finally, my special thanks goes to The Graduate Program in Chemistry of The Federal University of São Carlos (UFSCar) and The Coordenação de Aperfeiçoamento de Pessoal de Nível Superior (CAPES) for the scholarship granted to study in Brazil.

Thanks

LIST OF ABBREVIATION

API   Active Pharmaceutical Ingredient

DSC   Differential scanning calorimetric

TGA   Thermogravimetric Analysis

XRPD   X-ray Powder Diffraction

SCXRD   Single crystal X-ray diffraction

BCS   Bio-pharmaceutics Classification System

SCF   Supercritical Fluid technology

USSC   Ultrasound assisted solution Cocrystallisation

CCSD   Cambridge Crystallographic Structural Database

FLZ   Fluconazole

FUM   Fumaric acid

LIST OF FIGURES

LIST OF TABLES

ABSTRACT

SYNTHESIS OF NEW COCRYSTAL STRUCTURE OF FLUCONAZOLE-FUMARIC ACID

Pharmaceutical cocrystals are multicomponent crystalline solids comprised of an active pharmaceutical ingredient (API) and one or more co-formers interacting through hydrogen bonding or other weak interactions like the π-stack and van der Waals interactions. Fluconazole (FLZ) is a triazole antifungal drug used in the treatment and prevention of superficial and systemic fungal infections. It is also used to prevent and treat meningitis. Cocrystallization is an alternative approach for enhancement of drug. It can be performed using neat grinding, solvent assisted grinding, solvent evaporation, cooling evaporation and slurry cocrystallization. In this work, a new cocrystal Fluconazol-Fumaric acid monohydrate was synthesized via 1:1 stoichiometric amount of FLZ and FUM at different conditions. The characterization of the synthesized cocrystals was achieved using Raman spectroscopy, differential scanning calorimetry, powder X-ray diffraction and single crystal X-ray diffraction. The results obtained for the characterization of the samples showed some obvious differences among the spectra, diffractograms and thermograms. The single crystal X-ray diffraction analysis of the new structure shows a cocrystal where the fluconazole molecules are attached to the fumaric acid and water molecules respectively through hydrogen bonds, gave unique cell dimensions for an assumed structure $C_{17}H_{18}F_2N_6O_6$ with a space group of $P2_1/n$, a = 17.053(3) Å, b = 5.5995(10), c=21.154(3), α = 90°, β=105.418(4)°, γ= 90°, V = 1947.3(6) $Å^3$. This work is the first to report a monohydrate cocrystal structure of fluconazole and fumaric acid.

Keywords : API, Coformer, Fluconazole, Pharmacutical cocrystal, Crystal enginering, Raman, PXRD , Single Crystal XRD.

RESUMO

SÍNTESE DE NOVAS ESTRUTURAS DE COCRISTAL DE FLUCONAZOL-ÁCIDO FUMÁRICO

Cocristais farmacêuticos são sólidos cristalinos multi-componentes compostos de um ingrediente ativo farmacêutico (API) e um ou mais co-formadores interagindo através de ligações de hidrogênio ou outras interações fracas como as π-stack e Van der Waals. Fluconazol (FLZ), é um fármaco anti-fúngico triazol utilizado no tratamento e prevenção de infecções fúngicas superficiais e sistémicas. É também utilizado para prevenir e tratar a meningite. Cocristalização é uma abordagem alternativa para melhorar as propriedades de fármacos. Pode ser realizada através de moagem a seco, moagem assistida por solvente, evaporação de solvente e cristalização em suspensão. Neste trabalho, um novo co-cristal Fluconazol-Ácido Fumarico monohidrato foi sintetizado utilizando uma estequimetria 1:1 em diferentes condições. A caracterização dos co-cristais sintetizados foi realizada utilizando espectroscopia Raman, calorimetria exploratória diferencial, difração de raios-X em pó é por monocristal. Os resultados obtidos para a caracterização das amostras mostrou algumas diferenças obvias entre os espectros, difratogramas e termogramas. A difração de raios-X de monocristal mostrou uma nova estrutura onde as moléculas de fluconazol estão ligadas ao ácido fumárico e a uma molécula de água através de ligações de hidrogênio, originando uma estrutura única $C_{17}H_{18}F_2N_6O_6$ de grupo espacial $P2_1/n$ e dimensões da célula unitária a = 17.053(3) Å, b = 5.5995(10), c=21.154(3), α = 90°, β=105.418(4)°, γ= 90°, V = 1947.3(6) $Å^3$. Este trabalho é o primeiro a relatar uma estrutura de co-cristal mono-hidrato de fluconazol e acido fumárico.

Palavra-chave : API, Coformer, Fluconazol,Cocristais farmacetica, Engenharia

SUMMARY

CHAPTER 1 - INTRODUCTION

1. INTRODUCTION

1.1 Pharmaceutical industry and solubility of drugs

To the pharmaceutical industry[1], a drug molecule represent a chemical substance that has known a biological effect on humans and other animals. In pharmacology[2,3] however, a drug is "any chemical substance administered for the treatment, cure, prevention, or diagnosis of diseases or used to otherwise enhance physical or mental well-being"[1]. Pharmaceutical medicines generally comprised of a crystalline Active Pharmaceutical Ingredient (API)[4], a formulation containing inactive ingredients as a carrier system[5], and a package for market performance and appeal. Crystalline API's are strongly preferred due to their relative ease of isolation, the rejection of impurities inherent to the crystallization process and the physicochemical stability that the crystalline solid state affords[6].

The most frequent and greatest challenge in the pharmaceutical industry is the formulation of less soluble compounds for oral delivery. Thus, with the advent of combinatorial chemistry[7] and high throughput screening[8-10], the number of low water soluble compounds[11] has dramatically increased. Low aqueous solubility is a growing problem in the pharmaceutical industry and it is having an impact on the productivity of drug research. The solubility issue hampers preclinical study of a new drug candidate, and can limit dosing and bioavailability[12].

However, the most frequent and greatest challenge to the formulation scientists in the pharmaceutical industry is to finding a potential route to achieving pharmaceutical material with improved solubility and bioavailability thereby improving the physicochemical properties for oral delivery / administration. Drug absorption from a solid dosage form after oral administration, depends on the release of the active drug substance in the drug product and the dissolution of this drug under physiological conditions depends on its permeability across the gastrointestinal tract[13]. Thus, the therapeutic effectiveness of a drug directly depends on its bioavailability (the fraction of an administered dose of unchanged drug that reaches the systemic circulation) which also depends on the solubility and dissolution rate of such drug

molecules. Poor soluble drugs will be inherently released at a slow rate owing to their limited solubility. Hence, solubility is one of the important parameter that must be considered towards achieving a desired concentration of drug in systemic circulation for pharmacological response[14].

1.2 Classes of Active Pharmaceutical crystalline solid materials

Major problems arising with the use of crystalline material are usually related to poor solubility properties and the existence of more than one crystalline form of an API. In terms of regulatory approval, crystalline forms of an API have traditionally been limited to polymorphs, salts and stoichiometric solvates (pseudopolymorphs)[15]. Neutral compounds and salt forms have the potential to be solvated (i.e. interact with solvent molecules) or cocrystallized (i.e. interact with a cocrystal formers, which is a pharmaceutical accepted substance, used to optimize the properties of the API but can also be used solely in the isolation and/or purification of the API, such as a separating enantiomers from each other, as well and removed preceding the production of the drug). Solvate molecules and cocrystal formers can include organic acids or bases that remain in their neutral form within the multi-component crystal. Thus, the primary difference is the physical state of the isolated pure components
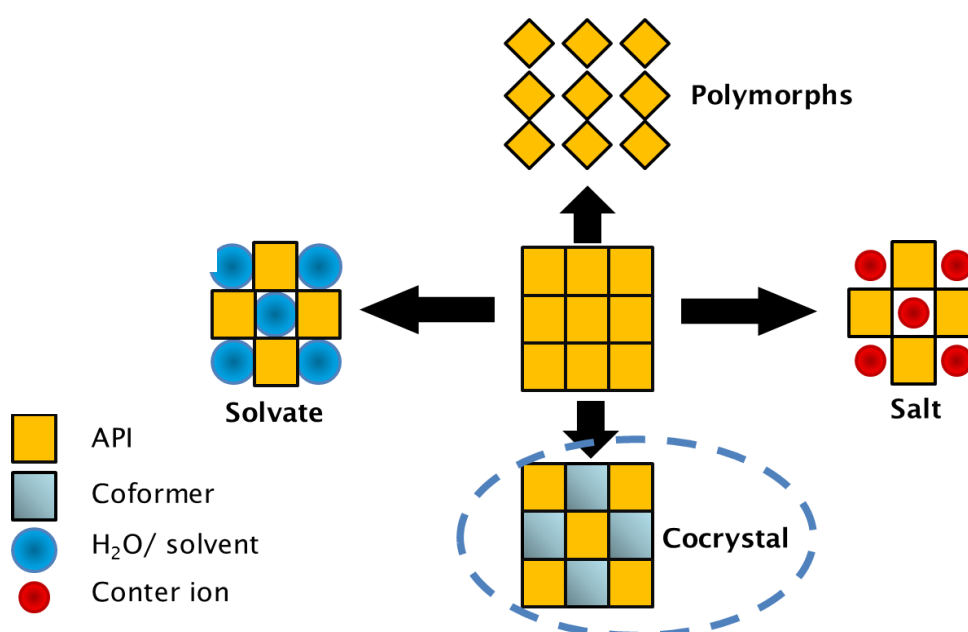
FIGURE 1.1‑ Different examples of possible multicomponent system which include cocrystals, salt cocrystals and derived multi-component solids.[16].

However, the advent of crystal engineering[17-20] has created a means for rapid development of pharmaceutical cocrystals[13,21-23]. Polymorphism and solid state polymorphic forms of an API are classified as either crystalline, amorphous, or solvate and hydrate forms, however, the applicable regulatory schemes for these solid-state polymorphic forms are well-defined and different cocrystal types are distinguishable from these traditional pharmaceutical solid-state forms.

The optimization[10] of the physical properties of less favourable APIs via cocrystallization mechanism is a reliable crystallization technique that most pharmaceutical industries are employing recently to tackle the problems arising from poor drug forms[24]. Many factors have been taken into consideration in the cause of producing drug compounds having properties within such acceptable quality range. Factors like the solubility rate, bioavailability, permeability, dissolution rates are taking into consideration during drug preparations to justify the quality rating of a drug compound[25].

1.3   The Bio-pharmaceutics Classification System (BCS)

The Bio-pharmaceutics Classification System (BCS) apart from being a tool in the scientific framework for classifying drug substances based on their aqueous solubility and intestinal permeability, has also served as a monitoring or considering factor in the synthesis and classification of drugs into four different classes based on their solubility and permeability[15]. The introduction of the BCS in 1995[26], was as a result of the continuous efforts on mathematical analysis for the elucidation of the kinetics and dynamics of the drug process in the gastrointestinal (GI) tract. BCS guidelines were quickly introduced into U.S. Food and Drug administration (USFDA), World Health Organization (WHO) and the European Medicines Evaluation Agency (EMEA) normative with the objective of predicting the in vivo pharmacokinetic performances of drugs from measurements of permeability and solubility. It has also stand the test of time as a regulatory tool for the replacement of certain bioequivalence (BE) studies with accurate in vitro dissolution tests. BCS recommends method for

classification according to dosage form dissolution along with the solubility-permeability characteristics of the drug products[27].

The pharmaceutical drugs are classified into four classes based on their solubility and permeability according to the Bio-pharmaceutics Classification System (Fig. 1.2). However, a drug substance is considered "highly soluble" when the highest dose strength is soluble in less than 250 ml water over a pH range of 1 to 7.5; and "highly permeable" when the extent of absorption in humans is determined to be higher than 90% of an administered dose, based on mass-balance or in comparison to an intravenous reference dose.

BCS CLASS I **High solubility** **High permeability**	BCS CLASS II **Low solubility** **High permeability**
BCS CLASS III **High solubility** **Low permeability**	BCS CLASS IV **Low solubility** **Low permeability**

FIGURE 1.2 – The Bio-pharmaceutical Classification System (BCS) for drugs.

Drugs of the BCS classes II and IV are problematic for effective oral administration. These classes of drugs have poor bioavailability and are usually not well absorbed through the intestinal mucosa, and a high variability is expected. The increasing number of poor drug forms classified as II and IV are however taken into consideration on ways of optimizing their physical properties (solubility and dissolution profiles); without altering the molecular structure. This process is a particular challenge for the successful development of a pharmaceutical product and it can be achieved by employing different crystal engineering principles[28,29]. Thus, on the cause of this project, attention is focused on improving the class II and IV drugs via simple cocrystallization

processes thereby synthesizing a new improved drug with improved physicochemical properties when compared to the previous starting materials using crystal engineering techniques.

1.4 Crystallization and Cocrystallization

Crystallisation was initially taken as a separation technique concerned with the evolution of a pure crystalline solid from saturated solution. As the saturated solution is allowed to cool, the solid will come out of the solution and crystals will start to grow. The crystals can then be collected and allowed to dry. The size of crystals depends on the rate of cooling. Fast cooling will result in a large number of small crystals. Slow cooling will result in a smaller number of large crystals. Cocrystallization technique[30] is an effective crystal engineering approach for modifying the crystal structure and properties of drugs in such that, when an API reacts with a cocrystal former(s) will provided an alternative to the physical properties of the neat API solid phases to produce a cocrystal.

Where traditional approaches such as salt screening fail, cocrystallization often still manages to solve the crystallization problems or improve a drug substance's physicochemical properties. This technique has offered the advantage of generating a diverse array of solid-state crystalline forms of stable and physically improved properties of API like the shelf life[31], dissolution rate, and bioavailability[12,32-35]. Furthermore, cocrystallization technique has also offered a potential to monitor and selectively improve the physicochemical properties of a drug preparation to an optimum specification, with remarkable consequences also in the field of the intellectual properties protection.

Cocrystallization of different components represents the supramolecular synthesis, where weak interactions link molecules together. This is in contrast to organic synthesis which is based on the formation or cleavage of covalent bonds. For pharmaceutical products it is expected to be an increasing importance in the design of modified drugs based on known agents as it is for polymorphs. Cocrystals are distinct different from solid solutions or mixed crystals, and can be considered as multicomponent crystals[36]. The two most

important reasons underlying the rapid success of cocrystallization as a method of constructing advanced materials can be identified as the ability to construct cocrystals following a simple design based on supramolecular synthons, and the modularity of the design that allows the exchange of cocrystal components with the intention of improving a particular solid-state property.

1.5   Polymorphism

Polymorphism (or crystal polymorphism) is a phenomenon related to the solid state; it is the ability of a compound in the solid state to exist in different crystalline forms having the same chemical composition but different structure and eventually making them to be therapeutically different. Polymorphic cocrystals attract extensive study due to the ability to change their physicochemical properties such as melting point, density and solubility. Whilst at times the changes in these properties may be beneficial, it can also reduce desired properties such as solubility, bioavailability and stability. Figure1.3 shows different polymorphic arrangements that can possibly existing in solid compounds.
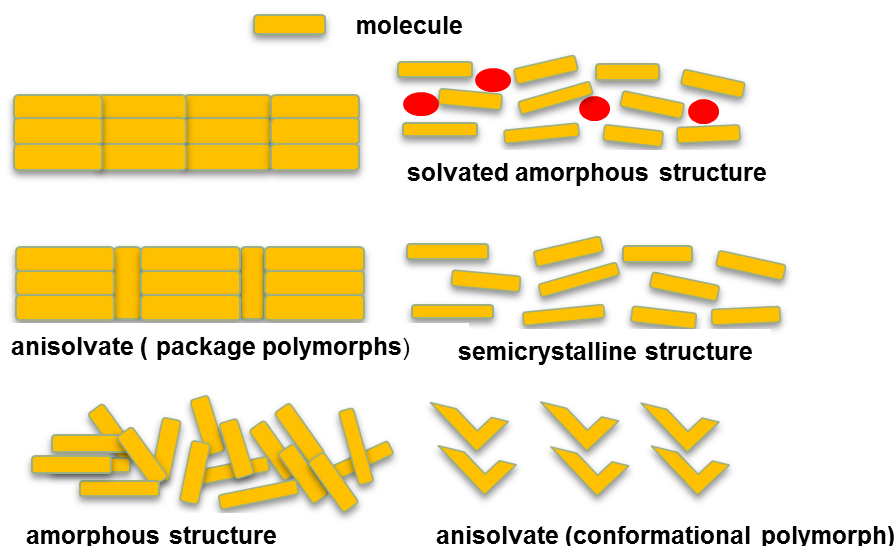
FIGURE 1.3 - Schematic illustration of polymorphism of solid compounds.

There are many examples of both single component systems and polymorphs. Fluconazole confirms the high frequency of hydrate occurrence in

APIs. Different polymorphic forms of fluconazole; a monohydrate and solvates are known[37-44]. Polymorph II form of fluconazole has been found to absorb humidity and form the monohydrate phase from both the environment and the excipient during either the storage phase or the manufacturing phase thereby indicating characteristic instability.

1.5.1 Hydrates and solvates

Pseudo-polymorphism [45-47] describes solvates (including hydrates) as a situation where a solvent is present in the crystal matrix in stoichiometric proportions; such matrix is called a hydrate when the solvent happens to be water.

The majority of the solvates and hydrates cocrystals formed during cocrystallisation experiments are from solution, so the presence of solvent within the crystal lattice is not surprising. Water molecules are small and can form multiple hydrogen bonds and hence inclusion as a hydrate within a crystal structure is frequently observed. It has been reported that in certain systems where there is an imbalance of donor and acceptor molecules, that the presence of water or other solvent can stabilize the structure. The CSD database search carried out to investigate the number of cocrystal structures that exist as either solvates or hydrates. The results of this search showed that ~12% of the 3624 entries were hydrates with a further ~11% being solvates (with methanol, ethanol and acetonitrile being the most common solvate to be incorporated into the structure[48-52].

The thermal stability of a range of hydrated cocrystals was investigated by cleark et al.; In their work, they addressed the role of water molecules in crystal engineering by studying the crystal structures and thermal stabilities of 11 new cocrystal hydrates and it was observed that the more tightly bound the water molecules, the higher the temperature required before the water is lost. For example, it was observed that samples in which the water was held in channels was lost at temperatures less than 100ºC, though temperatures greater than 120 ºC were required before dehydration of the samples in which the water was tightly bound within the crystalline lattice. Furthermore, the CSD

analysis was used to address the supramolecular heterosynthons that water molecules exhibit with two of the most relevant functional groups in the context of active pharmaceutical ingredients, carboxylic acids, and alcohols. It however suggest, unlike cocrystals, that there is great diversity in the supramolecular heterosynthons exhibited by water molecules when they form hydrogen bonds with carboxylic acids or alcohols.[53,54] It can therefore be said that the promiscuity of water molecules in terms of their supramolecular synthons and their unpredictable thermal stability makes them a special challenge in the context of crystal engineering and this we encountered in the course of this work. However, different crystalline forms or solvates may be produced by varying the crystallization conditions (temperature, pressure, solvent, concentration, rate of crystallization medium, presence and concentration of impurities). The stability and other physical properties of both hydrates and solvates differ from the unsolvated forms, and can be either detrimental or beneficial to a pharmaceutical product.

1.6   COCRYTALS

Cocrystals are multi-component crystalline solid substances in which its neutral components are in a definite stoichiometric ratio and interact through weak intermolecular bonds (hydrogen bonding, van der Waals and so on). This represent a known class of crystalline solid which allow an improvement in its physicochemical properties, a prototypal example of which is the improvement of the solubility and residence time at the site of action for sulfacetamide, a popular antibiotic prescribed for the treating of ocular infection. reported by Goud et al.[55]

The term and the definition of cocrystal has been a subject of topical debate between different reseachers/authors in the crystallography field. Jones, defines cocrystal as a crystalline complex of two or more neutral molecular constituents bound together in the crystal structure through non-covalent interactions, often including hydrogen bonding[56], and Zaworotko says that cocrystals are formed between a molecular or ionic API and a cocrystal former

that is a solid under ambient conditions[21]. However, hydrates[57-59] and other solvates[48,60,61] are excluded which, in principle, eliminates compounds that are typically classified as clathrates[62-64] or inclusion compounds (where the guest molecule is a solvent or a gas molecule), solvates or pseudopolymorphs[65-68].

Therefore, cocrystal is a crystalline material consisting of two or more components that are solids under ambient conditions and a liquid component might be called a cocrystal solvate or, if appropriate, a cocrystal hydrate[69,70]. Thus, a multi-component system made of molecular cocrystal former and an ionic API would simply be classified as a pharmaceutical cocrystal[71,72].

Cocrystals have attracted increasing interests from both industrial and academic researchers. They are attracted to the pharmaceutical scientists because of their significantly diversify in the number of crystal forms that can exist for a particular class of crystalline solids mostly the active pharmaceutical ingredient (API), and they can lead to improvements in physical properties of clinical relevance.

An alternative approach that arises conceptually from applying the concepts of supramolecular chemistry and crystal engineering is that a cocrystal is the consequence of a molecular recognition event between different molecular species[73]. Thus, the synthon-based design of cocrystals is continuously being expanded with hydrogen bonding functional groups and supramolecular synthons, expanding the diversity of potential cocrystals and cocrystal components

1.7 Crystal Engineering

Crystal engineering is the design and synthesis of molecular solid-state structures with desired properties, based on an understanding and exploitation of intermolecular interactions. The two main strategies currently in use for crystal engineering are based on hydrogen bonding and coordination complexation. [17,18,24,74]. The roots of crystal engineering can be traced back as far as 1930's, when Pauling defined the chemical bond in both covalent and non-covalent terms. The term "*crystal engineering*" was coined by Pepinsky in

1955 but was not implemented until Schmidt studied a series of solid state reactions of crystalline solids in connection with photodimerisation[75] reactions in crystalline cinnamic acids.

However, since this initial use, the meaning of the term has broadened considerably to include many aspects of solid-state supramolecular chemistry[76]. Gautam Radhakrishna Desiraju defined crystal engineering as "the understanding of intermolecular interactions in the context of crystal packing and the utilization of such understanding in the design of new solids with desired physical and chemical properties. Thus, the properties of molecular materials are dictated by the manner in which their molecules are ordered in the solid state, and it is clear that an ability to control this ordering would afford control over these properties.

Crystal engineering offers many alternative approaches and potential methods for the optimization of less active properties of an API with appropriate selection of a coformers with much better properties. Thus, by considering the nature of the supramolecular synthons present within the parties, the crystal is described with improved physicochemical properties while still maintaining the suitable physical and chemical nature of such API[77-84]. To the chemists, it has been described as the exploitation of non-covalent interactions between molecular or ionic components for the rational design of solid-state structures that might exhibit a better and interesting property. It is also recognised that it 'is becoming increasingly evident that the specificity, directionality, and predictability of intermolecular hydrogen bonds can be utilized to assemble supramolecular structures of, at the very least, controlled dimensionality[85]. Example is the synthesis of Voriconazole–*p* and hydroxybenzoic acid cocryst (1:1): VZL–PABA cocrystal crystallized from a solution of methanol and ethanol. Figure 1.4 show the helix of VZL and PABA connected via O−H···N and N−H···N hydrogen bonds. The connection is through carboxylic acid-pyrimidine two-point synthon and one-point N−H···N hydrogen bond between the amino group of PABA and triazole of VZL.
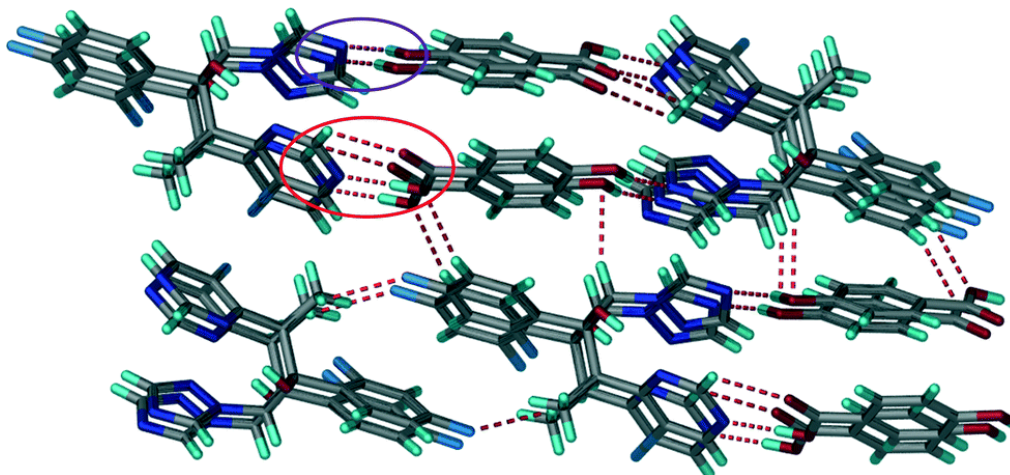
FIGURE 1.4 **-** Supermolecular hydrogen bonding synthons sites in a 1:1 Voriconazole–*p*hydroxybenzoic acid cocrystal.

There are diverse aspects of crystal engineering techniques that may be used to manipulate, improve the solubility and/or the dissolution rate of an API in the crystalline state. At the centre of these available approaches is the need to change surface and molecular assembly in equilibrium with a solvent and the basic knowledge of possible synthon interaction in the solutes will save time and materials. Carboxylic acids are an excellent starting point for synthon interaction in crystal engineering of pharmaceutical cocrystals. Their complementary hydrogen bond donor and acceptor sites make supramolecular homosynthon very favorable. However, as shown in fig 1.5, the formation of an acid dimer synthon is unlikely in competitive situations since the formation of acid-pyridine synthon will always be fovoured. Thus, statistical experiment was performed for the determination of the probability of forming 75 bimolecular hydrogen bonded ring synthons in organic crystal structures. It was observed that the probability of forming an acid dimer synthon was found to be only 33%. This relatively low probability was attributed to the competition with other hydrogen-bonded acceptors (like, COO, pyridine N, Amide C—O, S—O, P– –O, and so on.)[86].

In addition, a recent CSD study on carboxyl donors indicated that carboxylic acid–pyridine interactions through **O-H----N** hydrogen bonding is more favoured to be formed than the carboxylic acid dimer synthon. Indeed, the

acid-pyridine synthon is a highly reliable supramolecular heterosynthon and has been widely exploited in crystal engineering[87].

acid dimer synthon
33%

amide dimer synthon
35%

Homosynthon

acid-pyridine synthon
91%

acid-amide synthon
47%
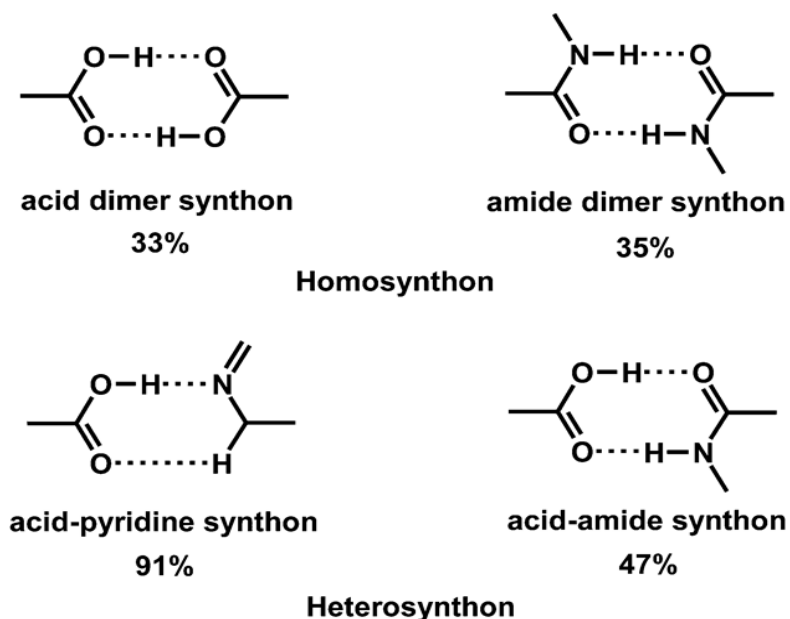
Heterosynthon

FIGURE 1.5 **-** Supramolecular synthons adopted by imides and carboxylic acids showing homosynthon and heterosynthon interaction.

Experimental calculations support the idea that the acid-amide synthon is energetically favoured over acid dimer synthon and that the acid-amide supramolecular heterosynthon with 47% [88] is favoured over acid dimer and acid-pyridine heterosynthon [89]. These observations are particularly relevant for design of cocrystals since robust supramolecular heterosynthons represent perhaps the most reliable and rational route to cocrystals synthesis. The complementary supramolecular heterosynthons that seem to clearly favour formation of cocrystals are not limited to carboxylic acids. The alcohol-amine[90] and alcohol-pyridine[9192] supramolecular heterosynthons are also shown to be well established in crystal engineering.

1.8 Cocrystallization methods/ techniques

Several different methods of cocrystals formation have been described in the literature, and the most common formation methods are based on solvent assisted crystallization (solution method) and the mechanochemical methods which can be neat grinding or solvent assisted grinding[20,93-95]. The solution methods which include cocrystallization by evaporation of stoichiometric solutions is one of the most important tool for a quick cocrystal screening experiments and it was the method considered and used in this (project) dissertation. Thus, in order to design a successful cocrystal screening experiments, it is very important to consider the reactants solubility[96]. In this method, the solution must contain a stoichiometric equimolar concentration of the components. When the ratio is not equivalent, a crystallization of only one component is likely obtained, while other drug remain in solution[35,97].

Cooling crystallisation method involves varying the temperature of the crystallisation system. First, large amounts of reactants and solvent are mixed in a reactor and then the system is heated to a higher temperature to make sure all solutes are totally dissolved in the solvent and is followed by a cooling down step. Cocrystals will precipitate when solution becomes supersaturated with respect to cocrystal as the temperature drops down. This method has recently attracted much more attention for potential of a large scale of cocrystal production.

Slurry cocrystallization technique is the simple process of adding a solvent to the mixture of a host and a guest leads to cocrystallization and is readily useful for systematic cocrystal screening without requiring a robotic system. In cocrystallization process, the dissolutions of the host and guest into a solvent create a supersaturation with respect to the cocrystal, that is, solution-mediated transformation into the cocrystal occurs similar to the transformation between polymorphs[98]. In addition, the slurry technique has been applied to determine the most stable form and the relationship of thermodynamic stability among polymorphs[20,99-102]. Figure 1.6 (1), represents a phase diagram of a cocrystal synthesized by slow evaporation cocrystallization method. Two cocrystal components A and B have similar solubility in solvent S and the 1:1

pure cocrystal can be formed and obtained by evaporation when equimolar components are dissolved in the solvent. The simplicity of this method mostly favors it to be employed especially for screening of new types of cocrystals[98,103-105]. It involves obtaining a supersaturated solution of the components in solution, followed by the addition of the second reagent. When the equilibrium shift to the product side, the crystallization process begins and crystals are observed. The components A and B have a similar solubility in the solvent at the end of the reaction (depending on the amount of each component) it is possible to obtain the pure crystal (6) a mixture between cocrystal and one of the components (2 or 4).
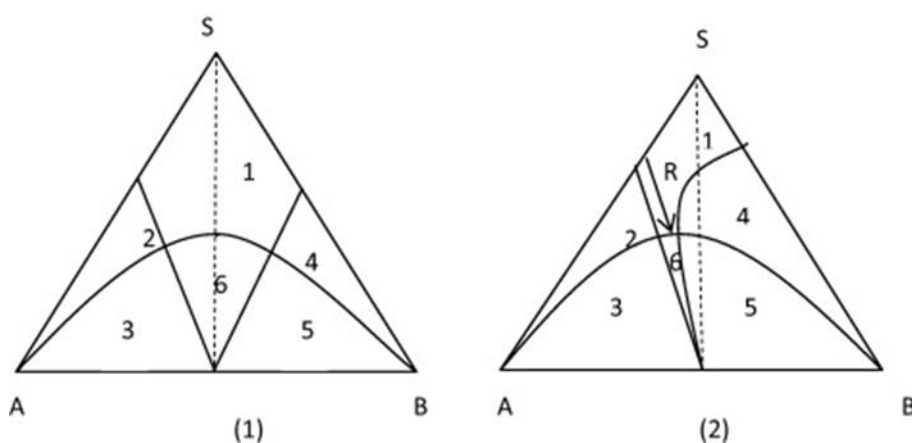
FIGURE 1.6 - Isothermal ternary phase diagrams (TPDs) with two components having similar (1) or dissimilar solubility (2). Region: 1: solution; 2: A + solvent; 3: A + cocrystal; 4: B + solvent; 5: B + cocrystal; 6: cocrystal. Path R indicates the evolution of solution composition as a result of adding reactant B to solutions at close to saturation with B.

The figure 1.6 (2) is a phase diagram for cocrystalization reaction. In the diagram, the components A and B have different solubility in the reaction solvent. For this system, the method of slow evaporation resulted in a precipitation of just a single component (4). The ideal to change the state of supersaturation region of the component A and then adding the component B the reaction mixture, thereby changing the synthetic route leading to the formation of the cocrystal (6).

For a large-scale cocrystals formation, the cooling crystallization method is preferred being used[100,106,107]. The solvent methods are of great importance due to that, most of the cocrystals which can qualify for single crystal X-ray diffraction (SCXRD) testing can only be prepared through this method. Another advantage of solvent evaporation cocrystallization method is the possibility of using spectroscopic analysis in situ to get information about the process of crystallization and chemical interactions present in the process[108,109]. Apart from the said methods, there are also many newly emerging methods, such as crystallization using supercritical fluid, hot-stage microscopy and ultrasound assisted crystallization[110]. While solvo-thermal methods are also used although less frequently[94,111-114].

The technique of mechanochemical cocrystallization started to develop following efforts of Paul and Curtin as well as Etter after they demonstrated that supramolecular synthesis in the solid state provides a degree of molecular recognition and a diversity of products matching and indeed extending those observed in solution cocrystallization.[115]. The application of mechanochemical synthesis for the construction of multicomponent hydrogen-bonded crystals compounds has been extensively studied. The observed increased the efficiency of different grinding methodologies for cocrystal synthesis over solution-based approaches, avoiding the effects of solubility and solvent competition that cannot be avoided during solution crystallization[108,115-118].

Cocrystal formation via grinding method focusing on the mechanistic aspects of cocrystal synthesis as a result milling of the API and conformer together. There are two different techniques for cocrystal formation via grinding. The first method is neat grinding which is also called dry grinding, consisting of mixing the stoichiometric cocrystal components together and grinding them either manually, using a mortar and pestle, or mechanically, using a ball mill or a vibratory mill. This method requires one or both reactants exhibiting significant vapour pressures in the solid state. To date, many kinds of pharmaceutical cocrystals have been successfully synthesised via neat grinding[108]. Various mechanisms have been employed to describe the process of neat grinding, involving different types of intermediate phases, such as molecular diffusion, eutectic formation, and amorphous phase.[119-123].

The second technique for cocrystal synthesis via grinding is the liquid-assisted grinding (also referred as kneading, solvent-drop, wet co-grinding). Significant improvements in kinetics of cocrystal formation by grinding can be achieved by the addition of minor amounts of an appropriate solvent. The improvements in kinetics might be rationalised by the additional degrees of orientational and conformational freedom as well as the enhancement of opportunities for molecular collisions. In addition, tiny cocrystal seeds may be envisaged to form within the solvent during the grinding process so the rate of cocrystallisation can be increased. Besides increasing the cocrystallisation rate, the method of liquid-assisted grinding can control over the polymorphic outcome of cocrystallisation. A detailed look at crystal packing reveal a difference which may be important in rationalising the observation that solvent polarity together with solid state grinding offers the means of controlling polymorphism.[56,123-129]. Finally, the nature of solvents used in grinding method may have a profound effect on the mechanochemical reaction process[130,131].

Recently, new methods like *Supercritical Fluid Technology* (SFT)[132] and *Ultrasound Assisted Solution Cocrystallisation* (USSC)[133],[134-136] were introduced for cocrystal formation. The utilisation of SCF is based on its three fundamental properties: solvent power, miscibility with organic liquids (anti-solvent), atomisation enhancement while the USSC is used to prepare cocrystals from solution or suspension/slurry. In Padrela's work[137], indomethacin–saccharin cocrystals with different morphologies and sizes (nano-to-micron) were produced using supercritical fluid techniques, demonstrating the potential of SCF technologies as screening method for cocrystals. USSC also has been studied using a non- congruently soluble pair of caffeine and maleic acid in methanol, in which pure caffeine/maleic acid 2:1 cocrystal was obtained[138]. It is suggested that ultrasound applications in USSC must have altered supersaturation conditions of caffeine and maleic acid in solution, favouring generation of caffeine/maleic acid 2:1 cocrystal nuclei. Further investigations need to be carried out for understanding the nucleation mechanisms during USSC.

1.9 Pharmaceuticals Ingredients

In this dissertation, different API with less favourable properties like solubility, stability, low dissolution rate were taken into consideration for cocrystal screening exercise in order to obtain an improved form of these APIs. Most of them are of the BCS class II and the BCS class IV, which are known with low solubility (class II) and low permeability (class IV). These APIs include: Indomethacin (IND), Candesartan (CDS), Valsartan (VST), Simvastatin (SVT), Ibuprofen (IBP), Clopidogrel (CLP), Gemfibrozil (GMF), Lamotrigine (LMT), tadalafil (TDF), Ezetimibe (EZT), Cabarmazepina (CBZ), and some which are not in these class like Taurin (TAR), Nicotinamide (NCT) and Fluconazole (FLZ).

The coformers were selected based on their excellent properties like high solubility, stability and the presence of synthon for possible molecular interaction via cocrystallization with the APIs. It were evaluated Ascobic acid (ASC) Aspirin (ASP), Benzoic acid (BEZ), Citric acid (CTR), Fumaric acid (FUM), L-Aspartic acid, Glycine (GLY) and saccharine (SAC).

However, this work was based on fluconazole which gave different structures in the screening experiments with fumaric acid through synthon interactions.

1.9.1 Fumaric acid

Fumaric acid or trans-butenedioic acid ($HO_2CCH=CHCO_2H$) molar mass of 116.07g/mol and melting point of 287 ^{o}C (Fig. 1.7), is a white crystalline compound with fruit like taste and is one of the two isomeric unsaturated dicarboxylic acids. The salts and esters of fumaric acid are known as fumarates. Dimethyl fumarate is known to significantly reduce disability progression in multiple sclerosis. The presence of two acid functionalities aids its ability to interact with other molecules through supramolecular interaction.
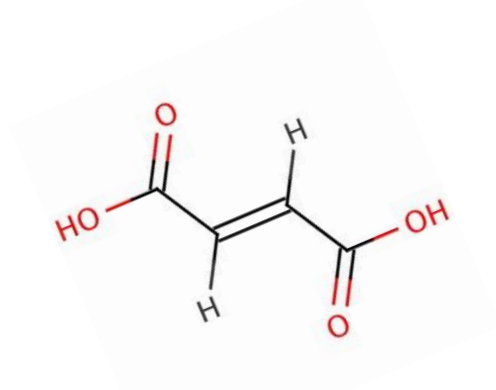
FIGURE 1.7 - Structure of fumaric acid molecule

1.9.2 Fluconazole

Fluconazole [2-(2,4-difluorophenyl)-1,3-bis (1H-1,2,4 triazole-1-yl)-propan-2-ol], molar mass 306.27g/mol and a melting point of between 138-140 ^{o} C. As shown in (Figure 1.8) is a triazole antifungal agent, used in the treatment of localized candidiasis and systemic therapy of candidial infections, dermatophytic fungal infections, and cryptococcal meningitis. That is, it is used to treat fungal infections, including yeast infections of the vagina, mouth, throat, esophagus, abdomen, lungs, blood, and other organs.
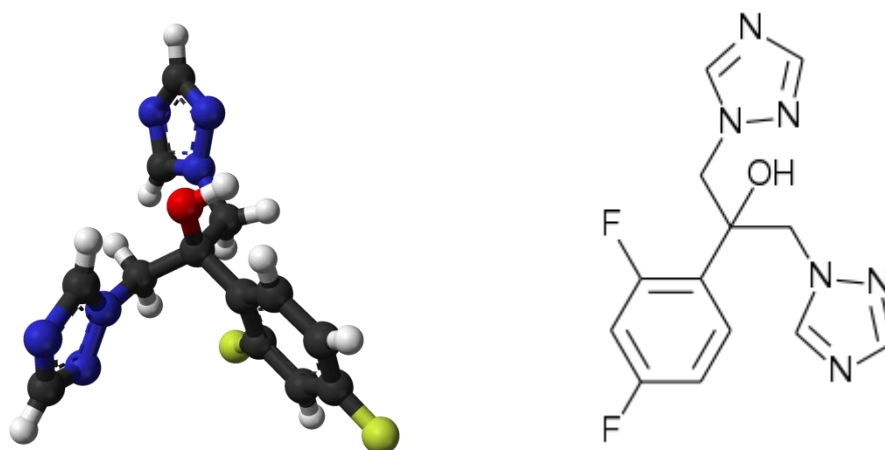
FIGURE 1.8 – Structures of fluconazole molecule

Fluconazole is also used to treat meningitis (infection of the membranes covering the brain and spine) caused by fungus and also used to prevent yeast infections in patients who are likely to become infected because they are being treated with chemotherapy or radiation therapy before a bone marrow transplant. It is commonly used as accompanying therapy for immunodeficient

patients, that is, patients with AIDS or cancer and patients taking immune-depressive agents[139].

As it appears, fluconazole is a white crystalline powder which is slightly soluble in water and is a very weak base with a pKa value of 1.76 for its conjugated acid, which limits its ability to form salts. It is generally accepted that for salt formation a pKa difference greater than two units between the acid and the base is needed, which means that only very strong acids would be considered appropriate for salt screening.

Different crystalline forms of fluconazole (cocrystals, monohydrates and several solvates) have been reported[140]. Scientists from Pfizer[39,42] have reported the existence of three polymorphic forms of fluconazole, which they have designated as form-I, II, III and a hydrate[37-44]. The Raman spectra[38,39,41,42,141,142] of different polymorphs of FLZ and the XRPD[39] were observed. The polymorph II was our starting material in this dissertation. The calculated PXRD patterns of the different crystalline forms of fluconazole and fumaric acid are shown in figure 1.9, with the PXRD FLZ-FUM corresponds to the only reported cocystal.

A 2FLZ-1FUM cocrystal was also reported and stored as UPOQEW in the CCSD, which was obtained from a 2:1 mixture of fluconazole and fumaric acid dissolved in boiling ethanol [40].The cocrystals suitable for single crystal X-ray diffraction were prepared by dissolving fluconazole and fumaric acid in 1 mL of boiling methanol. This cocrystal shows an amide dimer synthon O-H----N connection and presents the PI space group. The asymmetric unit consists of one molecule of a neutral FLZ and one-half of a FUM acid molecule as shown in figure 1.10.

Structures of reported cocrystals of FLZ with carboxylic acids; (malonic acid, glutaric acid, maleic acid and 2-hydroxybnzoic acid are deposited in the CSD with refcode MEWTAL, UPOQIA, UPOQAS and EZEGIA respectively). The five FLZ polymorphs as IVUQOZ, IVUQOZ01 - IVUQOZ04, monohydrates of FLZ as IVUQIZ, IVUQIZ01 - IVUQIZ05 and the fluconazole ethyl acetate solvate with CSD refcode IVUQEV. The figure 1.11 shows different FLZ molecules interact through the O-H----N hydrogen bonded molecular chain or dimer and forming a strong supramolecular assemblies. Apart from the strong

O-H----N hydrogen bonded interaction; different polymorphic structures of FLZ dimers in the same asymmetric unit also show different weak interactions involving intramolecular C-H----O, C-H----F and C-H----N hydrogen bonds. These different polymorphs observed are conformational and were due to the orientation of the phenyl ring and the two triazole rings as shown in the CCSD.
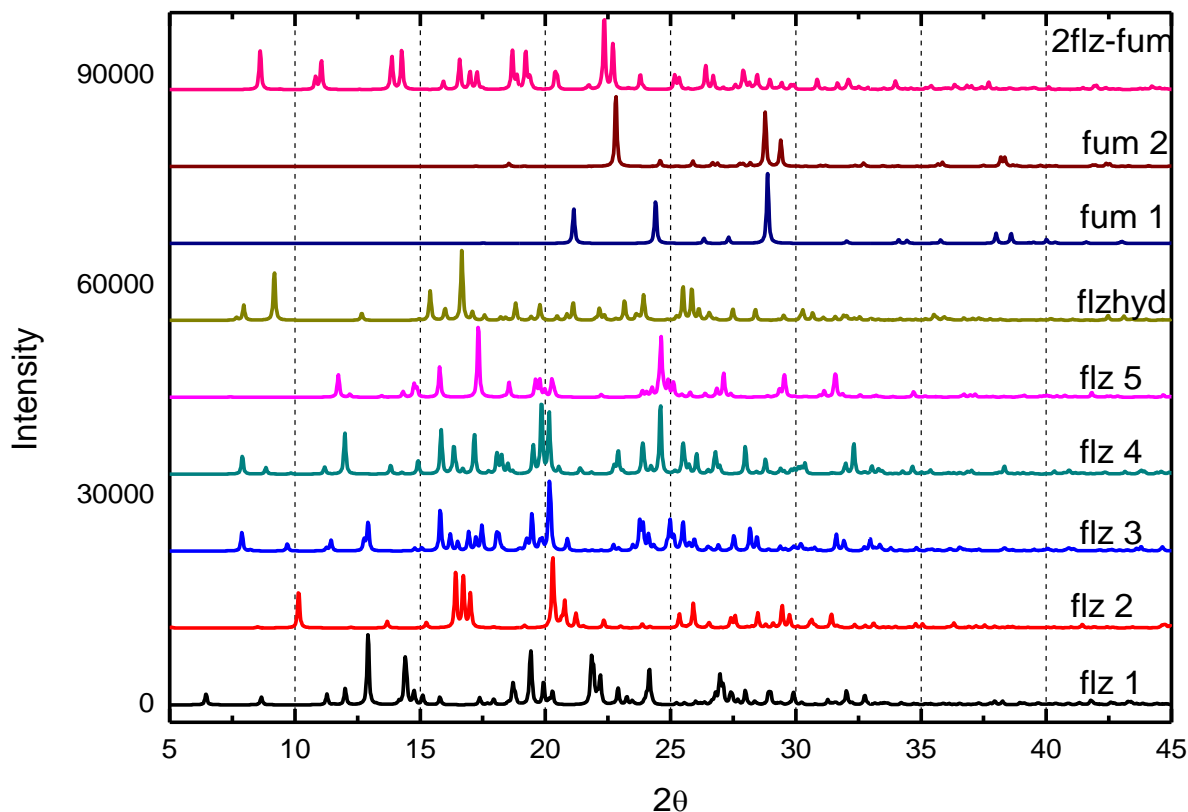
FIGURE 1.9 – Calculated PXRD patterns of reported Fluconazole polymorphs, fumaric acid and the 2FLZ-FUM cocrystal.
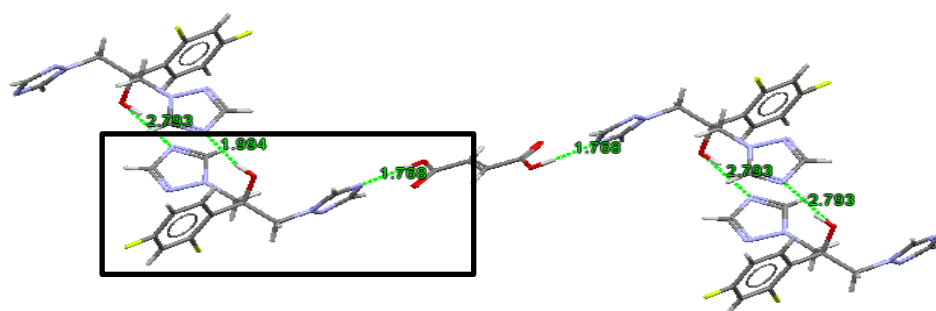
FIGURE 1.10 - 2FLZ-FUM cocrystal structure showing the asymmetric unit[40].
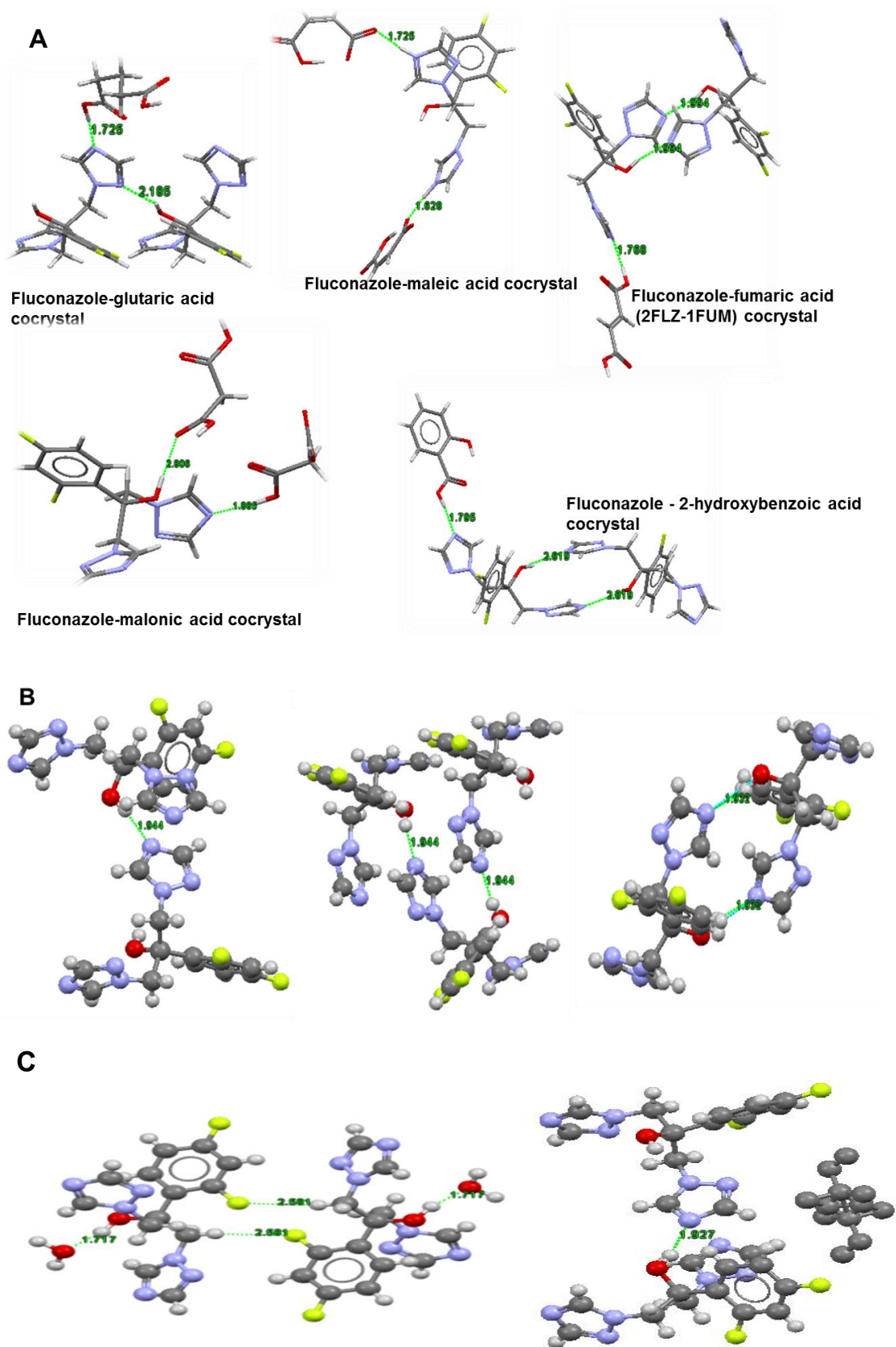
FIGURE 1.11 Supramolecular assemblies of synthon connection and bond distances (A) strong O-H----N interaction in FLZ cocrystals with carboxylic acids (B) C-H----N interaction in FLZ polymorphs (C) O-H----N, O-H----O and H----F in solvate and hydrate of FLZ.

1.10   Characterization methods

Structure resolution by characterization is the ultimate and most important part of cocrystal research, in that, it confirms synthon interactions in the formation of a new structures. It also allows for the determination of whether the adduct synthesized is a salt, solvate or other class into which the cocrystal might belong and it aids the resolution of solvent or water molecules that may be present within the crystal lattice and facilitates the determination of structure-property relationships.

There are different characterization techniques and the single-crystal X-ray diffraction is currently the most widely used technique for cocrystal structure solution, though NMR spectroscopy, Raman spectroscopy, and solid state IR spectroscopy are all techniques used to complement this method. Powder X-ray diffraction and other thermal analysis like the DSC and the Thermogravimetric analysis are also used within this field. Powder X-ray diffraction is used more as a screening technique for new materials although it does have the potential for full structure analysis [143-147].

1.10.1   Raman Spectroscopy

The Raman spectroscopy provides information about molecular vibrations that can be used for sample identification and quantitation[148]. The technique involves shining a monochromatic light source (i.e. laser) on a sample and detecting the scattered light (Fig. 1.12), the majority of the scattered light is of the same frequency as the excitation source; this is known as Rayleigh or elastic scattering (Fig1.13). A very small amount of the scattered light (ca. 0.0001% of the incident light intensity) is shifted in energy from the laser frequency due to interactions between the incident electromagnetic waves and the vibrational energy levels of the molecules.
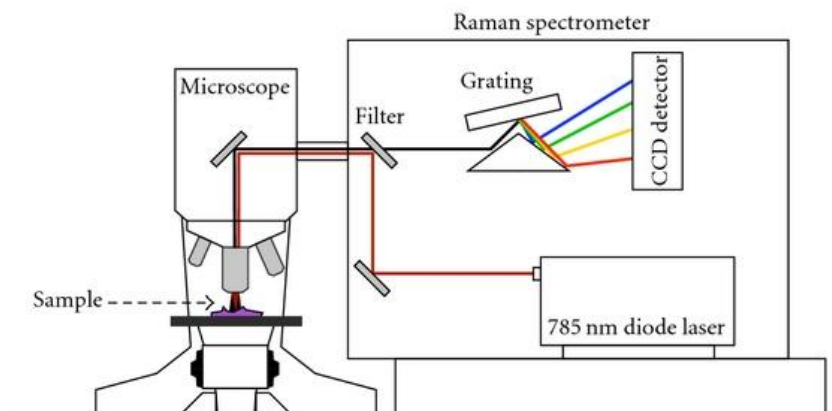
FIGURE 1.12 – A sketch showing a typical set up of Raman spectroscopy attached to a microscope.

Generally, Raman spectra are plotted with respect to the laser frequency such that the Rayleigh band lies at 0 cm^{-1}. On this scale, the band positions will lie at frequencies that correspond to the energy levels of different vibrations. The Raman spectrum can thus be interpreted similar to the infrared absorption spectrum.
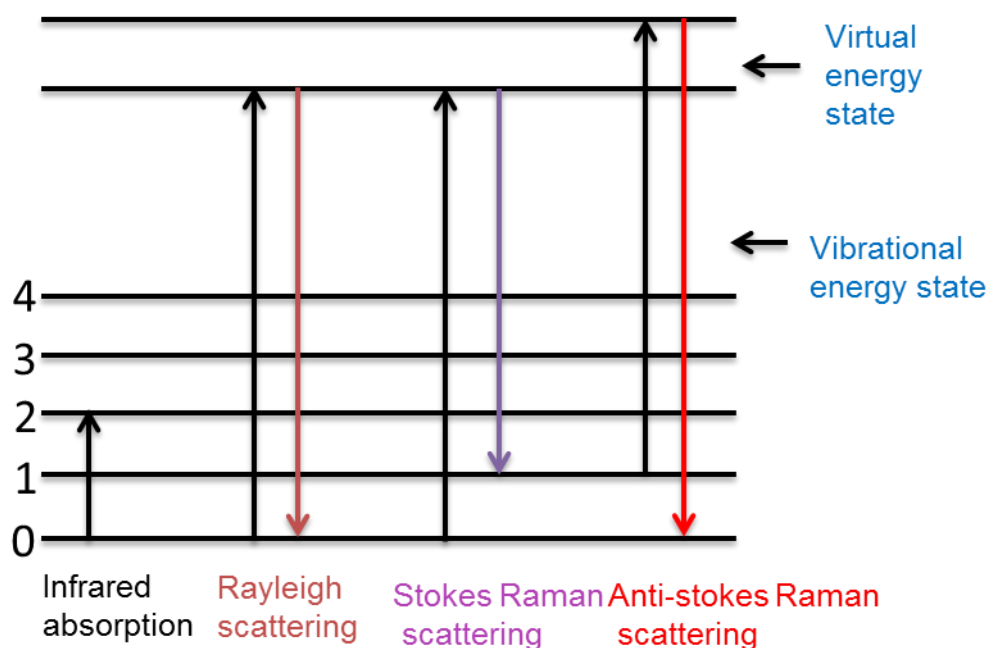
FIGURE 1.13 - Electromagnetic waves shifted in energy from the incident radiation by Raman spectrum.

Raman scattering is a spectroscopic technique that is complementary to infrared absorption spectroscopy. Raman offers several advantages over mid-IR and near-IR spectroscopy, including:

- Water is a weak scatterer - no special accessories are needed for measuring aqueous solutions

- Water and CO_2 vapors are very weak scatterers - purging is unnecessary

- Inexpensive glass – sample holders are ideal in most cases

- Fibre optics (up to 100's of meters in length) can be used for remote analyses

- Raman spectra are "cleaner" than mid-IR spectra - Raman bands are narrower, and overtone and combination bands are generally weak

- The standard spectral range reaches well below 400 cm^{-1}, making the technique ideal for both organic and inorganic species

- Raman spectroscopy can be used to measure bands of symmetric linkages which are weak in an infrared spectrum (e.g. -S-S-, -C-S-, -C=C)

- The major disadvantages of the Raman spectroscopy is the weak Raman effect, which leads to low sensitivity in measuring low concentration of substances, it can also experiences fluorescence in some materials and give no result for metals and alloys samples.

1.10.2 X-ray Powder Diffraction (XRPD)

X-ray diffraction from crystalline solids is an established phenomenon discovered by a German physicist, Max von Laue in 1912, who was interested in the way light and crystals interacted with one another. Von Laue demonstrated mathematically that X-rays were diffracted by crystalline materials and established that X-rays are electromagnetic in nature. Subsequent work allowed Sir William Bragg and his son Sir Lawrence Bragg to establish a new

area of science, which led to the analysis of crystal structure by the means of X-ray diffraction. The use of X-rays as a device for discovering the precise three dimensional crystal structures of molecular solids was entirely due to the Braggs work. It was shown that electromagnetic radiation (X-rays) with a wavelength similar to an inter-planar distance (d) in crystal planes (of the order of 1Å) incident on planes of atoms, results in X-rays being scattered both constructively and de-constructively.

The Bragg's law (equation 1) is the central to diffraction as it gives the geometric conditions under which a diffracted beam can be observed. The Bragg model can be seen (figure 1.14), as the reflection of the incident radiation by parallel planes of atoms. The planes which are defined by Miller indices (hkl) will only give rise to constructive interference when the second beam, which has travelled the extra distance of A'B' + B'C', is an integral (n) multiple of the wavelength (λ).

$$n\lambda = 2d \sin\theta \qquad\qquad \text{(eq. 1)}$$
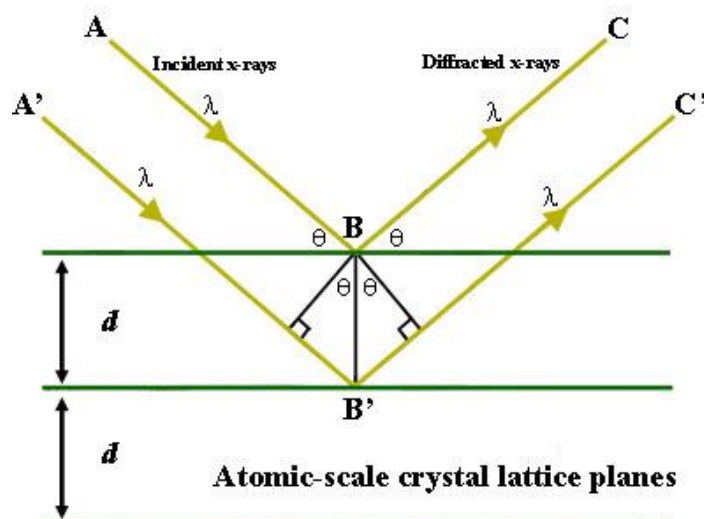
FIGURE 1.14 - The geometric conditions required for Bragg diffraction. The diffracted X-rays exhibit constructive interference when the distance between paths ABC and A'B'C' differs by an integer number of wavelengths (λ).

The source of an X-rays in the X-ray diffraction equipment is an X-ray tube (Fig. 1.15), which generates this electromagnetic radiation when strong moving electrons decelerate as a consequence of hitting a metal target (most commonly copper or molybdenum) in an evacuated enclosure. More intense X-rays can be produced from a synchrotron storage ring in which electrons moving at relativistic speed are contained by magnetic fields.
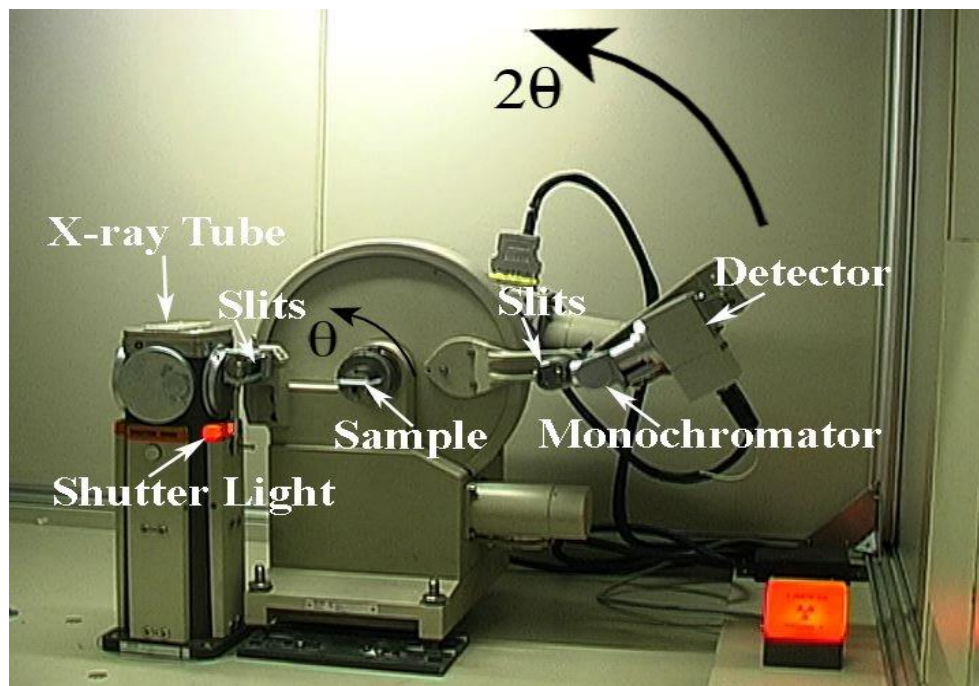
FIGURE 1.15 – A picture of a typical XRD device setup.

In any typical X-ray diffraction (XRD) experiment, the interplanar spacing (d-spacing) of a crystal is used for identification and characterization of the crystal. When X-rays interact with electrons in a solid crystal, the X-ray diffraction obtained gives a measurement of electron density within a unit cell of the crystalline system [149-155].
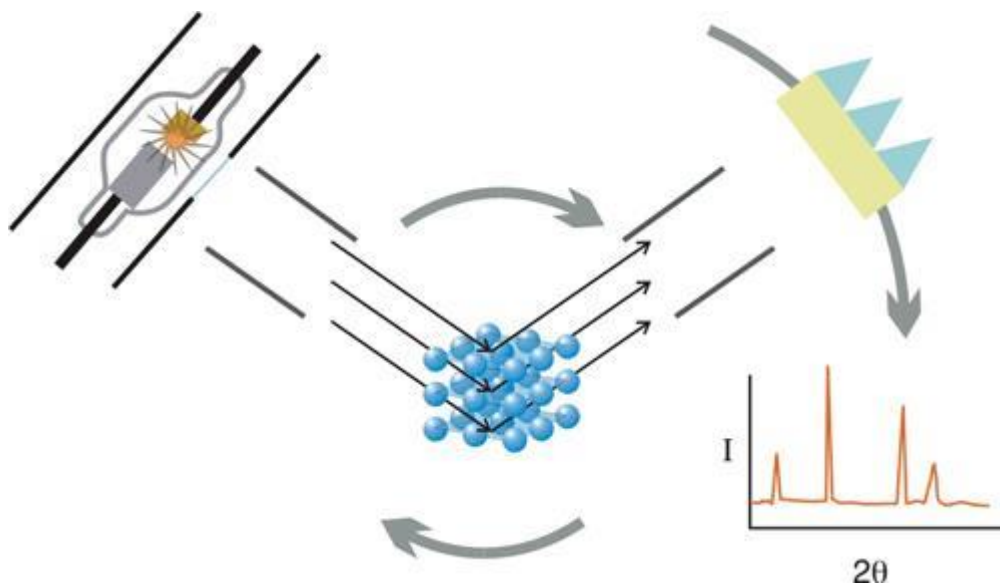
FIGURE 1.16 – A sketch showing the X-ray interaction with crystal samples to generate diffraction.

The X-rays are scattered from the electron cloud surrounding an atom at the same frequency as the primary beam, known as Thomson scattering, and are collected on a detector. In the forward direction ($2\theta = 0°$) all the X-rays electrons scatter in the same phase, but as 2θ increases, the intensity of the scattered X-rays decreases due to destructive interference (fig 1.16). The value of the scattering factor is therefore proportional to the number of electrons in the atom. Solving Bragg's Equation gives the d-spacing between the crystal lattice planes of atoms that produce the constructive interference. A given unknown crystal is expected to have many rotational planes of atoms in its structure; therefore, the collection of "reflections" of all the planes can be used to uniquely identify an unknown crystal. In general, crystals with high symmetry (e.g. isometric system) tend to have relatively few atomic planes, whereas crystals with low symmetry (in the triclinic or monoclinic systems) tend to have a large number of possible atomic planes in their structures.

1.10.3   Single crystal X-Ray Diffraction

The main experimental tool for investigating atomic structure of single crystals with X-ray diffraction is the SCXRD with CMOS detector (fig.1.17). It allows for very exact measurement of satellite reflections of a periodic crystal. Most SCXRD has x-ray tubes with copper or molybdenum anode. The molybdenum tube provides x-rays of the wavelength 0.71073 Å collimated with fibre-optics collimator. The beam diameter can be set from 0.3 to 0.8 mm. This radiation can be used for studies of inorganic and organometallic materials including strongly absorbing samples.

a)   b)
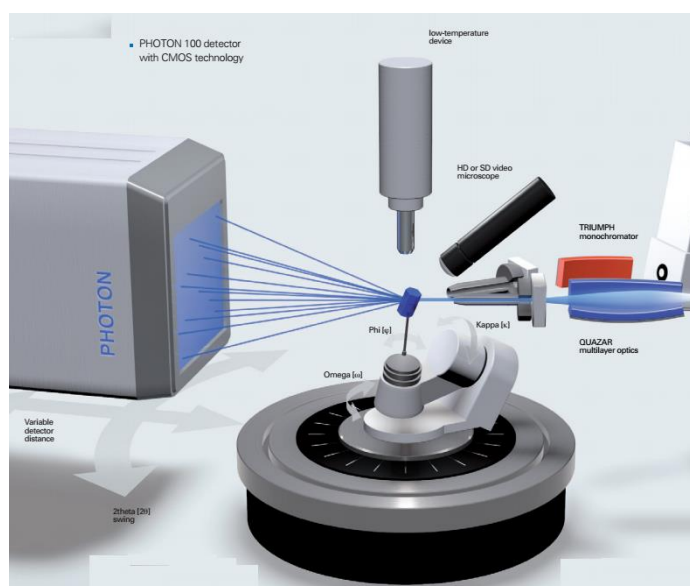
FIGURE 1.17 – (A) Picture of Single Crystal X-Ray Diffraction device (B) Image of the devices showing X-rays interaction with crystal sample.

The copper tube provides x-rays of the wavelength 1.54184 Å collimated with thin-layers mirrors to a beam of the diameter 0.3 mm. The intensity of the

focused beam is sufficient for measurement of organic samples, from small molecules to well diffracting proteins.

Single crystal X-ray diffraction (SXRD)[156,157] is a non-destructive analytical technique which provides detailed information about the internal lattice of crystalline substances, including unit cell dimensions, bond-lengths, bond-angles, and details of site-ordering.

In order for X-ray crystallography to be successful, the sample must be crystalline; that is, having a periodic long range order. A crystal lattice is formed of unit cells; a unit cell contains the smallest repeating unit and is connected to other identical unit cells in three dimensions. It has parameters which define both the axes (a, b and c) and the angles (α, β, and γ)[158,159]. This labelling of parameters is the standardised scheme for a unit cell as shown in figure 1.18.
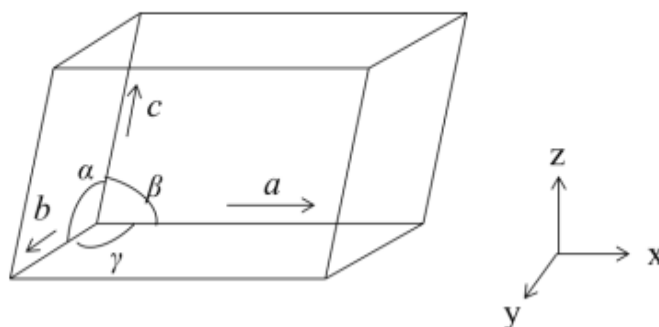
FIGURE 1.18 - A unit cell in three dimensions parameters which define both the axes (a, b and c) and the angles (α, β, and γ).

TABLE 1.1 – Showing the relationship between different crystal system, unit cell parameters and the possible Bravais lattice types.

Crystal system	Restrictions on Unit Cell parameters	Possible Bravais types
Cubic	$a = b = c$ $\alpha = \beta = \gamma = 90^\circ$	P, I, F
Hexagonal	$a = b \neq c$ $\alpha = \beta = 90^\circ$ $\gamma = 120^\circ$	P
Trigonal	$a = b = c$ $\alpha = \beta = \gamma \neq 90^\circ$	R
Tetragonal	$a = b \neq c$ $\alpha = \beta = \gamma = 90^\circ$	P, I
Orthogonal	$a \neq b \neq c$ $\alpha = \beta = \gamma = 90^\circ$	P, I, F, A, B, C
Monoclinic	$a \neq b \neq c$ $\alpha = \gamma = 90^\circ$ $\beta \neq 90^\circ$	P, C
Triclinic	$a \neq b \neq c$ $\alpha \neq \beta \neq \gamma \neq 90^\circ$	P

The contents of the unit cell can often be reduced to sub-units known as the asymmetric unit. Each asymmetric unit is related to others by symmetry elements (rotation, reflection, inversion and so on), to form the complete crystal structure. The planes within a set are parallel and equidistant (interplanar distance known as d-spacing) and are labelled by Miller indices (h,k,l); integer values which are mathematically related to the unit cell parameters.

A crystal structure is assigned a space group which represents all of the symmetry elements within the system. The combination of possible symmetry elements, the seven crystal systems and fourteen Bravais lattices means there are only 230 different space groups. The possible symmetry elements include

inversion, rotation, reflection, screw axes and glide planes [160-166]. Figure 1.19 shows the common four of the fourteen bravais lattice.
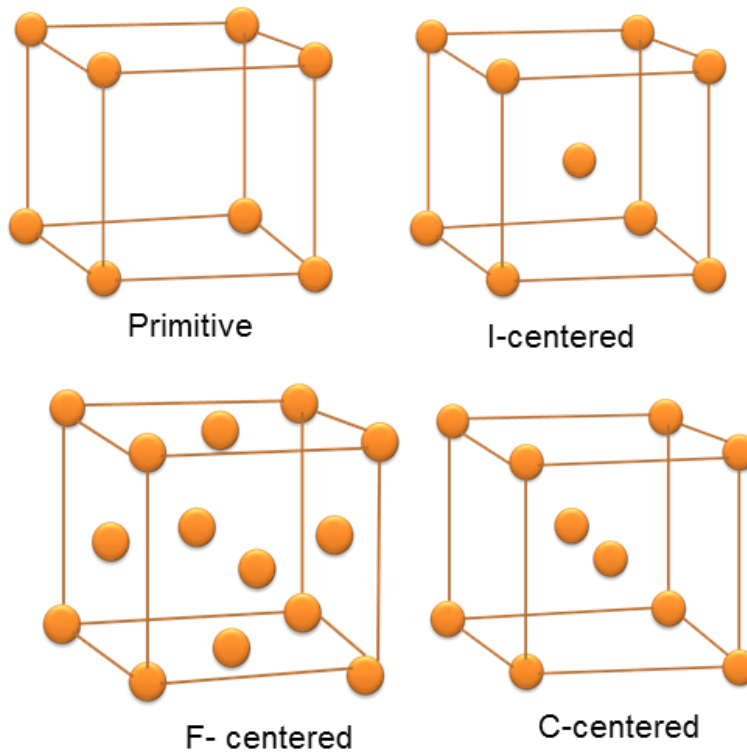
FIGURE 1.19 - The four Bravais lattice types.

1.10.4 Differential scanning calorimetric (DSC)

Differential scanning calorimetric is a thermal analysis technique that detects the temperatures and heat flows caused by changes in heat capacity or by endothermic and exothermic processes of materials as a function of time and temperature. For this, the equipment measures the energy necessary to establish a nearly zero difference of temperature between a substance and an inert reference material, as the two specimens are subjected to identical temperature regimes in an environment heated or

cooled at a controlled rate. An accurate measurement of the melting temperature, fusion heat, latent heat of melting, reaction energy and temperature, glass transition temperature, crystalline phase transition temperature and energy, precipitation energy and temperature, denaturisation temperatures, oxidation induction times and specific heat or heat capacity are obtained from this device[167].

With advancement in DSC equipment, several different modes of operations exist and it can enhance the applications of DSC. Scanning mode typically refers to conventional DSC, which uses a linear increase or decrease in temperature.
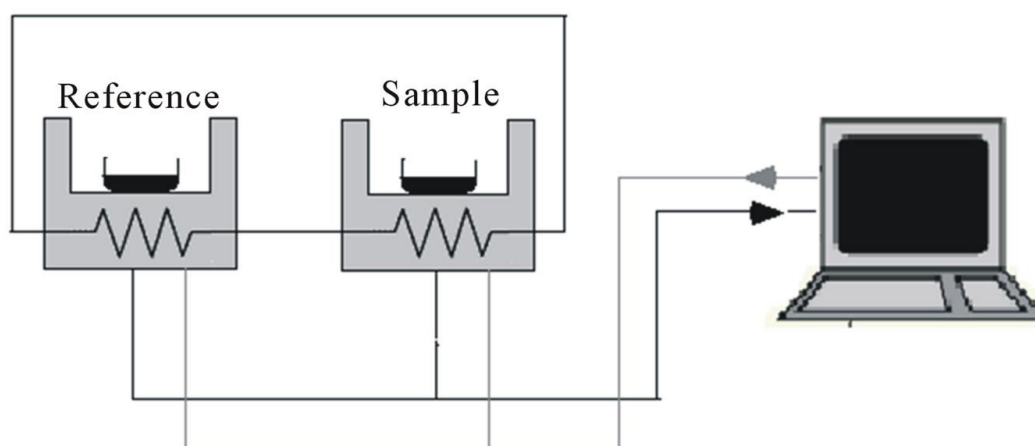
FIGURE 1.20 - Common features of the Differential scanning calorimeter

An example of an additional mode often found in DSC equipment is an isothermal scan mode, which keeps temperature constant. This allows for stability studies at constant temperatures, particularly useful in shelf life studies for pharmaceutical drugs [168-170].

In the DSC equipment, sample is placed in a suitable pan (Al, Cu, Au, Pt, alumina, and graphite are available and need to be chosen to avoid reactions with samples) and sits upon a constantan disc on a platform in the DSC cell with a chromel wafer immediately underneath as shown in (Fig. 1.20). A

chromel-alumel thermocouple under the constantan disc measures the sample temperature. An empty reference pan sits on a symmetric platform with its own underlying chromel wafer and chromel-alumel thermocouple. Heat flow is measured by comparing the difference in temperature across the sample and the reference chromel wafers and this depends on the equipment used.

The equipment plots the difference in heat output for the two heaters against the temperature achieved (Fig.1.21). If the material is just heating up, then the rate of heat flow will be constant, and determined by the specific heat of the sample. When there are changes in state, as for example when a polymer crystallises or reaches its glass transition temperature, then there is either a dip or an increase in the plot. A permanent change in increase represents a permanent change in state.
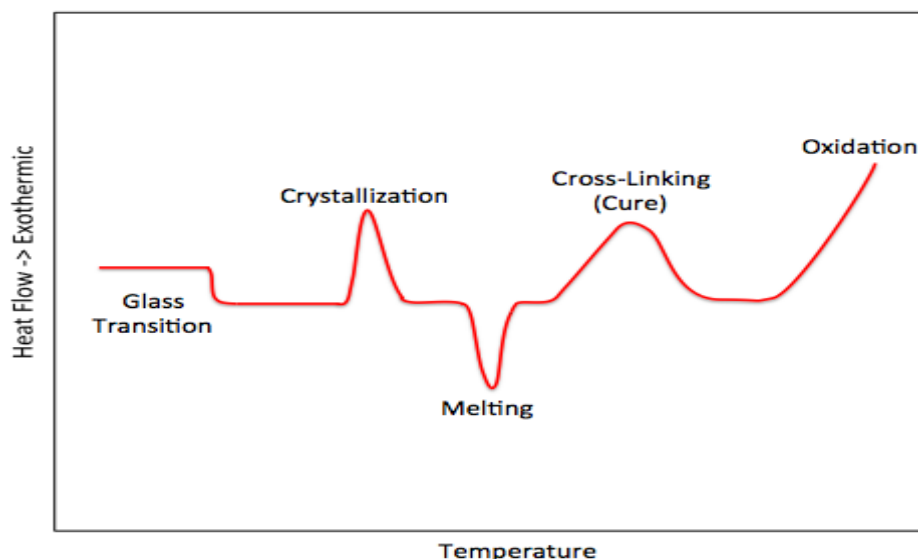
FIGURE 1.21 - An idealized DSC curve showing the shapes associated with particular phase transitions.

1.10.5 Thermogravimetric Analysis (TGA)

Thermogravimetric analysis or thermal gravimetric analysis (TGA) is a method of thermal analysis in which changes in physical and chemical properties of materials are measured as a function of increasing temperature (with constant heating rate), or as a function of time (with constant temperature and/or constant mass loss). That is, TGA is based on the measurement of the

mass loss of a material as a function of temperature. Based on this, it provides information about physical phenomena, such as second-order phase transitions, including vaporization, sublimation, absorption, adsorption, and desorption. It also provide information about chemical phenomena including chemisorptions, desolvation (especially dehydration), decomposition, and solid-gas reactions (e.g., oxidation or reduction). Thus, It is a useful technique for the study of polymeric and pharmaceutical materials[171].
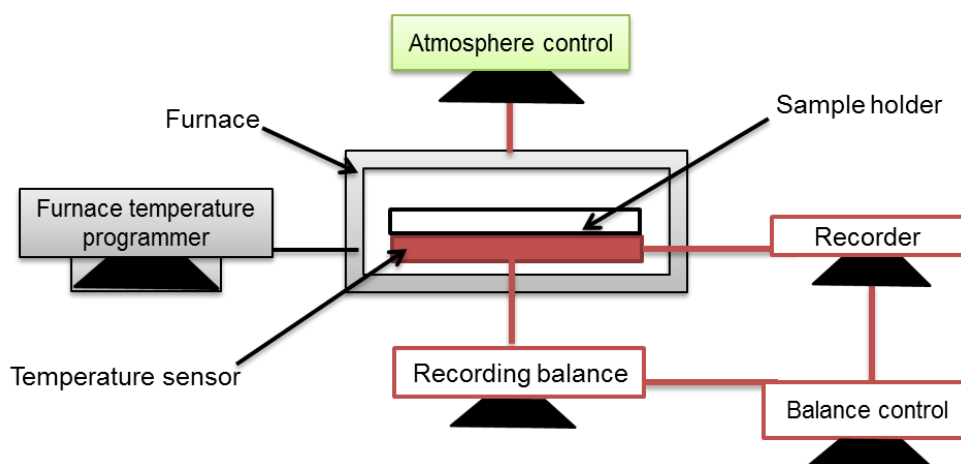
FIGURE 1.22 - Block diagram of TGA (Description of Thermogravimetry).

Figure 1.22 shows the balance beams for the sample and the reference located in the furnace. The masses of the sample and the reference are measured by the sensitivity-calibrated drive coils separately. The mass difference is sent as TG signal. By the differential mass measurement, the effects of the beam expansion, the convection flow, and buoyant force are cancelled. Thus the highly sensitive thermogravimetry measurement is achieved. The mass measurement of the sample and the reference by the independent drive coils enables the easy adjustment of the TG baseline drift electrically. Also, thermocouple is located in each holder which enables the simultaneous DTA signal output.

In addition, within the thermogravimetry, a continuous graph of modified mass against temperature is acquired while a substance is heated at a uniform rate or kept at constant temperature. The plot of mass change versus temperature (T) is referred to as the thermogravimetric curve (TG curve). For the TG curve, a plot of mass (m) is decreasing downwards on the y axis

(ordinate), and temperature (T) increasing to the right on the x axis (abscissa) as described in (Fig. 1.23). Within a TG curve of a single stage decomposition, there are two features temperatures; the initial Ti and the last temperature Tf of an event. Ti is described as the lowest temperature at that the onset of a mass change could be detected through thermobalance operating under particular conditions and Tf as the final temperature at that the particular decomposition appear to be complete[172].
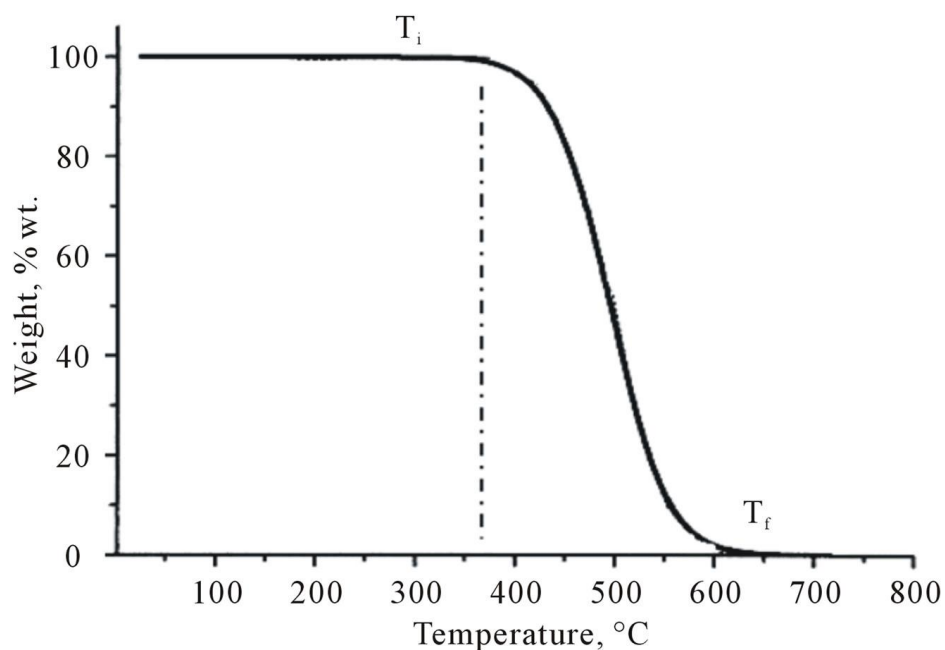
FIGURE 1.23 – A typical TGA curve

TGA is commonly used to determine selected characteristics of materials that exhibit either mass loss or gain due to decomposition, oxidation, or loss of volatiles (such as moisture). Common applications of TGA are (1) materials characterization through analysis of characteristic decomposition patterns, (2) studies of degradation mechanisms and reaction kinetics, (3) determination of organic content in a sample, and (4) determination of inorganic (e.g. ash) content in a sample[173].

CHAPTER 2 - OBJECTIVE

2. Objective

The objective of this work is to improve the unfavourable pharmaceutical characteristics of less active APIs having deficiencies in terms of solubility, bioavailability, stability and shelf life using crystal engineering techniques to perform cocrystalization of APIs. It will be used the knowledge of supramolecular synthons and the understanding of the hydrogen bonding to forge molecular interaction between the API and pharmaceutically acceptable coformers, selected based on their favourable properties like high solubility and stability. It is expected that the forging of a simple molecular interaction between the less active API and the selected coformer will lead to a new crystalline structure with improved physicochemical properties.

The evaluated APIs were Indomethacin (IND), Candesartan (CDS), Valsartan (VST), Simvastatin (SVT), Ibuprofen (IBP), Clopidogrel (CLP), Gemfibrozil (GMF), Lamotrigine (LMT), tadalafil (TDF), Ezetimibe (EZT), Cabarmazepina (CBZ) of BCS class II and IV, and some which are not in these classes like Taurin (TAR), Nicotinamide (NCT) and Fluconazole (FLZ) of BCS class III. The conformers used are Ascobic acid (ASC) Aspirin (ASP), Benzoic acid (BEZ), Citric acid (CTR), Fumaric acid (FUM), L-Aspartic acid, Glycine (GLY) and saccharine (SAC).

However, this process of obtaining a new cocrystal solid structure with additional improved physicochemical properties starts with the selection of a problematic API and the pharmaceutically acceptable cocrystal formers, selected based on the knowledge of supramolecular interaction (using the Cambridge Crystallography Structure Database). The characterization of this solid crystal structure using the Raman spectroscopy, X-ray Powder diffraction, Differential scanning calorimeter, thermogravimetric analysis and the Single crystal x-ray diffraction will confirm the synthesis of a new crystalline structure.

CHAPTER 3 - MATERIALS AND METHODS

3. Materials and methods

3.1 Materials

The fluconazole (API) used for this experiment present a similar XRD pattern of polymorph 2 previously reported and was donated from Medley Pharmaceuticals Limited as a primary material. The API was used as obtained without further purification. Other APIs used in this experiment which did not result into a new crystal structure were either obtained from pharmaceutical companies or pharmacies. Fumaric acid (coformer) used was purchased from Sigma-Aldrich chemical company at a >99% purity (Analytical reagent grade).

The solvents used for the experiment were pure water obtained from a MiliQ sytem (18.2 mΩ cm); Acetonitrile HPLC grade, purchased from J.T Bakers Ltd. The other solvents like Ethanol, Methanol used at different experimental stages was HPLC grade likewise and purchased from J.T Bakers Ltd.

The Raman spectroscopy used for the screening experiment is a B&W Tek model *i*-Raman BWS 415-785H, with a red laser (785 nm), spectral resolution of 3.5 cm^{-1}. Attached to an optical microscope used to observe the crystal at different magnifications. Each spectrum was obtained with 30s of acquisition time and a laser power 160 mW.

For the X-ray powder diffraction studies, Rigaku Multiflex diffractometer with a Cu source was employed maintained at a voltage of 40 kV and current of 30 mA. The choice of scanning angle was from 5° to 45° (2θ) and using a step of 0.2 °θ/ minute.

For the single-crystal X-ray diffraction, it was used a Bruker D8 Quest with monochromatic Cu source, voltage of 40 kV and current of 30 mA coupled to a Photon 100 detector.

The DSC thermal analyses of all samples were recorded on a Differential Scanning Calorimeter Netzsch DSC 204 with a Al_2O_3 pan crucible used at a heating rate of 10 K/min. It was employed over a temperature range of 298 K to 733 K, under N_2 gas (with a fixed flow rate of 2 ml/min).

Thermogravimetric analysis (TGA) was performed using the Netzsch TG 209 F1, with Al_2O_3 crucible as the reference used under O_2 gas (flow rate of 2 ml/min), 10 °C/min and range of 333 K to 633 K.

3.2   Method employed

Cocrystal screening is a process similar to salt screening and is particularly suited to high-throughput technologies. Once an API has been selected for cocrystallisation studies, a pharmaceutically acceptable, non-toxic cocrystallising agent(s), coformer, is chosen to result in a pharmaceutically acceptable product. This limits the crystallizing agent to those that have been approved for consumption by humans, for example pharmaceutical excipients and compounds classified as generally recognised as safe (GRAS) for use as food additives (as classified by the U.S. Department of Health and Human Services). Thus, APIs and coformer selection will be the first step in the screening process using the knowledge and understanding of supramolecular synthon interaction and the guide on synthon reported in the CSD. Since the aim of performing this experimental is to improve the pharmaceutical properties of less desirable drugs, focus will be on the less soluble APIs of the BCS class II and IV.

Publications and recent studies on the materials used for the synthesis and the methods employed of a particular drug (API of choice) will be an advantage in the course of further research on the drug. Thus, knowledge on the different classes of hydrates, solvates and cocrystal polymorphs of this particular API with their structural parameters obtained from Cambridge Structural Database (CSD) will be an advantage and a guide to a good screening experiment and the final resolution and conclusion since it will confirms the newness of the structure obtained when compared to all previously obtained structures.

According to the chat on figure 3.1, the method employed for the synthesis of new cocrystal in this research starts with the selection of APIs and coformers which have the tendency of dissolving in a given solvent, and via different solvent cocrystallization techniques, with varying cocrystallization conditions like

changing the coformers, temperature and solvent to favour the synthesis of a new solid cocrystal. However, the dried cocrystal obtained will undergo the first

characterized using the Raman spectroscopy to detect changes in the spectra of the starting materials, the less favourable API and selected conformer
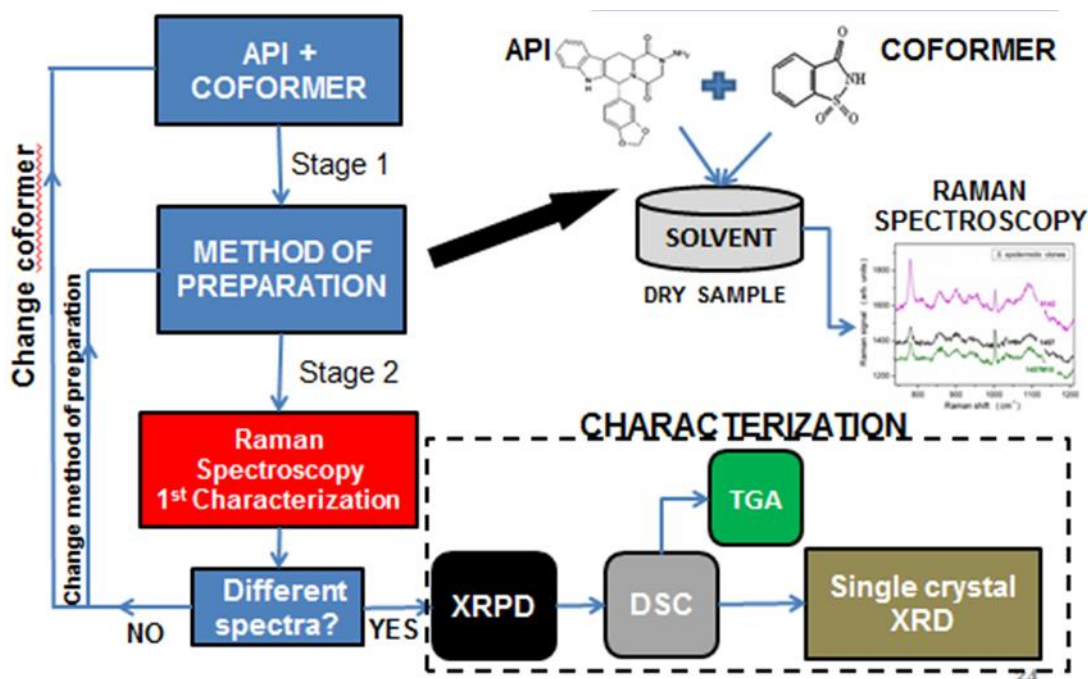
FIGURE 3.1 - A chart showing the crystal engineering processes and stages for the synthesis of new cocrystal structures.compared

with that of the dry synthesized solid crystal and the result obtained will indicate for further characterization using XRD, TGA, DSC and the SCXRD to obtain information about the structure of the new crystal molecule.

Different characterization tools like the Raman spectroscopy, DSC, XRD, TGA and the SCXRD were employed in this study to provide information about the possible cocrystals structures, by considering the changes in physical and chemical properties like melting temperature, spectral profile, diffraction pattern and the bonding interactions. The spectra of pure API and conformer can be easily compared with that of the new cocrystal to reveal whether or not there is an interaction or strong recognition between the less active ingredient and coformer or with the solvent as the case may be. This is the first stage in

the research, which focusing more on the screening experiments, in order to find and evaluate possible new cocrystals structures**.**

In this work, different cocrystal screening experiments were performed as shown in (Table 3.2), using small amount of the APIs and coformers at different stoichiometric ratio of FLZ:FUM at 1:1, 2:1, 3:1, 1:2, 1:3, using grinding and solvent evaporation crystallization as screening experiment using different

Table 3.1 – Screening experiment using different API and coformers

API/coformer	Citric (CTR)	Fumaric (FUM)	Aspirin (ASP)	Benzoic (BEZ)	L-Aspartic (ASR)	Glycine (GLY)	Saccharine (SAC)
Indomethacine (IND)	IND-CTR	IND-FUM	IND-ASP	IND-BEZ	IND-ASR	IND-GLY	IND-SAC
Candesartan (CDS)	CDS-CTR	CDS-FUM	CDS-ASP	CDS-BEZ	CDS-ASR	CDS-GLY	CDS-SAC
Valsartan (VST)	VST-CTR	VST-FUM	VST-ASP	VST-BEZ	VST-ASR	VST-GLY	VST-SAC
Sinvastatin (SVT)	SVT-CTR	SVT-FUM	SVT-ASP	SVT-BEZ	SVT-ASR	SVT-GLY	SVT-SAC
Ibuprofen (IBP)	IBP-CTR	IBP-FUM	IBP-ASP	IBP-BEZ	IBP-ASR	IBP-GLY	IBP-SAC
Clopidogrel (CLP)	CLP-CTR	CLP-FUM	CLP-ASP	CLP-BEZ	CLP-ASR	CLP-GLY	CLP-SAC
Lamotrigine (LMT)	LMT-CTR	LMT-FUM	LMT-ASP	LMT-BEZ	LMT-ASR	LMT-GLY	LMT-SAC
Tadalafila (TDF)	TDF-CTR	TDF-FUM	TDF-ASP	TDF-BEZ	TDF-ASR	TDF-GLY	TDF-SAC
Ezetimiba (EZT)	EZT-CTR	EZT-FUM	EZT-ASP	EZT-BEZ	EZT-ASR	EZT-GLY	EZT-SAC
Carbamazephina (CBZ)	CBZ-CTR	CBZ-FUM	CBZ-ASP	CBZ-BEZ	CBZ-ASR	CBZ-GLY	CBZ-SAC
Nicotinamida (NCT)	NCT-CTR	NCT-FUM	NCT-ASP	NCT-BEZ	NCT-ASR	NCT-GLY	NCT-SAC
Fluconazole (FLZ)	FLZ-CTR	FLZ-FUM	FLZ-ASP	FLZ-BEZ	FLZ-ASR	FLZ-GLY	FLZ-SAC

Solvent used for screening experiment; Acetonitrile, methanol and water. The solvent and components were heated and left to evaporate at room conditions

solvents. The product obtained through the screening experiments was characterised firstly using the Raman spectroscopy which is a fas characterization technique in the identification for the possible cocrystal formation by spectra comparison. Finally, when a new crystal is observed, the screening method is repeated using large amount of samples of the API and coformer and further characterization studies will be performed to know the classes and other physicochemical properties of the new crystal.

However, from the first screening test and the results obtained from the Raman spectroscopy characterization, the combination showed to be promising for samples of FLZ:FUM mixed at a stoichiometric ratio of 1:1. By comparing the Raman spectra of the less soluble FLZ and the pure FUM, the obvious differences in the spectra peak observed was taken as an evidence for the possible formation of a new crystalline structure as shown in (Fig 3.2). The presence of peaks from both coformer and API in the FLZ-FUM between 1600 and 1750 cm^{-1} can be related to a crystalline structure with both components.
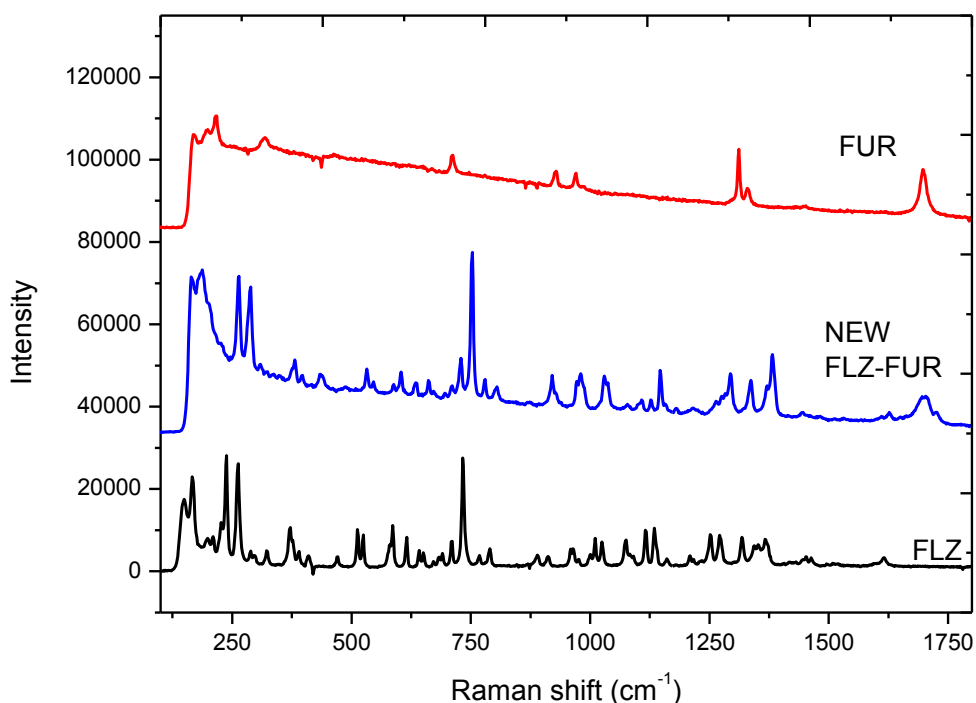
FIGURE 3.2 - Raman spectra comparison of FLZ, FUM and the new FLZ-FUM cocrystal for the first characterization process.

However, the differences which really distinguish the new FLZ-FUR from the starting materials were observed in the region between 800 -1400cm^{-1}. This is the first characterisation evidence from the Raman spectroscopy that confirm the changes in the chemical composition of the synthesized solid crystal.

In addition, the XRD analysis of the suspected 1:1 FLZ-FUM cocrystal solid formed was performed and compared to that of FLZ and FUM according to figure 3.3. The patterns were compared and peak positioning and intensity was observed and taken as more evidences for the formation of a new crystalline structure. It was observed that the polymorphic form of FLZ used in the experiments is the form II, compared to the reported powder diffractions of polymorphic forms in figure 1.9.
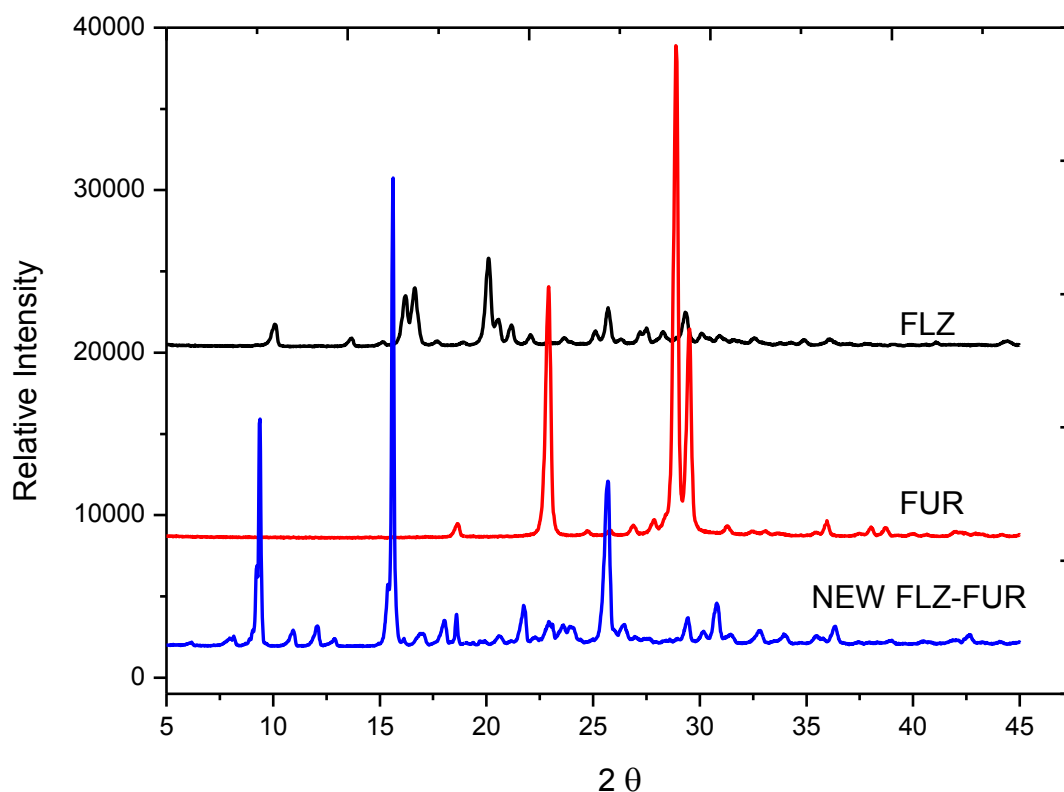
FIGURE 3.3 – Experimental PXRD patterns of the new FLZ-FUM solid form compared to that of FLZ and FUM.

CHAPTER 4 – RESULTS AND DISCUSSION

4. Results

4.1 Synthesis and characterization of FLZ-FUM cocrystals

In this confirmatory experiment, five samples of FLZ-FUM cocrystals were synthesised through the promising 1:1 stoichiometric mixing ratio at different conditions and methods as shown in the table 4.1. Using simple solvent based cocrystallization techniques, the characterization of the dry crystal obtained was achieved by comparing the Raman spectra, diffraction patterns and thermograms curves of the crystal samples to that of the starting materials. In this experiment, efforts were made to find the most pure means of synthesizing the purest form of FLZ: FUM at 1:1 stoichiometric ratio by considering the five samples and the results obtained gave some similarities and differences in terms of purity when analysed.

TABLE 4.1 – Screening experiments conditions for FLZ-FUM prepared through solvent evaporation methods.

Name	API (Amount)	Coformer (Amount)	Solvent	Method of preparation
Am 0	FLZ 0.1mmol	FUM 0.1mmol	Boiling ACN-H_2O (1:1) (4mL)	Solvent evaporation
Am 1	FLZ 0.05mmol	FUM 0.05mmol	Boiling H_2O (2mL)	Solvent evaporation
Am 2	FLZ 1mmol	FUM 1mmol	Boiling ACN-H_2O (1:1) (2mL)	Solvent evaporation
Am 3	FLZ 0.1mmol	FUM 0.1mmol	Boiling ACN-H_2O (1:1) (2mL)	Solvent evaporation
Am 5	FLZ 0.05mmol	FUM 0.05mmol	ACN-H_2O (1:1) (5mL)	Slow crystallisation

The sample Am 4 was performed using boiling ethanol as reported in the publication for the synthesis of 2FLZ-1FUM cocrystal. The results obtained from the characterization studies, considering the Raman spectra and the XPRD pattern analysis of the synthesized crystal gave a similar result to that of the publication but with some little differences in peak positioning and was excluded from the Table 4.1. The powder XRD patterns of previously reported polymorphs of FLZ in the Cambridge Crystallographic Structure Database (CCSD) were used for the characterization in this experiment.

Thus, we bring to mind that in this experiment, the fluconazole and fumaric acid were dissolved in either boiling ACN-H_2O (2:1), ACN-H_2O (1:1) or boiling H_2O with the API and the coformer totally dissolved and resulting into a clear solution at 1:1 stoichiometric ratio. After, the solution was then left to slowly cool off at room temperature and crystals were obtained in water after 24-48 hours. The little water remaining alongside with some samples was filtered off and the crystals obtained were dried at a room temperature. The dry crystals obtained were then used for the further characterisation experiment

Considering the first characterisation study performed using Raman spectroscopy, the full spectrum obtained for the samples as shown in (Fig.4.1 A) gave some similarities with one another. However, by focusing on some selected regions of spectra around 370 - 400cm^{-1}, region between 800 cm^{-1} - 1400 cm^{-1} and 1350 -1450 cm^{-1}, some obvious differences in peak positioning and intensity in the spectra of the five samples was observed.

The selection of the most pure sample and further characterization of the samples was carried out based on the differences in the Raman spectra and the diffractograms obtained from the X-ray diffractions analysis. The obtained XRD pattern of the pure crystals selected was compared with the previously reported patterns of FLZ polymorphs in the CSD. The structure determination was carried out using the single crystal XRD analysis and the data obtained was compared to the reported structures of the polymorphs of FLZ. All the analysis and result obtained were discussed below.

Raman spectra analysis

The Raman spectra of the synthesized crystalline solid of FLZ-FUM and the starting materials were taken and plotted with minor differences spotted when compared with one another and wit the starting materials (Figure 4.1A). However, in the figure 4.1(B), the Raman spectra of all the samples were analysed focusing on some spectral regions that gave clear differences between the spectra of the starting materials when compared to the synthesized crystalline solids around 890 cm^{-1} to 920 cm^{-1}, 960 cm^{-1}, 1050 cm^{-1}, 1250cm^{-1} and between 1260 to 1330 cm^{-1}, with peak presence or absence, peak intensity and peak width.

(A)
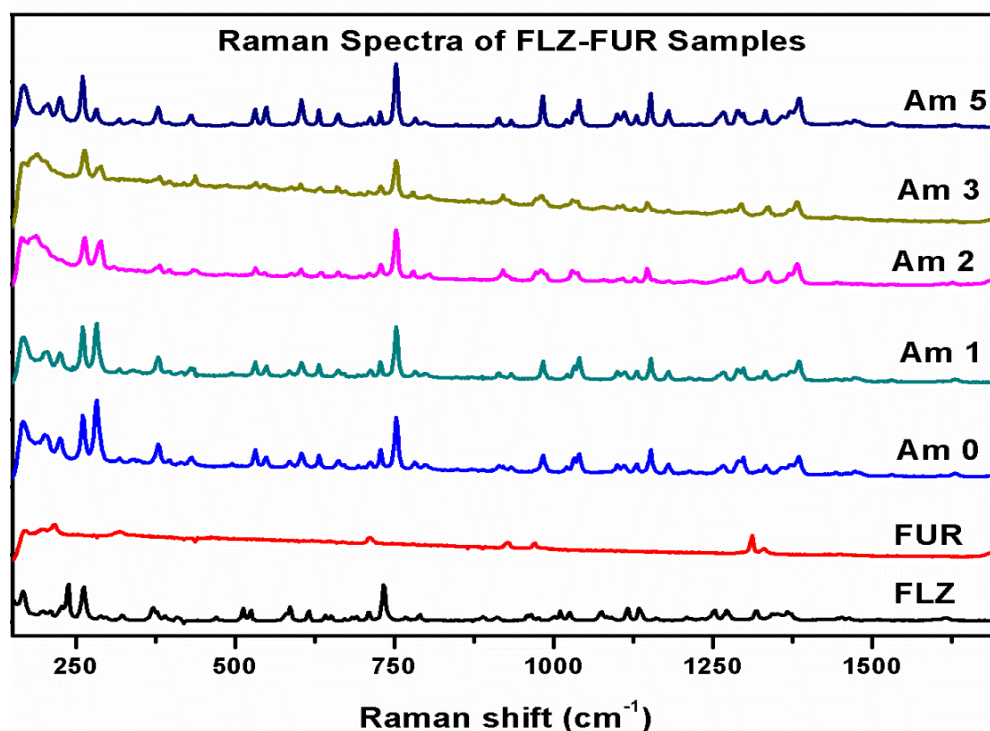
(B)
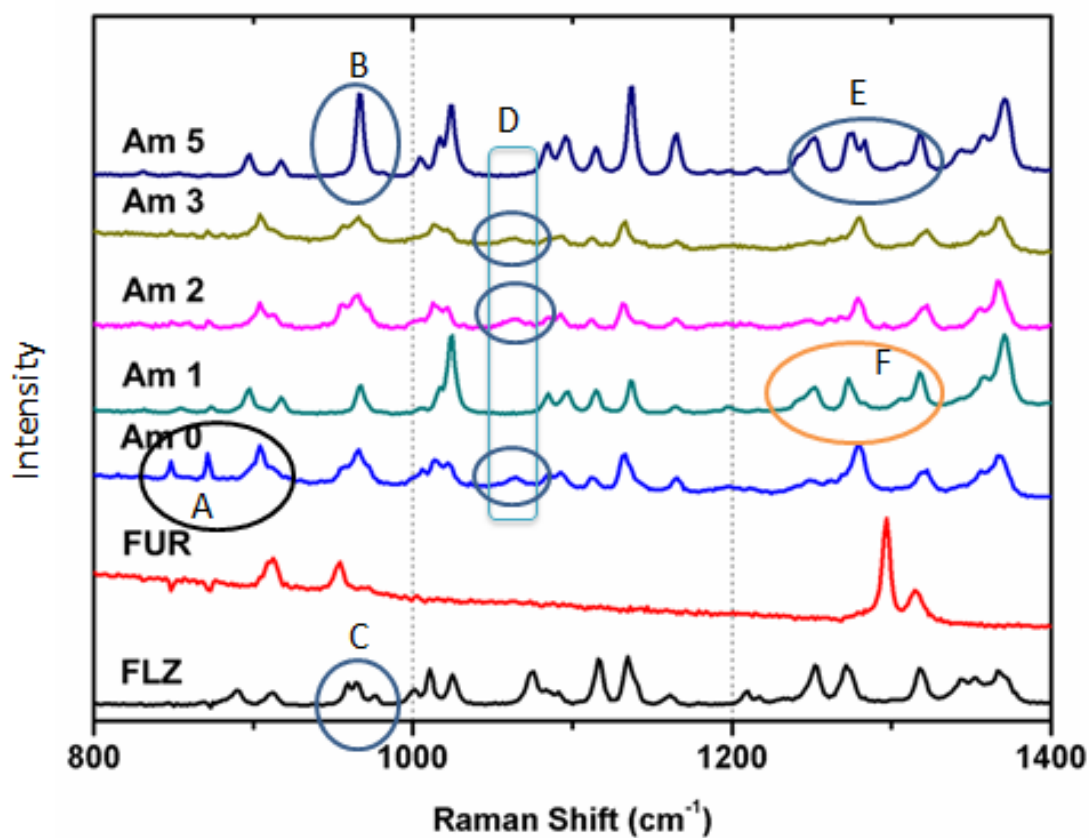
FIGURE 4.1 – (A) Raman spectra of the five samples compared to the starting materials (FLZ and FUM), from approximately 150 to 1700 cm^{-1}. (B) Raman spectra showing major differences in the spectra of the five samples when compared to the starting materials, from 800 to 1400 cm^{-1}.

The first region of interest is the point **A,** three obvious peaks on **Am 0** at 890-920cm^{-1}, with the third a broad peak at 920 cm^{-1}. These peaks are slightly shifted from other peaks observed in **Am 1**, **Am 5** and the starting materials. This peak is also presented in samples **Am 2** and **Am 3**, but with less intensity. Samples **Am 1** and **Am 5** is observed to present a spectral profile most similar to FLZ peaks, in this region.

The **Am 5** gave a unique sharp peak at point **B** at 970 cm^{-1}, which is a unique peak with a high intensity when compared to all other broad peaks observed at this region. Sample **Am 1**, also presents the same peak, but less intense. However, samples **Am 2** and **Am 3** presents mixed peaks that look more like FLZ peaks at this region **C**. Sample **Am 1** presents both signals, the sharp peak of **Am 5** and the mixed peaks from samples **Am 2** and **Am 3**, This might be an indicative that sample **Am 0** is a mixture of more than one crystal. Samples **Am 0, 2** and **3** gave nearly the same peak as shown by point **D at** 1050 cm^{-1}. The **Am 5** gave different peaks especially at point **E** (1250 -1320 cm $^{-1}$), but seems more like a mixture of a crystal formed in **Am 1** and samples **Am 2** and **Am 3**.

The **Am 0** spectrum looks unique and seems a bit like the **Am 3** and **Am 2** but with some little peak differences observed at **A**. The point **F** on **Am 1** looks more like the peak observed at point **E** on **Am 5,** with little peak differences observed for the latter and this is also a point that shows the differences between the samples and FLZ. Hence, **Am 2** and **Am 3** show some unique differences between each other when their spectra are compared. The broad peaks observed on FLZ at 990 -1010cm^{-1} is observed in **Am 2 and 3** with a low intense peak, and observed to be missing on **Am 1** or obviously replaced with an intense peak at 1020 cm^{-1}.

Raman spectroscopy served well as a characterization technique since it targets molecular vibrations, thus, specific chemical bonds and structures displaying characteristic Raman peaks. However, the spectral differences in these mention regions on the Raman spectra indicate that the major differences in this case was the chemical environment accompanied by differences in some molecular interactions, when compared to the starting materials

XRD pattern analysis
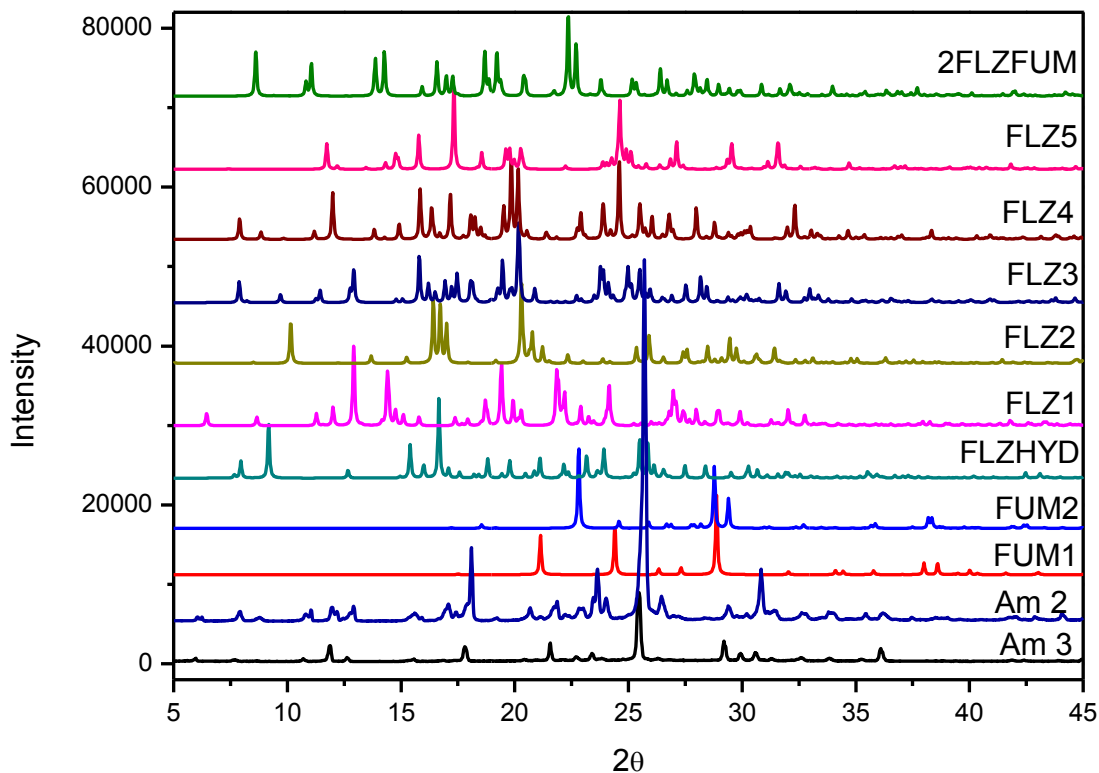
FIGURE 4.2. Calculated PXRD patterns of the new FLZ-FUR solid samples (Am2 and 3) compared to the diffraction patterns of reported FLZHYD, 2FLZ-FUR cocrystal and (FLZ and FUR polymorphs).

The PXRD patterns show obvious differences in diffraction patterns for the PXRD of each sample. The five new FLZ-FUM crystal samples gave different peaks when compared to the starting materials and the previously reported cocrystal, hydrate and polymorphs with a characteristic peaks at different points 2θ; 6.25^{o}, 7.65^{o}, 9.00^{o}, 11.00^{o}, 12.00^{o} and 13.70^{o} as shown in figure 4.2 to be common with **Am2** and **Am 3,** while **Am 0, Am 1** and **Am 5** gave peaks that looks alike.

However, it was observed that some unique peaks of the new FLZ-FUM solid crystals samples are either missing or shifted in their diffraction pattern position when compared to one another, thus indicating some differences in the structural arrangement and as a result of conformational changes. Thus, a few

of these new peaks observed in the new synthesized FLZ-FUM solid samples can however be traced to the initial FLZ crystalline phases at (2θ); 26.00^{o}, and look alike with one another with varying intensities at 2θ: 7.65^{o}, 9.00^{o}, 10.30^{o}, 11.00^{o}, 13.00^{o} and 26.00^{o} indicating other phases or mixtures of other phases.

To gain further insight into the purity and uniqueness of these crystalline solid crystal samples, attention was once again given to **Am 2** and **Am 3** that have similarity with peak positioning as expected, with the former showing some characteristic differences in peak shift, broadness and peak intensity when compared to the latter (Fig 4.3) and this can be due to the shape of the crystal, differences in the height of the crystal powder in the loader and other conformational changes and conditions that may result during the PXRD analysis.

In addition, the **Am 3** can be said to display high level of purity compared to **Am 2** taking into their PXRD account on peak patterns. **Am 3** gave unique sharp peaks which are characteristic of a pure crystal. While **Am 0** and **Am 1** showed low intensity peaks similar to that of **Am 2** and **Am 3** at 2θ; 6.00^{o}, 8.00^{o}, 10.50^{o}, 11.00^{o} and 13.00^{o} and interestingly with the presence of an intense peak located at (2θ) $8.00^{o} - 9.00^{o}$ with differences in positioning.
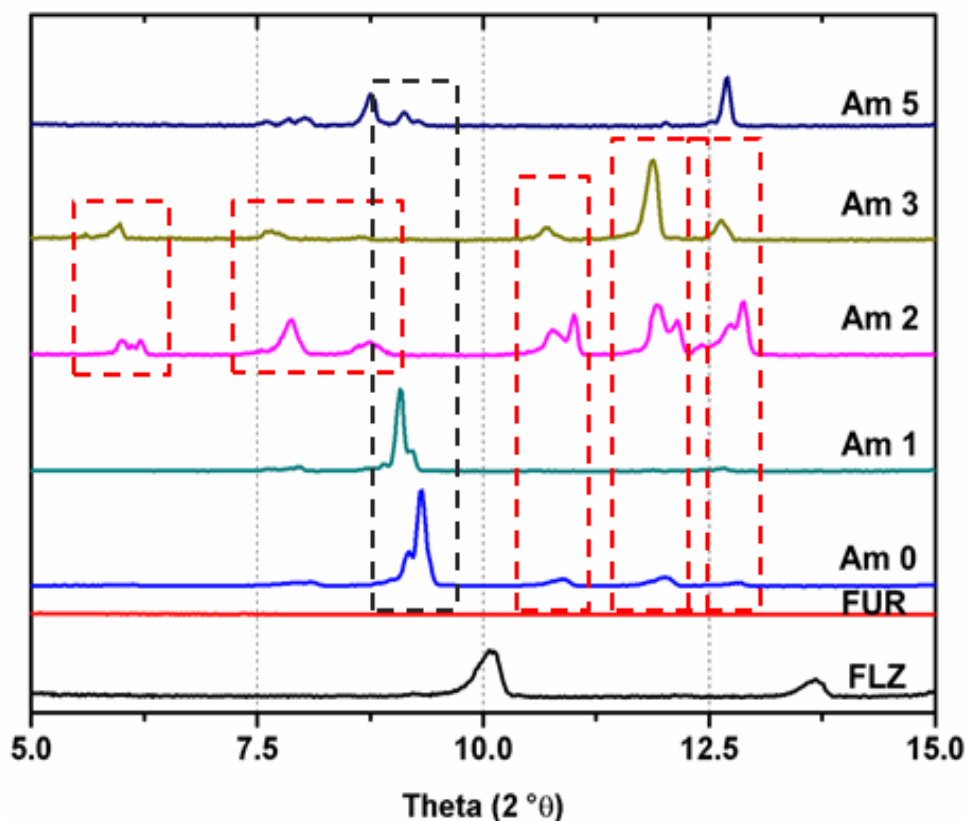
FIGURE 4.3 – A selected region of the XRD patterns showing clearly the comparisons of the products, FLZ and FUM.

As shown in Figure 4.3, **Am 5** have peaks similar in positioning with **Am 1** but quite different from FLZ PXRD pattern, thereby indicate the formation of a different crystalline phase. Thus, the results obtained indicate a high possibility of obtaining two novel solid forms of FLZ-FUM from the XRD analysis as said earlier while considering the results obtained from the Raman spectra characterization. The PXRD patterns observed for **Am 0**, **Am 2** and **Am 3** are different from all the patterns already observed for the polymorphs and hydrates of FLZ.

DSC thermal analysis

It is expected that the DSC thermal analysis of the samples will give more information about the purity and forms of the crystals. All the samples (**Am 0, 1, 2, 3 and 5**), gave a different thermal events compared to the peaks obtained for FLZ and FUM. All the crystal samples gave a characteristic broad peak between 75 ^{o}C and 125 ^{o}C with **Am 3** and **Am 1** presenting single peaks at 100 ^{o}C and 110 ^{o}C respectively (Fig 4.4).
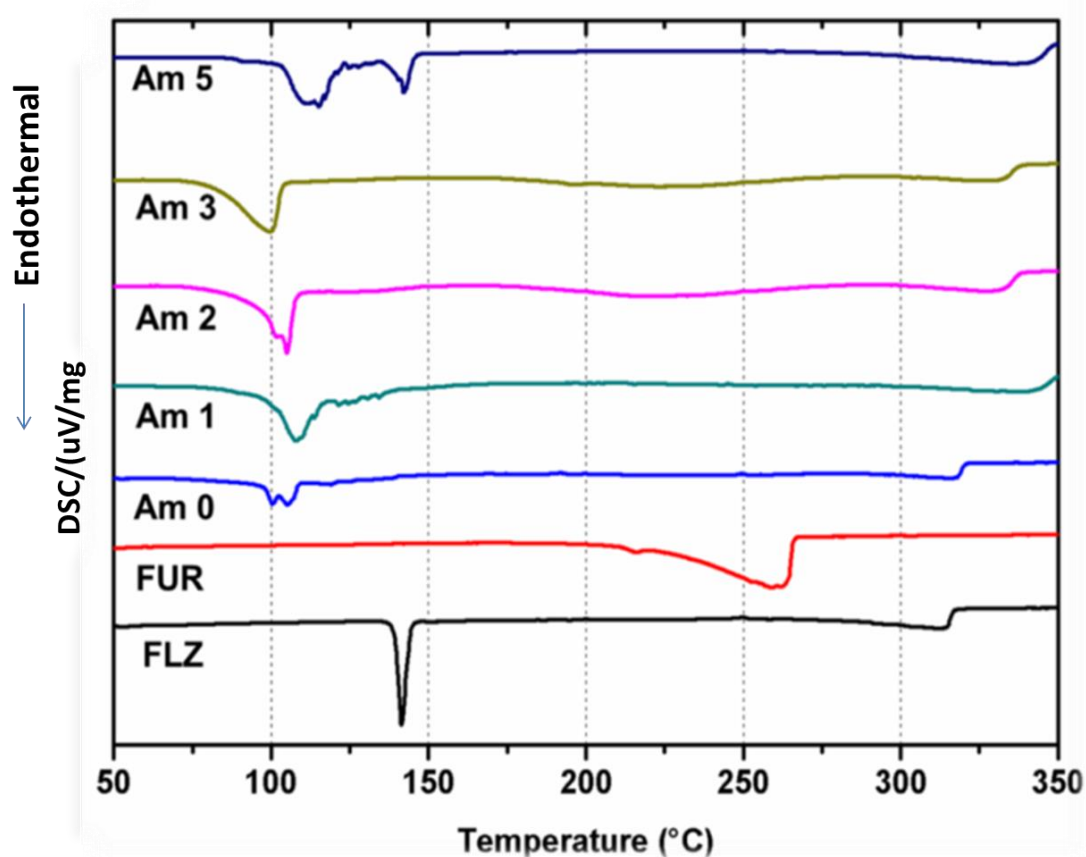
FIGURE 4.4 – DSC thermal peaks of samples showing different melting points when compared to FLZ and FUM.

Am 0 looks like a mixture of the crystal **Am 3** and **Am 1** with two closely observed peaks. **Am 5** gave two peaks, with the first, a broad peak between 110 - 120 ^{o} C and the seconds, having a characteristic peak of FLZ melting range (138 -140 ^{o} C). The possibility of obtaining two new solid forms of FLZ-FUM remain a certainty with the results obtained from **Am 1** and **Am 0, 2** and **3** in this experiment.

TGA curve analysis

The TG Analysis was employed to certify the nature of the five cocrystal and thereby confirming the class to which they can be classified (monohydrates, polyhydrates, solvates and so on). In this analysis, it was observed from the TG curves that all the FLZ-FUM samples showed a characteristic mass loss of approximately 6 - 7% of the total mass of the samples, which is possibly a water molecule, between the temperature range of 65 - 140 ^{o} C, while the curve of FLZ and FUM shows no such characteristic at this said temperature range (Fig 4.5).
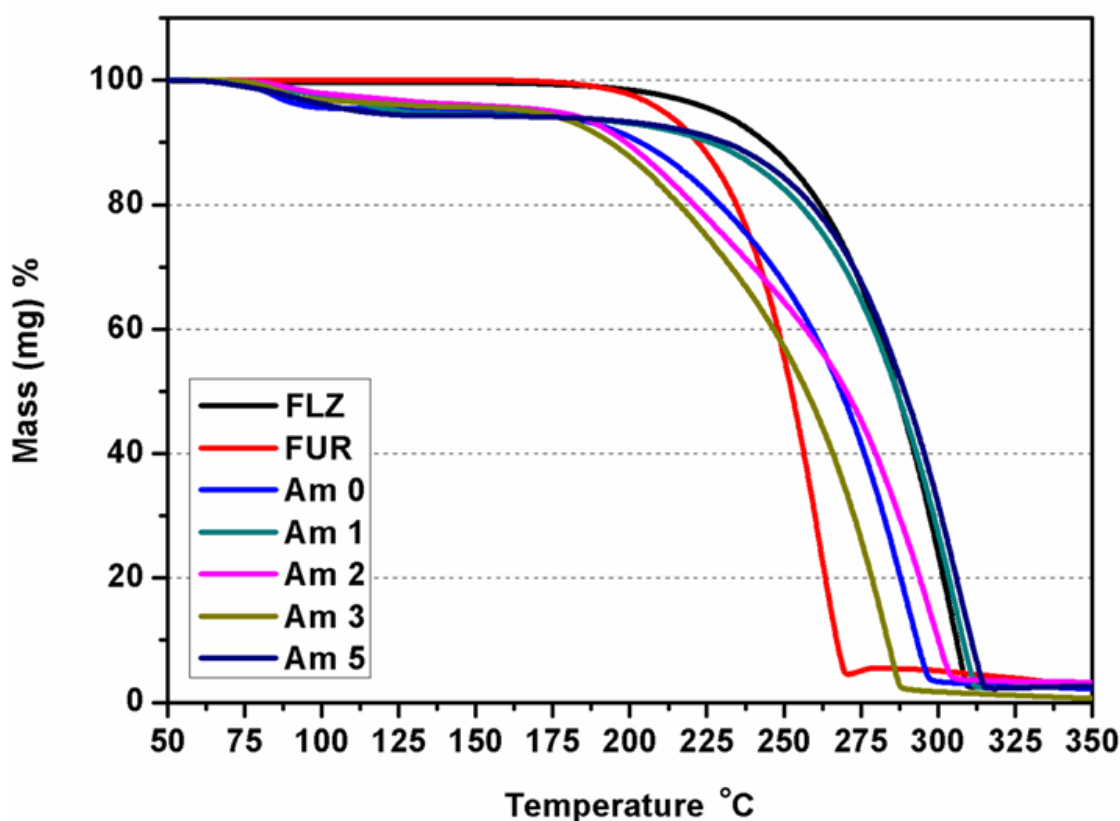
FIGURE 4.5 - TGA curves of the cocrystal samples compared to FLZ and FUM.

Apart from FLZ and FUM, all crystal samples started mass loss around 63 ^{o}C except for Am 2 and 3 that begin at 75 ^{o}C and gave similar curve. Am 0 and Am 5 show a gradual loss while Am 1 gave a unique steep curve showing two levels loss, which may be taken to be a loss of more than a molecule of water when compared to the other curve, with possible crystalline transition.
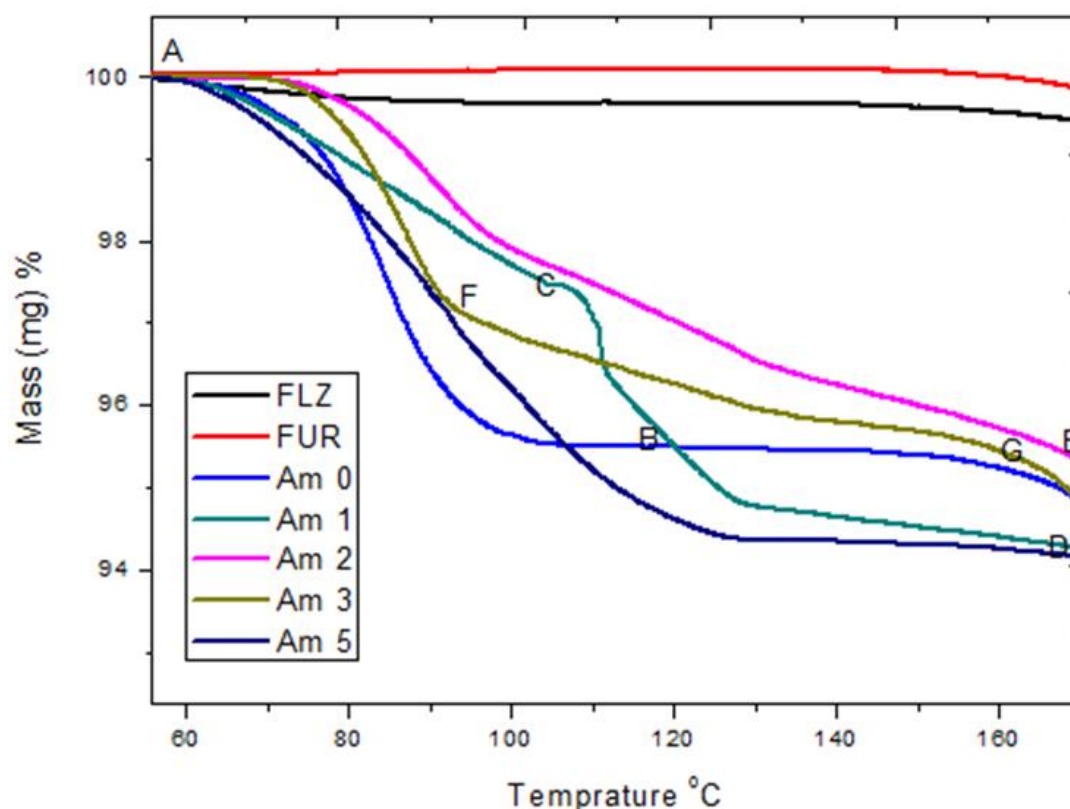
FIGURE 4.6 - TGA curve analysis to determine mass loss and ratio of anhydrous crystal to water.

The mole ratio calculations of the anhydrous crystal to the water loss were carried out according to table 4.2 and the ratio of the samples were obtained and compared. **Am 0, Am 2** and **Am 3** gave a **1:1** ratio of anhydrous to water while **Am 5** indicate the possibility of more than a mole of water with a ratio of **1:1.7. Am 0** lost 0.315mg which account for 4.5% of the total mass and in the range of 4.6%, which is the range which correlates to the loss of a single water molecule. The differences in the TGA curve of **Am 1** and **Am 3** remain uncertain due to the impurities and other factors like moisture in this sample which has altered the TGA curve.

TABLE 4.2 – TGA mass loss calculation and mole ratio of anhydrous to water.

	100% Mass of hydrate cocrystal	Mass of anhydrous	Mass of H_2O loss	Mole Ratio of anhydrous to water
Am 0	7.056mg	6.738mg	0.318mg	1:1
Am 1	10.42mg	**A – C** 10.15mg **C – D** 9.83mg	0.27mg 0.32mg	uncertain
Am 2	12.165mg	11.61mg	0.555mg	1:1
Am 3	5.485mg	**A - F** 5.326mg **F – G** 5.22mg	0.159mg 0.104mg	uncertain
Am 5	11.06mg	10.44mg	0.62mg	1: 1.7

Single Crystal XRD analysis

The structural resolution analysis of single crystal is generally considered the best way to characterize crystalline compounds, defining its absolute structure. In this work, it were performed Single Crystals XRD analyses for the crystals with good quality obtained in the experiments using FLZ and FUM. The best result was found for a crystal presented in the experiment **Am 0**, where it was found a new cocrystal hydrate FLZ-FUM- H_2O, which was not present in the CCDS.

The calculated PXRD pattern for the new FLZ-FUM-H_2O was compared with the experimental PXRD patterns earlier reported for **Am 2** and **Am 3** as presented in the Figure 4.7, which were considered very similar. The differences in peaks intensity due to the characteristics of either instrument, preferential orientation and crystal size are common issues which bring slight differences to the diffractgrams. Based on this, the observed condition strongly confirms the presence of a novel molecular structure.
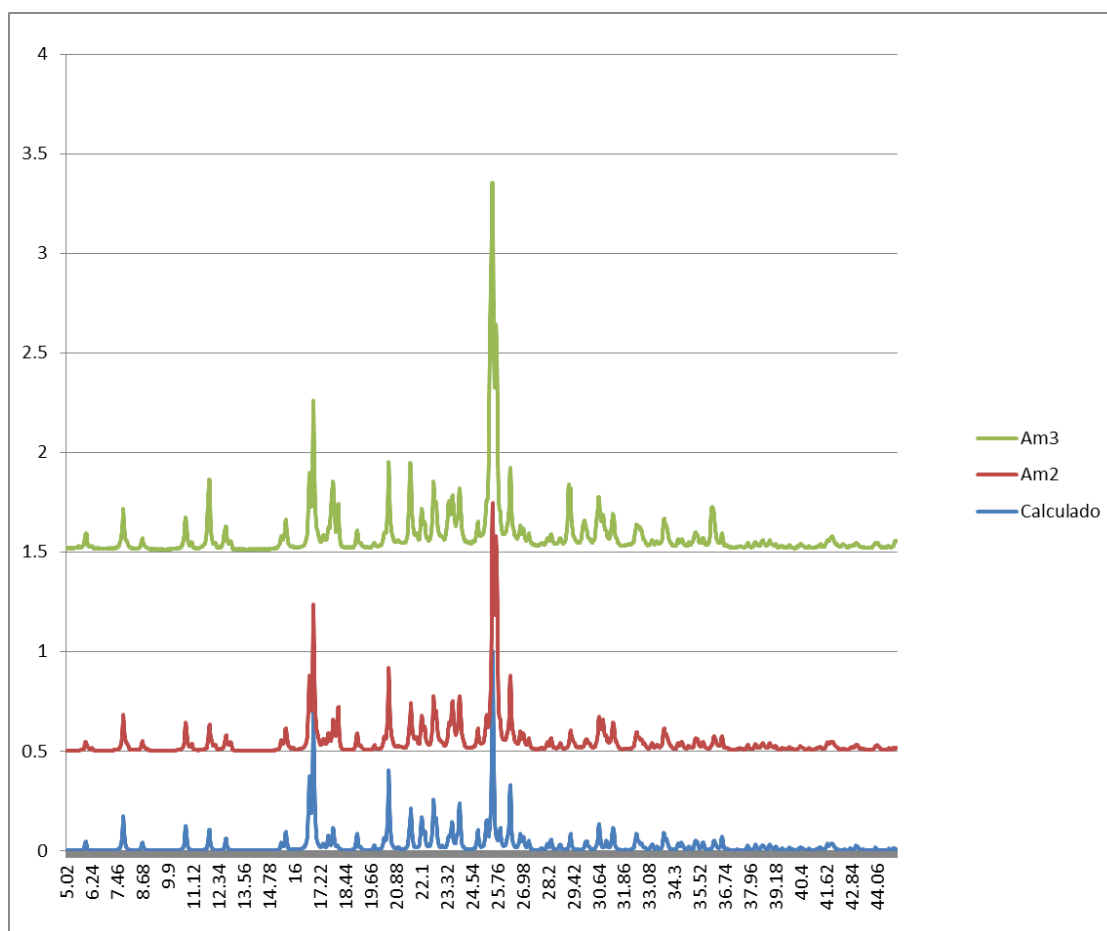
FIGURE 4.7 – Similarities between the calculated PXRD of the new FLZ-FUM monohydrate and the experimental PXRD of experiments Am 2 and Am 3.

The whole profile comparison between the calculated powder XRD and the experimental requires that the variables factors like the peak intensity, width, positions, shapes and background intensity distribution describing the aspect of the calculated patterns. The calculated XRD of FLZ-FUM-H_2O showed significant similarities and agree on the previously mentioned structure determination conditions with the experimental powder XRD patterns of **Am 2** and **Am 3**, as expected.

The single crystal structure determination clearly indicate that the molecule is a monohydrate cocrystal of FLZ-FUM-H_2O of a monoclinic P21/n

space group in which a molecule of water (H_2O) is attached to one of the triazole ring of FLZ and also form a hydrogen bond to a FUM molecule. There are four molecules observed in the asymmetric unit as reported in Table 4.3.

TABLE 4.3 – Cell parameters for the new FLZ-FUM-H2O monohydrate.

$C_{17}H_{18}F_2N_6O_6$	$P2_1/n$
a = 17.054(3) Å	α = 90°
b = 5.5995(10) Å	β = 105.418(4)°
c = 21.154(3) Å	γ = 90°
V = 1947.4(6) Å^3	R1 = 6.22%
Z = 4	Z' = 1

The FLZ, is attached to the fumaric acid molecule through a strong intermolecular O-H-----N hydrogen bond interaction (2.680 Å) as shown in the left side of Figure 4.8A. At the other side, the fluconazole is bonded to a water through a HO-H----N hydrogen bond (2.681Å), and this water molecule is bonded to a carbonyl group of a fumaric acid molecule through a H_2O---H-O-C hydrogen bond (2.618 Å). We can observe that these hydrogen bonds create a linear chains of "…FLZ --- H2O --- FUM --- FLZ --- H2O --- FUM…", which is clearly seen in Figure 4.8B. These chains are attached side by side by hydrogen bonds HO-H----O=C between the water molecule and the lateral carbonyl group of a fumaric acid (2.679 Å). Figure 4.8C shows that the 2D-tapes formed by hydrogen bonds (the Figure 4.8B represents a part of these 2D-tapes) are connected by a strong C-F----H-C bonds (2.383 Å), giving stability to the structure. The π staking interactions are not observed between the aromatic rings of fluconazole molecule.

(A
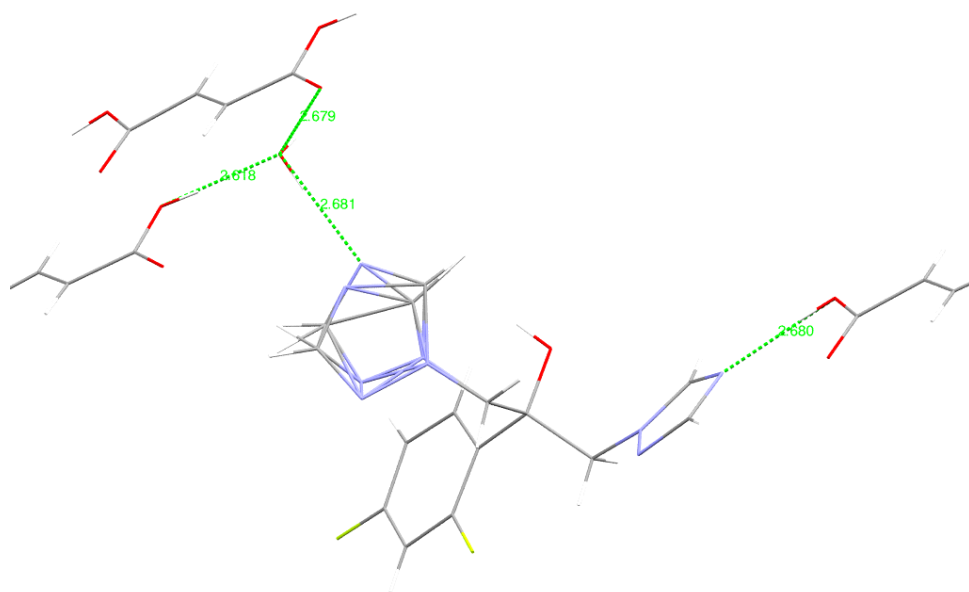
(B)
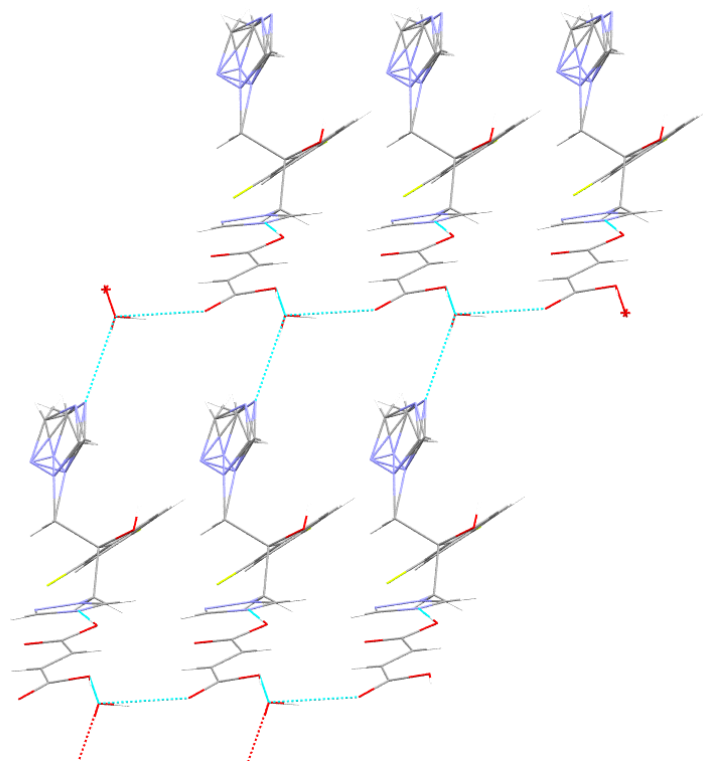
Figure 4.8 continues in the next page…

C)
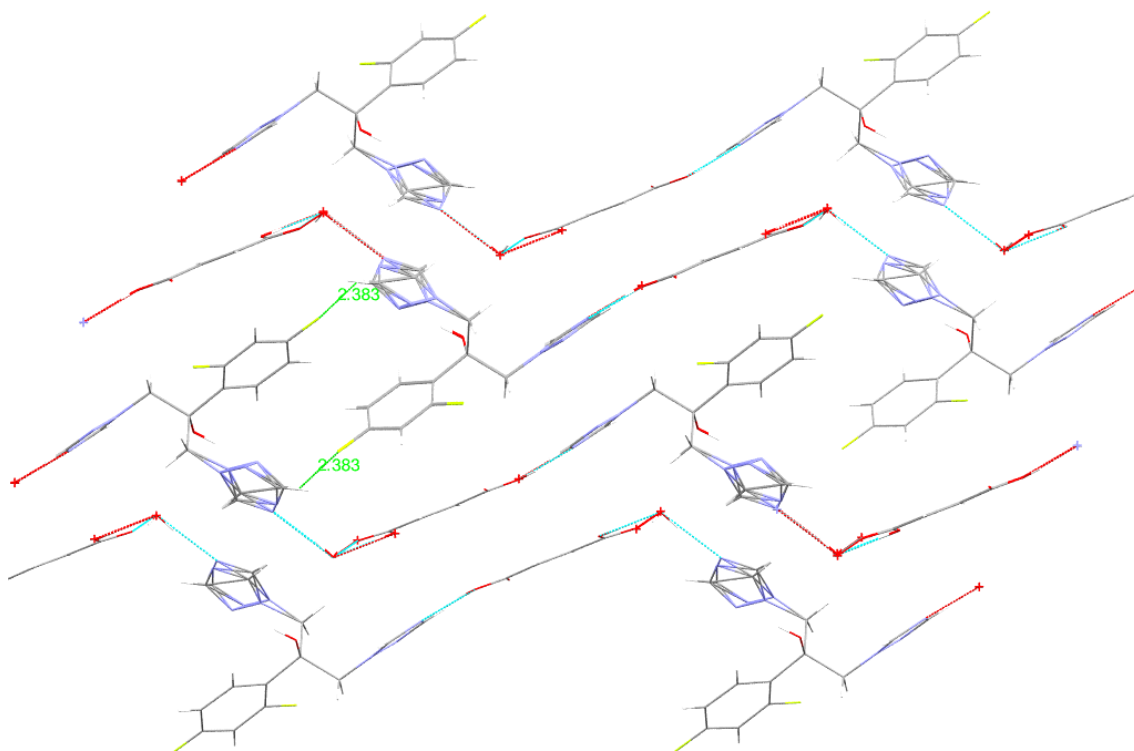
FIGURE 4.8 – (A) Distance between the main hydrogen bonds for the FLZ-FUM-H_2O; (B) Connections among the chains of FLZ-FUM-H_2O; (C) Connection among the 2D-Tapes formed by the hydrogen bonds.

The ANNEX I bring the structural information of the obtained single crystal FLZ-FUM-H_2O after the structure refining. ANNEX II presents the CIF/REPORT for the structure showing a good agreement between the proposed structure and the experimental data with a R1 = 6.22%.

CHAPTER 5 - CONCLUSIONS

5. Conclusions

Most active pharmaceutical ingredients are associated less favourable properties like low solubility, low permeability and instability. The aim of this research was justified through the synthesis of a new cocrystal solid form of fluconazole-fumaric acid monohydrate via crystal engineering technique. Thus, through a careful analysis of the samples using Raman spectroscopy as the starting characterization device, differences in the Raman spectra peaks comparison indicated a different intermolecular interaction (indicated by the shift in peak position and intensity.

The powder XRD analysis gave similar diffraction patterns for samples having similar condition of preparation. The diffractograms of the experiments were compared to the previously reported diffractograms for FLZ polymorphs, where obvious differences were observed. The experimental XRD patterns obtained for the most pure samples **Am 2** and **Am 3** was compared to the calculated XRD pattern of FLZ-FUM-H_2O, showing a high correlation in terms of peak positioning, intensity and width.

Further thermal analysis using the DSC and the TGA gave an insight on the level of purity and the class into which the samples belong. The TGA curve shows a stoichiometric loss of a mole of water according to the TGA curve calculations.

Finally, the single crystals structural analysis gave the ultimate conclusion about this new cocrystal structure. The unit cell parameters was obtained successfully with no other match found in the CSD, and it was observed to be a novel monohydrate FLZ:FUM:H_2O cocrystal with the H_2O molecule attached between the FLZ and FUM in a 1:1:1 molar ratio. This work is the first to report a monohydrate cocrystal structure of FLZ with a carboxylic acid (FUM).

.

CHAPTER 6 – FUTURE PERSPECTIVES

6. PERSPECTIVE

The search for a new crystalline molecular structure mostly pharmaceutical is considered tedious and reasonable devoted time and huge amount money is spent on both successful and fruitless search. Notwithstanding, such search must be a continuous venture, with the application of the knowledge of supramolecular chemistry, considering different crystal engineering techniques and a well monitored characterization process, the synthesis of new improved drug forms are possible from less active drugs via molecular interaction with selected coformer.

In crystallography, the SCXRD remains the ultimate means of characterizing crystalline samples and obtaining convincing atomic and molecular information about structural properties. Thus, the SCXRD of all observed crystal sample should be analysed to confirm the possibility of another unique molecular structure. The studies on solubility and bioavailability of the cocrystal produced should also be analysed and compared to previous known forms.

CHAPTER 7 - REFERENCES

7. REFERENCES

1. CALIARI, T. & RUIZ, R.M., "Brazilian pharmaceutical industry and generic drugs policy: Impacts on structure and innovation and recent developments". *Science and Public Policy*. **41**(2): 245, 2014.

2. BEYER, K.H., "What Pharmacology Is All About". *Pharmacologist*. **13**(2): 129, 1971.

3. LAURENCE, D., "What is pharmacology? A discussion". *Trends in Pharmacological Sciences*. **18**(5): 153, 1997.

4. ARENAS-GARCIA, J.I.; HERRERA-RUIZ, D.; MONDRAGON-VASQUEZ, K.; MORALES-ROJAS, H. & HOPFL, H., "Co-Crystals of Active Pharmaceutical Ingredients - Acetazolamide". *Cryst Growth Des*. **10**(8): 3732, 2010.

5. CHAN, H.C.S.; WOOLLAM, G.R.; WAGNER, T.; SCHMIDT, M.U. & LEWIS, R.A., "Can picolinamide be a promising cocrystal former?". *Crystengcomm*. **16**(21): 4365, 2014.

6. BLAGDEN, N.; COLESB, S.J. & BERRY, D.J., "Pharmaceutical co-crystals - are we there yet?". *Crystengcomm*. **16**(26): 5753, 2014.

7. SILLION, B., "Combinatory chemistry - New discipline or strategy for development?". *Actualite Chimique*, (9): 3, 2000.

8. BEERS, K.L.; DOUGLAS, J.F.; AMIS, E.J. & KARIM, A., "High throughput approach to crystallization in thin films of isotactic polystyrene.". *Abstr Pap Am Chem S*. **222**: U327, 2001.

9. MORISSETTE, S.L.; READ, M.J.; SOUKASENE, S.; TAUBER, M.K.; SCOPPETTUOLO, L.A.; APGAR, J.R.; GUZMAN, H.R.; SAUER, J.M.; COLLINS, D.S.; JADHAV, P.K.; ENGLER, T. & GARDNER, C.G., "High throughput crystallization of polymorphs and salts: Applications in early lead optimization.". *Abstr Pap Am Chem S*. **225**: U227, 2003.

10. WALTER, T.S.; DIPROSE, J.M.; MAYO, C.J.; SIEBOLD, C.; PICKFORD, M.G.; CARTER, L.; SUTTON, G.C.; BERROW, N.S.; BROWN, J.; BERRY, I.M.; STEWART-JONES, G.B.E.; GRIMES, J.M.; STAMMERS, D.K.; ESNOUF, R.M.; JONES, E.Y.; OWENS, R.J.; STUART, D.I. & HARLOS, K., "A procedure for setting up high-throughput nanolitre crystallization experiments. Crystallization workflow for initial screening, automated storage, imaging and optimization". *Acta Crystallographica Section D-Biological Crystallography*. **61**: 651, 2005.

11. CHEN, J.M.; WANG, Z.Z.; WU, C.B.; LI, S. & LU, T.B., "Crystal engineering approach to improve the solubility of mebendazole". *Crystengcomm*. **14**(19): 6221, 2012.

12. ZHANG, Y.Z.; CHE, E.X.; ZHANG, M.; SUN, B.X.; GAO, J.; HAN, J. & SONG, Y.L., "Increasing the dissolution rate and oral bioavailability of the poorly water-soluble drug valsartan using novel hierarchical porous carbon monoliths". *Int J Pharm*. **473**(1-2): 375, 2014.

13. QIAO, N.; LI, M.Z.; SCHLINDWEIN, W.; MALEK, N.; DAVIES, A. & TRAPPITT, G., "Pharmaceutical cocrystals: An overview". *Int J Pharm*. **419**(1-2): 1, 2011.

14. TEHLER, U.; FAGERBERG, J.H.; SVENSSON, R.; LARHED, M.; ARTURSSON, P. & BERGSTROM, C.A.S., "Optimizing Solubility and Permeability of a Biopharmaceutics Classification System (BCS) Class 4 Antibiotic Drug Using Lipophilic Fragments Disturbing the Crystal Lattice". *Journal of Medicinal Chemistry*. **56**(6): 2690, 2013.

15. BENET, L.Z., "The role of BCS (biopharmaceutics classification system) and BDDCS (biopharmaceutics drug disposition classification system) in drug development". *Journal of pharmaceutical sciences*. **102**(1): 34, 2013.

16. SCHULTHEISS, N. & NEWMAN, A., "Pharmaceutical Cocrystals and Their Physicochemical Properties". *Cryst Growth Des*. **9**(6): 2950, 2009.

17. "Crystal engineering". *Chemical & Engineering News*. **79**(49): 35, 2001.

18. "Crystal engineering networks". *Physical Chemistry Chemical Physics*. **6**(21): C88, 2004.

19. ADALDER, T.K. & DASTIDAR, P., "Crystal Engineering Approach toward Selective Formation of an Asymmetric Supramolecular Synthon in Primary Ammonium Monocarboxylate (PAM) Salts and Their Gelation Studies". *Cryst Growth Des*. **14**(5): 2254, 2014.

20. CHILDS, S.L.; CHYALL, L.J.; DUNLAP, J.T.; SMOLENSKAYA, V.N.; STAHLY, B.C. & STAHLY, G.P., "Crystal engineering approach to forming cocrystals of amine hydrochlorides with organic acids. Molecular complexes of fluoxetine hydrochloride with benzoic, succinic, and fumaric acids". *J Am Chem Soc*. **126**(41): 13335, 2004.

21. VISHWESHWAR, P.; MCMAHON, J.A.; BIS, J.A. & ZAWOROTKO, M.J., "Pharmaceutical co-crystals". *Journal of pharmaceutical sciences*. **95**(3): 499, 2006.

22. TRASK, A.V., "An overview of pharmaceutical cocrystals as intellectual property". *Mol Pharmaceut*. **4**(3): 301, 2007.

23. STEED, J.W., "The role of co-crystals in pharmaceutical design". *Trends Pharmacol Sci*. **34**(3): 185, 2013.

24. MASTALERZ, M., "CRYSTAL ENGINEERING Covalent crystal growth". *Nature Chemistry*. **5**(10): 810, 2013.

25. TIEKINK, E.R.T., "Adventures in crystal engineering". *Acta Chimica Slovenica*. **50**(2): 343, 2003.

26. SHAH, V.P. & AMIDON, G.L., "GL Amidon, H. Lennernas, VP Shah, and JR Crison. A Theoretical Basis for a Biopharmaceutic Drug Classification: The Correlation of In Vitro Drug Product Dissolution and In Vivo Bioavailability, Pharm Res 12, 413-420, 1995-Backstory of BCS". *Aaps J*. **16**(5): 894, 2014.

27. BERGSTROM, C.A.S.; ANDERSSON, S.B.E.; FAGERBERG, J.H.; RAGNARSSON, G. & LINDAHL, A., "Is the full potential of the biopharmaceutics classification system reached?". *Eur J Pharm Sci*. **57**: 224, 2014.

28. LENNERNAS, H.; ABRAHAMSSON, B.; PERSSON, E.M. & KNUTSON, L., "Oral drug absorption and the biopharmaceutics classification system". *J Drug Deliv Sci Tec*. **17**(4): 237, 2007.

29. JUNG, S.J.; CHUNG, M.W.; URN, S.Y. & OH, H.Y., "Drug evaluation by biopharmaceutics classification system". *Drug Metab Rev*. **38**: 156, 2006.

30. HERRMANN, M.; FORTER-BARTH, U.; KROBER, H.; KEMPA, P.B.; JUEZ-LORENZO, M.D. & DOYLE, S., "Co-Crystallization and Characterization of Pharmaceutical Ingredients". *Part Part Syst Char*. **26**(3): 151, 2009.

31. KREITNER, R., "Shelf Life". *Nation*. **299**(21): 37, 2014.

32. CHEN, C.H.; YANG, J.C.; UANG, Y.S. & LIN, C.J., "Improved dissolution rate and oral bioavailability of lovastatin in red yeast rice products". *Int J Pharm*. **444**(1-2): 18, 2013.

33. MUTALIK, S.; ANJU, P.; MANJ, K. & USHA, A.N., "Enhancement of dissolution rate and bioavailability of aceclofenac: A chitosan-based solvent change approach". *Int J Pharm*. **350**(1-2): 279, 2008.

34. PANDEY, A.; RATH, B. & DWIVEDI, A.K., "Enhancement of dissolution rate and bioavailability of Paliperidone by Hot Melt Extrusion technique". *J Sci Ind Res India*. **73**(10): 680, 2014.

35. WANG, P.X.; LUO, Q.; MIAO, Y.Q.; YING, L.; HE, H.B.; CAI, C.F. & TANG, X., "Improved dissolution rate and bioavailability of fenofibrate pellets prepared by wet-milled-drug layering". *Drug Dev Ind Pharm*. **38**(11): 1344, 2012.

36. DUNITZ, J.D., "Crystal and co-crystal: a second opinion". *Crystengcomm*. **5**: 506, 2003.

37. ALKHAMIS, K.A.; OBAIDAT, A.A. & NUSEIRAT, A.F., "Solid-state characterization of fluconazole". *Pharm Dev Technol*. **7**(4): 491, 2002.

38. GU, X.J. & JIANG, W., "Characterization of Polymorphic Forms of Fluconazole Using Fourier-Transform Raman-Spectroscopy". *Journal of pharmaceutical sciences*. **84**(12): 1438, 1995.

39. KARANAM, M.; DEV, S. & CHOUDHURY, A.R., "New Polymorphs of Fluconazole: Results from Cocrystallization Experiments". *Cryst Growth Des*. **12**(1): 240, 2012.

40. KASTELIC, J.; HODNIK, Z.; SKET, P.; PLAVEE, J.; LAH, N.; LEBAN, I.; PAJK, M.; PLANINSEK, O. & KIKELJ, D., "Fluconazole Cocrystals with Dicarboxylic Acids". *Cryst Growth Des*. **10**(11): 4943, 2010.

41. OBAIDAT, R.M.; ALKHAMIS, K.A. & SALEM, M.S., "Determination of factors affecting kinetics of solid-state transformation of fluconazole polymorph II to polymorph I using diffuse reflectance Fourier transform spectroscopy". *Drug Dev Ind Pharm*. **36**(5): 570, 2010.

42. PARK, H.J.; KIM, M.S.; KIM, J.S.; CHO, W.; PARK, J.; CHA, K.H.; KANG, Y.S. & HWANG, S.J., "Solid-State Carbon NMR Characterization and Investigation of Intrinsic Dissolution Behavior of Fluconazole Polymorphs, Anhydrate Forms I and II". *Chem Pharm Bull*. **58**(9): 1243, 2010.

43. PARK, H.J.; KIM, M.S.; LEE, S.; KIM, J.S.; WOO, J.S.; PARK, J.S. & HWANG, S.J., "Recrystallization of fluconazole using the supercritical antisolvent (SAS) process". *Int J Pharm*. **328**(2): 152, 2007.

44. THAKUR, A.; KUMAR, D.; THIPPARABOINA, R. & SHASTRI, N.R., "Exploration of crystal simulation potential by fluconazole isomorphism and its application in improvement of pharmaceutical properties". *J Cryst Growth*. **406**: 18, 2014.

45. BETTINETTI, G.; SORRENTI, M.; CATENACCI, L.; FERRARI, F. & ROSSI, S., "Polymorphism, pseudopolymorphism, and amorphism of peracetylated alpha-, beta-, and gamma-cyclodextrins". *J Pharmaceut Biomed*. **41**(4): 1205, 2006.

46. SCHMIDT, A.C.; SCHWARZ, I. & MEREITER, K., "Polymorphism and pseudopolymorphism of salicaine and salicaine hydrochloride crystal polymorphism of local anaesthetic drugs, part V". *Journal of pharmaceutical sciences*. **95**(5): 1097, 2006.

47. SUITCHMEZIAN, V.; JESS, I. & NATHER, C., "Investigations on the polymorphism and pseudopolymorphism of the glucocorticoid triamcinolone: New findings for a well-known drug". *Cryst Growth Des*. **7**(1): 69, 2007.

48. AITIPAMULA, S.; CHOW, P.S. & TAN, R.B.H., "Polymorphs and Solvates of a Cocrystal Involving an Analgesic Drug, Ethenzamide, and 3,5-Dinitrobenzoic Acid". *Cryst Growth Des*. **10**(5): 2229, 2010.

49. AITIPAMULA, S.; CHOW, P.S. & TAN, R.B.H., "Solvates and a monohydrate of N-4-acetylsulfamerazine: Structural, thermochemical, and computational analysis". *J Mol Struct*. **1005**(1-3): 134, 2011.

50. AITIPAMULA, S.; CHOW, P.S. & TAN, R.B.H., "Solvates and polymorphic phase transformations of 2-chloro-4-nitrobenzoic acid". *Crystengcomm*. **13**(3): 1037, 2011.

51. AITIPAMULA, S.; CHOW, P.S. & TAN, R.B.H., "Solvates of the antifungal drug griseofulvin: structural, thermochemical and conformational analysis". *Acta Crystallogr B*. **70**: 54, 2014.

52. AITIPAMULA, S.; VANGALA, V.R.; CHOW, P.S. & TAN, R.B.H., "Cocrystal Hydrate of an Antifungal Drug, Griseofulvin, with Promising Physicochemical Properties". *Cryst Growth Des*. **12**(12): 5858, 2012.

53. CLARKE, H.D.; ARORA, K.K.; BASS, H.; KAVURU, P.; ONG, T.T.; PUJARI, T.; WOJTAS, L. & ZAWOROTKO, M.J., "Structure-Stability Relationships in Cocrystal Hydrates: Does the Promiscuity of Water Make Crystalline Hydrates the Nemesis of Crystal Engineering?". *Cryst Growth Des*. **10**(5): 2152, 2010.

54. CLARKE, H.D.; ARORA, K.K.; WOJTAS, L. & ZAWOROTKO, M.J., "Polymorphism in Multiple Component Crystals: Forms III and IV of Gallic Acid Monohydrate". *Cryst Growth Des*. **11**(4): 964, 2011.

55. GOUD, N.R.; KHAN, R.A. & NANGIA, A., "Modulating the solubility of sulfacetamide by means of cocrystals". *Crystengcomm*. **16**(26): 5859, 2014.

56. JONES, W.; MOTHERWELL, S. & TRASK, A.V., "Pharmaceutical cocrystals: An emerging approach to physical property enhancement". *Mrs Bull*. **31**(11): 875, 2006.

57. VANGALA, V.R.; CHOW, P.S. & TAN, R.B.H., "Co-Crystals and Co-Crystal Hydrates of the Antibiotic Nitrofurantoin: Structural Studies and Physicochemical Properties". *Cryst Growth Des*. **12**(12): 5925, 2012.

58. JACOBS, A. & NOA, F.M.A., "Co-crystals and co-crystal hydrates of vanillic acid". *Crystengcomm*. **17**(1): 98, 2015.

59. HENNINGS, E.; SCHMIDT, H. & VOIGT, W., "Crystal structures of hydrates of simple inorganic salts. II. Water-rich calcium bromide and iodide hydrates: CaBr2 center dot 9H(2)O, Cal(2)center dot 8H(2)O, Cal(2)center dot 7H(2)O and Cal(2)center dot 6.5H(2)O". *Acta Crystallogr C*. **70**: 876, 2014.

60. MADUSANKA, N.; EDDLESTON, M.D.; ARHANGELSKIS, M. & JONES, W., "Polymorphs, hydrates and solvates of a co-crystal of caffeine with anthranilic acid". *Acta Crystallogr B*. **70**: 72, 2014.

61. SUPONITSKY, K.Y.; LYSSENKO, K.A.; ANANYEV, I.V.; KOZEEV, A.M. & SHEREMETEV, A.B., "Role of Weak Intermolecular Interactions in the Crystal Structure of Tetrakis-furazano[3,4-c:3 ',4 '-g:3 '',4 ''-k:3 ''', 4 '''-o][1,2,5,6,9,10,13,14]octaazacyclohexadecine and Its Solvates". *Cryst Growth Des*. **14**(9): 4439, 2014.

62. DALE, S.H.; ELSEGOOD, M.R.J & COOMBS, A.E.L., "Hydrogen bond directed supramolecular arrays utilising hemimellitic acid: Solvent inclusion clathrates". *Crystengcomm*. **6**: 328, 2004.

63. DALE, S.H.; ELSEGOOD, M.R.J. & REDSHAW, C., "Polymorphism and pseudopolymorphism in calixarenes: acetonitrile clathrates of p-Bu-t-calix[n]arenes (n = 6 and 8)". *Crystengcomm*. **5**: 368, 2003.

64. KIRSANOVA, M.A. & SHEVELKOV, A.V., "Clathrates and semiclathrates of Type-I: crystal structure and superstructures". *Z Kristallogr*. **228**(5): 215, 2013.

65. NANGIA, A., "Pseudopolymorph: Retain this widely accepted term". *Cryst Growth Des*. **6**(1): 2, 2006.

66. BOLTE, M.; BRUSKO, V. & BOHMER, V., "A new pseudopolymorph of 5,11,17,23,29,35,41,47-octabromo-49,50,51,52,53,54,55,56-octamethoxycalix[8]arene". *Acta Crystallogr E*. **59**: O1691, 2003.

67. PROKOFIEV, A.V.; DAHLMANN, E.; RITTER, F.; ASSMUS, W.; MARGRAF, G. & WAGNER, M., "Crystal growth of a new pseudopolymorph modification of the polymer compound [CuC12H8N4O2](n)". *Cryst Res Technol*. **39**(11): 1014, 2004.

68. KATAGIRI, K.; KATO, T.; MASU, H.; TOMINAGA, M. & AZUMAYA, I., "Pseudopolymorph and Infinite Hydrogen Bonding Network of Cyclic Oligomers of m-Aminobenzenesulfonic Acid". *Cryst Growth Des*. **9**(3): 1519, 2009.

69. DYSON, P.J.; STEED, J.W. & SUMAN, P., "Reproducible growth of a neutral inorganic co-crystal: Pd{PPh2(C16H15)}(2)Cl-2 center dot[Pd{PPh2(C16H15)}Cl-2](2)center dot solvate (solvate = CH2Cl2 or Et2O)". *Crystengcomm*, (2) 1999.

70. HAN, L.J. & KONG, Y.J., "Pentafluorobenzoato-dimolybdenum(II) Solvate and Co-crystal Complexes with Benzene and Naphthalin". *Z Anorg Allg Chem*. **640**(10): 2007, 2014.

71. AAKEROY, C.B.; COOKE, T.I. & NIEUWENHUYZEN, M., "The crystal structure of the molecular cocrystal L-malic acid L-tartaric acid (1/1)". *Supramol Chem*. **7**(2): 153, 1996.

72. ARMAN, H.D.; KAULGUD, T.; MILLER, T.; POPLAUKHIN, P. & TIEKINK, E.R.T., "Crystal and Molecular Structures of the 2:1 Cocrystal of 4-Nitrophenylacetic acid and N,N '-bis(pyridin-3-ylmethyl)oxalamide, and with the Thioxalamide Analogue". *J Chem Crystallogr*. **42**(7): 673, 2012.

73. DESIRAJU, G.R., "Crystal and co-crystal". *Crystengcomm*. **5**: 466, 2003.

74. VISHWESHWAR, P.; MCMAHON, J.A.; PETERSON, M.L.; HICKEY, M.B.; SHATTOCK, T.R. & ZAWOROTKO, M.J., "Crystal engineering of pharmaceutical co-crystals from polymorphic active pharmaceutical ingredients". *Chem Commun (Camb)*, (36): 4601, 2005.

75. SIMAO, C.; MAS-TORRENT, M.; ANDRE, V.; DUARTE, M.T.; TECHERT, S.; VECIANA, J. & ROVIRA, C., "Solid state photodimerisation of tetrathiafulvalene derivatives bearing carboxylate and carboxylic acid substituents". *Crystengcomm*. **15**(46): 9878, 2013.

76. LEHN, J.M., "Supermolecular chemistry (Reprinted)". *Recherche*, (331): 74, 2000.

77. DESIRAJU, G.R., "Designer crystals: intermolecular interactions, network structures and supramolecular synthons". *Chem Commun*, (16): 1475, 1997.

78. DISKIN-POSNER, Y.; DAHAL, S. & GOLDBERG, I., "New effective synthons for supramolecular self-assembly of meso-carboxyphenylporphyrins". *Chem Commun*, (7): 585, 2000.

79. KONER, R. & GOLDBERG, I., "Probing the supramolecular interaction synthons of 1-benzofuran-2,3-dicarboxylic acid in its monoanionic form". *Acta Crystallogr C*. **65**: M37, 2009.

80. VISHWESHWAR, P.; THAIMATTAM, R.; JASKOLSKI, M. & DESIRAJU, G.R., "Supramolecular synthons based on N-H center dot center dot center dot N and C-H center dot center dot center dot O hydrogen bonds. Crystal engineering of a helical structure with 5,5-diethylbarbituric acid". *Chem Commun*, (17): 1830, 2002.

81. DESIRAJU, G.R., "Supramolecular Synthons in Crystal Engineering - a New Organic-Synthesis". *Angewandte Chemie-International Edition in English*. **34**(21): 2311, 1995.

82. REDDY, D.S.; OVCHINNIKOV, Y.E.; SHISHKIN, O.V.; STRUCHKOV, Y.T. & DESIRAJU, G.R., "Supramolecular synthons in crystal engineering .3. Solid state architecture and synthon robustness in some 2,3-dicyano-5,6-dichloro-1,4-dialkoxybenzenes". *J Am Chem Soc*. **118**(17): 4085, 1996.

83. REDDY, D.S.; CRAIG, D.C. & DESIRAJU, G.R., "Supramolecular synthons in crystal engineering .4. Structure simplification and synthon interchangeability in some organic diamondoid solids". *J Am Chem Soc*. **118**(17): 4090, 1996.

84. THALLADI, V.R.; GOUD, B.S.; HOY, V.J.; ALLEN, F.H.; HOWARD, J.A.K. & DESIRAJU, G.R., "Supramolecular synthons in crystal engineering. Structure simplification, synthon robustness and supramolecular retrosynthesis". *Chem Commun*, (3): 401, 1996.

85. DESIRAJU, G.R., "Weak hydrogen bonds: From crystal engineering to virtual screening". *Abstr Pap Am Chem S*. **233**: 151, 2007.

86. ALLEN, F.H.; MOTHERWELL, W.D.S.; RAITHBY, P.R.; SHIELDS, G.P. & TAYLOR, R., "Systematic analysis of the probabilities of formation of bimolecular hydrogen-bonded ring motifs in organic crystal structures". *New J Chem*. **23**(1): 25, 1999.

87. Steiner T. 2001. Competition of hydrogen-bonded acceptors for the strong carboxyl donors. Acta Crystallogr B57:103–106

88. Reddy LS, Nangia A, Lynch VM. 2004. Phenylperfluorophenyl synthon mediated cocrystallization of carboxylic acids and amides. Cryst Growth Des 4:89–94

89. Vishweshwar P, Nangia A, Lynch VM. 2002. Recurrence of carboxylic acid-pyridine supramolecular synthon in the crystal structures of some pyrazinecarboxylic acids. J Org Chem 67:556– 565.

90. Ermer O, Eling A. 1994. Molecular recognition among alcohols and amines: Super-tetrahedral crystal architectures of linear diphenol–diamine complexes and aminophenols. J Chem Soc Perkin Trans 2:925–944

91. Vishweshwar P, Nangia A, Lynch VM. 2003. Supramolecular synthons in phenol-isonicotinamide adducts. Cryst Eng Comm 5:164–168.

92. Papaefstathiou GS, MacGillivray LR. 2001. Discrete versus infinite molecular self-assembly: Control in crystalline hydrogen-bonded assemblies based on resorcinol. Org Lett 3:3835–3838.

93. AITIPAMULA, S.; WONG, A.B.H.; CHOW, P.S. & TAN, R.B.H., "Cocrystallization with flufenamic acid: comparison of physicochemical properties of two pharmaceutical cocrystals". *Crystengcomm*. **16**(26): 5793, 2014.

94. HOLAN, J.; RIDVAN, L.; BILLOT, P. & STEPANEK, F., "Design of co-crystallization processes with regard to particle size distribution". *Chem Eng Sci*. **128**: 36, 2015.

95. HONG, C.; XIE, Y.; YAO, Y.S.; LI, G.W.; YUAN, X.R. & SHEN, H.Y., "A Novel Strategy for Pharmaceutical Cocrystal Generation Without Knowledge of Stoichiometric Ratio: Myricetin Cocrystals and a Ternary Phase Diagram". *Pharm Res-Dordr*. **32**(1): 47, 2015.

96. RAGER, T. & HILFIKER, R., "Stability Domains of Multi-Component Crystals in Ternary Phase Diagrams". *Z Phys Chem*. **223**(7): 793, 2009.

97. YADAV, A.V.; SHETE, A.S.; DABKE, A.P.; KULKARNI, P.V. & SAKHARE, S.S., "Co-crystals: a novel approach to modify physicochemical properties of active pharmaceutical ingredients". *Indian J Pharm Sci*. **71**(4): 359, 2009.

98. CROKER, D.M.; DAVEY, R.J.; RASMUSON, A.C. & SEATON, C.C., "Solution mediated phase transformations between co-crystals". *Crystengcomm*. **15**(11): 2044, 2013.

99. AITIPAMULA, S.; CHOW, P.S. & TAN, R.B.H., "Crystal Engineering of Tegafur Cocrystals: Structural Analysis and Physicochemical Properties". *Cryst Growth Des*. **14**(12): 6557, 2014.

100. KOJIMA, T.; TSUTSUMI, S.; YAMAMOTO, K.; IKEDA, Y. & MORIWAKI, T., "High-throughput cocrystal slurry screening by use of in situ Raman microscopy and multi-well plate". *Int J Pharm*. **399**(1-2): 52, 2010.

101. TAKATA, N.; SHIRAKI, K.; TAKANO, R.; HAYASHI, Y. & TERADA, K., "Cocrystal screening of stanolone and mestanolone using slurry crystallization". *Cryst Growth Des*. **8**(8): 3032, 2008.

102. ZHANG, S.; CHEN, H. & RASMUSON, A.C., "Thermodynamics and crystallization of a theophylline-salicylic acid cocrystal". *Crystengcomm*. **17**(22): 4125, 2015.

103. GAGNIERE, E.; MANGIN, D.; PUEL, F.; VALOUR, J.P.; KLEIN, J.P. & MONNIER, O., "Cocrystal formation in solution: Inducing phase transition by manipulating the amount of cocrystallizing agent". *J Cryst Growth*. **316**(1): 118, 2011.

104. GRECO, K. & BOGNER, R., "Solution-mediated phase transformation: Significance during dissolution and implications for bioavailability". *Journal of pharmaceutical sciences*. **101**(9): 2996, 2012.

105. LEYSSENS, T.; SPRINGUEL, G.; MONTIS, R.; CANDONI, N. & VEESLER, S., "Importance of Solvent Selection for Stoichiometrically Diverse Cocrystal Systems: Caffeine/Maleic Acid 1:1 and 2:1 Cocrystals". *Cryst Growth Des*. **12**(3): 1520, 2012.

106. MIROSHNYK, I.; MIRZA, S. & SANDLERT, N., "Pharmaceutical co-crystals-an opportunity for drug product enhancement". *Expert Opin Drug Del*. **6**(4): 333, 2009.

107. PATIL, S.P.; MODI, S.R. & BANSAL, A.K., "Generation of 1:1 Carbamazepine:Nicotinamide cocrystals by spray drying". *Eur J Pharm Sci*. **62**: 251, 2014.

108. FRISCIC, T.; CHILDS, S.L.; RIZVI, S.A.A. & JONES, W., "The role of solvent in mechanochemical and sonochemical cocrystal formation: a solubility-based approach for predicting cocrystallisation outcome". *Crystengcomm*. **11**(3): 418, 2009.

109. HAN, L.L.; LI, Z.H.; CHEN, J.S.; WANG, X.P. & SUN, D., "Solution and Mechanochemical Syntheses of Two Novel Cocrystals: Ligand Length Modulated Interpenetration of Hydrogen-Bonded 2D 6(3)-hcb Networks Based on a Robust Trimeric Heterosynthon". *Cryst Growth Des*. **14**(3): 1221, 2014.

110. GOYAL, S.; THORSON, M.R.; ZHANG, G.G.Z.; GONG, Y.C. & KENIS, P.J.A., "Microfluidic Approach to Cocrystal Screening of Pharmaceutical Parent Compounds". *Cryst Growth Des*. **12**(12): 6023, 2012.

111. ANTUNES, A.B.D.; DE GEEST, B.G.; VERVAET, C. & REMON, J.P., "Solvent-free drug crystal engineering for drug nano- and micro suspensions". *Eur J Pharm Sci*. **48**(1-2): 121, 2013.

112. MIRZAEI, M.; ESHTIAGH-HOSSEINI, H.; ALIPOUR, M. & FRONTERA, A., "Recent developments in the crystal engineering of diverse coordination modes (0-12) for Keggin-type polyoxometalates in hybrid inorganic-organic architectures". *Coordination Chemistry Reviews*. **275**: 1, 2014.

113. SANSAM, B.C.R.; ANDERSON, K.M. & STEED, J.W., "A simple strategy for crystal engineering water clusters". *Cryst Growth Des*. **7**(12): 2649, 2007.

114. THOMAS, N.W.; RAMDAS, S. & THOMAS, J.M., "A New Approach to the Crystal Engineering of Organic-Compounds - Application to a Solid-State Photoreactive System". *Proceedings of the Royal Society of London Series a-Mathematical and Physical Sciences*. **400**(1819): 219, 1985.

115. FRISCIC, T. & JONES, W., "Recent Advances in Understanding the Mechanism of Cocrystal Formation via Grinding". *Cryst Growth Des*. **9**(3): 1621, 2009.

116. BRUNI, G.; MAIETTA, M.; BERBENNI, V.; MUSTARELLI, P.; FERRARA, C.; FRECCERO, M.; GRANDE, V.; MAGGI, L.; MILANESE, C.; GIRELLA, A. & MARINI, A., "Mechanochemical Synthesis of Bumetanide-4-Aminobenzoic Acid Molecular Cocrystals: A Facile and Green Approach to Drug Optimization". *J Phys Chem B*. **118**(31): 9180, 2014.

117. CINCIC, D.; FRISCIC, T. & JONES, W., "A stepwise mechanism for the mechanochemical synthesis of halogen-bonded cocrystal architectures". *J Am Chem Soc*. **130**(24): 7524, 2008.

118. HASA, D.; RAUBER, G.S.; VOINOVICH, D. & JONES, W., "Cocrystal Formation through Mechanochemistry: from Neat and Liquid-Assisted Grinding to Polymer-Assisted Grinding". *Angew Chem Int Edit*. **54**(25): 7371, 2015.

119. KARKI, S.; FRISCIC, T. & JONES, W., "Control and interconversion of cocrystal stoichiometry in grinding: stepwise mechanism for the formation of a hydrogen-bonded cocrystal". *Crystengcomm*. **11**(3): 470, 2009.

120. SANPHUI, P.; KUMAR, S.S. & NANGIA, A., "Pharmaceutical Cocrystals of Niclosamide". *Cryst Growth Des*. **12**(9): 4588, 2012.

121. SPRINGUEL, G.; NORBERG, B.; ROBEYNS, K.; WOUTERS, J. & LEYSSENS, T., "Advances in Pharmaceutical Co-crystal Screening: Effective Co-crystal Screening through Structural Resemblance". *Cryst Growth Des*. **12**(1): 475, 2012.

122. STROBRIDGE, F.C.; JUDAS, N. & FRISCIC, T., "A stepwise mechanism and the role of water in the liquid-assisted grinding synthesis of metal-organic materials". *Crystengcomm*. **12**(8): 2409, 2010.

123. TRASK, A.V.; MOTHERWELL, W.D.S. & JONES, W., "Pharmaceutical cocrystallization: Engineering a remedy for caffeine hydration". *Cryst Growth Des*. **5**(3): 1013, 2005.

124. ALTHEIMER, B.D.; PAGOLA, S.; ZELLER, M. & MEHTA, M.A., "Mechanochemical Conversions Between Crystalline Polymorphs of a Complex Organic Solid". *Cryst Growth Des*. **13**(8): 3447, 2013.

125. FUCKE, K.; MYZ, S.A.; SHAKHTSHNEIDER, T.P.; BOLDYREVA, E.V. & GRIESSER, U.J., "How good are the crystallisation methods for co-crystals? A comparative study of piroxicam". *New J Chem*. **36**(10): 1969, 2012.

126. NIJHAWAN, M.; SANTHOSH, A.; BABU, P.R.S. & SUBRAHMANYAM, C.V.S., "Solid state manipulation of lornoxicam for cocrystals - physicochemical characterization". *Drug Dev Ind Pharm*. **40**(9): 1163, 2014.

127. PATEL, J.R.; CARLTON, R.A.; NEEDHAM, T.E.; CHICHESTER, C.O. & VOGT, F.G., "Preparation, structural analysis, and properties of tenoxicam cocrystals". *Int J Pharm*. **436**(1-2): 685, 2012.

128. SOWA, M.; SLEPOKURA, K. & MATCZAK-JON, E., "A 1:1 pharmaceutical cocrystal of myricetin in combination with uncommon piracetam conformer: X-ray single crystal analysis and mechanochemical synthesis". *J Mol Struct*. **1058**: 114, 2014.

129. TRASK, A.V.; MOTHERWELL, W.D.S. & JONES, W., "Solvent-drop grinding: green polymorph control of cocrystallisation". *Chem Commun*, (7): 890, 2004.

130. BRAGA, D.; GIAFFREDA, S.L.; GREPIONI, F.; CHIEROTTI, M.R.; GOBETTO, R.; PALLADINO, G. & POLITO, M., "Solvent effect in a "solvent free" reaction". *Crystengcomm*. **9**(10): 879, 2007.

131. PFEIFFER, C.R.; FOWLER, D.A. & ATWOOD, J.L., "Establishing trends based on solvent system changes in cocrystals containing pyrogallol[4] arenes and fluorescent probes rhodamine B and pyronin Y". *Crystengcomm*. **17**(24): 4475, 2015.

132. PADRELA, L.; RODRIGUES, M.A.; VELAGA, S.P.; FERNANDES, A.C.; MATOS, H.A. & DE AZEVEDO, E.G., "Screening for pharmaceutical cocrystals using the supercritical fluid enhanced atomization process". *J Supercrit Fluid*. **53**(1-3): 156, 2010.

133. DHUMAL, R.S.; BIRADAR, S.V.; PARADKAR, A.R. & YORK, P., "Ultrasound Assisted Engineering of Lactose Crystals". *Pharm Res-Dordr*. **25**(12): 2835, 2008.

134. AMBELE, M.A.; SEWELL, B.T.; CUMMINGS, F.R.; SMITH, P.J. & EGAN, T.J., "Synthetic Hemozoin (beta-Hematin) Crystals Nucleate at the Surface of Neutral Lipid Droplets that Control Their Sizes". *Cryst Growth Des*. **13**(10): 4442, 2013.

135. FRYDENBERG, R.P.; HAMMERSHOJ, M.; ANDERSEN, U. & WIKING, L., "Ultrasonication Affects Crystallization Mechanisms and Kinetics of Anhydrous Milk Fat". *Cryst Growth Des*. **13**(12): 5375, 2013.

136. WAGTERVELD, R.M.; MIEDEMA, H. & WITKAMP, G.J., "Effect of Ultrasonic Treatment on Early Growth during CaCO3 Precipitation". *Cryst Growth Des*. **12**(9): 4403, 2012.

137. PADRELA, L.; RODRIGUES, M.A.; VELAGA, S.R.; MATOS, H.A. & DE AZEVEDO, E.G., "Formation of indomethacin-saccharin cocrystals using supercritical fluid technology". *Eur J Pharm Sci*. **38**(1): 9, 2009.

138. AHER, S.; DHUMAL, R.; MAHADIK, K.; PARADKAR, A. & YORK, P., "Ultrasound assisted cocrystallization from solution (USSC) containing a non-congruently soluble cocrystal component pair: Caffeine/maleic acid". *Eur J Pharm Sci*. **41**(5): 597, 2010.

139. SWEETMAN, S.C., "Dose adjustment in renal impairment - Response from Martindale: the Complete Drug Reference". *Brit Med J*. **331**(7511): 292, 2005.

140. KASTELIC, J.; LAH, N.; KIKELJ, D. & LEBAN, I., "A 1:1 cocrystal of fluconazole with salicylic acid". *Acta Crystallographica Section C-Crystal Structure Communications*. **67**: O370, 2011.

141. IBELINGS, M.S.; MAQUELIN, K.; ENDTZ, H.P.; BRUINING, H.A. & PUPPELS, G.J., "Rapid identification of Candida spp. in peritonitis patients by Raman spectroscopy". *Clin Microbiol Infec*. **11**(5): 353, 2005.

142. UDELHOVEN, T.; NAUMANN, D. & SCHMITT, J., "Development of a hierarchical classification system with artificial neural networks and FT-IR spectra for the identification of bacteria". *Appl Spectrosc*. **54**(10): 1471, 2000.

143. CHADHA, R.; SAINI, A.; JAIN, D.S. & VENUGOPALAN, P., "Preparation and Solid-State Characterization of Three Novel Multicomponent Solid Forms of Oxcarbazepine: Improvement in Solubility through Saccharin Cocrystal". *Cryst Growth Des*. **12**(8): 4211, 2012.

144. GROSSJOHANN, C.; ECCLES, K.S.; MAGUIRE, A.R.; LAWRENCE, S.E.; TAJBER, L.; CORRIGAN, O.I. & HEALY, A.M., "Characterisation, solubility and intrinsic dissolution behaviour of benzamide: dibenzyl sulfoxide cocrystal". *Int J Pharm*. **422**(1-2): 24, 2012.

145. HEIDEN, S.; TROBS, L.; WENZEL, K.J. & EMMERLING, F., "Mechanochemical synthesis and structural characterisation of a theophylline-benzoic acid cocrystal (1:1)". *Crystengcomm*. **14**(16): 5128, 2012.

146. PALUCH, K.J.; TAJBER, L.; ELCOATE, C.J.; CORRIGAN, O.I.; LAWRENCE, S.E. & HEALY, A.M., "Solid-State Characterization of Novel Active Pharmaceutical Ingredients: Cocrystal of a Salbutamol Hemiadipate Salt with Adipic Acid (2:1:1) and Salbutamol Hemisuccinate Salt". *Journal of pharmaceutical sciences*. **100**(8): 3268, 2011.

147. SHEN, J.P.; DUAN, X.H.; LUO, Q.P.; ZHOU, Y.; BAO, Q.L.; MA, Y.J. & PEI, C.H., "Preparation and Characterization of a Novel Cocrystal Explosive". *Cryst Growth Des*. **11**(5): 1759, 2011.

148. ELBAGERMA, M.A.; EDWARDS, H.G.M.; MUNSHI, T.; HARGREAVES, M.D.; MATOUSEK, P. & SCOWEN, I.J., "Characterization of New Cocrystals by Raman Spectroscopy, Powder X-

ray Diffraction, Differential Scanning Calorimetry, and Transmission Raman Spectroscopy". *Cryst Growth Des*. **10**(5): 2360, 2010.

149. BATAILLE, T. & LOUER, D., "Powder and single-crystal X-ray diffraction study of the structure of [Y(H2O)](2)(C2O4)(CO3)(2)". *Acta Crystallogr B*. **56**: 998, 2000.

150. DELGADO, G. & MORA, A.J., "Crystal structure determination of p-bromoaniline using laboratory X-ray powder diffraction data". *Mater Sci Forum*. **378-3**: 795, 2001.

151. HAMMOND, R.B.; JONES, M.J.; ROBERTS, K.J.; KUTZKE, H. & KLAPPER, H., "A structural study of polymorphism in phenyl salicylate: determination of the crystal structure of a meta-stable phase from X-ray powder diffraction data using a direct space systematic search method". *Z Kristallogr*. **217**(9): 484, 2002.

152. KARIUKI, B.M.; ZIN, D.M.S.; TREMAYNE, M. & HARRIS, K.D.M., "Crystal structure solution from powder X-ray diffraction data: The development of monte carlo methods to solve the crystal structure of the gamma-phase of 3-chloro-trans-cinnamic acid". *Chem Mater*. **8**(2): 565, 1996.

153. MIURA, H.; USHIO, T.; NAGAI, K.; FUJIMOTO, D.; LEPP, Z.; TAKAHASHI, H. & TAMURA, R., "Crystallization of a desired metastable polymorph by pseudoseeding, crystal structure solution from its powder X-ray diffraction data, and confirmation of polymorphic transition". *Cryst Growth Des*. **3**(6): 959, 2003.

154. POOJARY, D.M. & CLEARFIELD, A., "Application of X-ray powder diffraction techniques to the solution of unknown crystal structures". *Accounts Chem Res*. **30**(10): 414, 1997.

155. SIDHU, P.S.; ENRIGHT, G.A.; RIPMEESTER, J.A. & PENNER, G.H., "Polymorphism, structure, guest conformation, and dynamics in the inclusion, compound of 1,2-dichloroethane with tris(5-acetyl-3-thienyl) methane: a combined single crystal and powder X-ray diffraction, C-13 CP/MAS, and H-2 NMR study". *J Phys Chem B*. **106**(34): 8569, 2002.

156. AAKEROY, C.B.; BEATTY, A.M.; TREMAYNE, M.; ROWE, D.M. & SEATON, C.C., "A combination of X-ray single-crystal diffraction and Monte Carlo structure solution from X-ray powder diffraction data in a structural investigation of 5-bromonicotinic acid and solvates thereof". *Cryst Growth Des*. **1**(5): 377, 2001.

157. SCHMIDTMANN, M.; COSTER, P.; HENRY, P.F.; TING, V.P.; WELLERE, M.T. & WILSON, C.C., "Determining hydrogen positions in crystal engineered organic molecular complexes by joint neutron powder and single crystal X-ray diffraction". *Crystengcomm*. **16**(7): 1232, 2014.

158. DINNEBIER, R.E.; SIEGER, P.; NAR, H.; SHANKLAND, K. & DAVID, W.I.F., "Structural characterization of three crystalline modifications of telmisartan by single crystal and high-resolution X-ray powder diffraction". *Journal of pharmaceutical sciences*. **89**(11): 1465, 2000.

159. KALAKEWICH, K.; IULIUCCI, R. & HARPER, J.K., "Establishing Accurate High-Resolution Crystal Structures in the Absence of Diffraction Data and Single Crystals-An NMR Approach". *Cryst Growth Des*. **13**(12): 5391, 2013.

160. BROWNACQUAYE, H.A. & LANE, A.P., "The Single-Crystal Polarized Vibrational-Spectra of Namnf3 and Nacof3 and the Assignment to Their Correct Space Group". *J Inorg Nucl Chem*. **43**(12): 3143, 1981.

161. DAVIES, J.A.; DUTREMEZ, S.G. & PINKERTON, A.A., "Studies of Cis-[Ptcl2(Pph2npr)(Bzs(O)Bz)] by Solid-State Cp Mas P-31 Nmr-Spectroscopy, Single-Crystal X-Ray-Diffraction and X-Ray-Powder Diffraction - Investigation of a Question Concerning Polymorphism Versus Space Group Ambiguity". *Magn Reson Chem*. **31**(5): 435, 1993.

162. LEROUX, S.D. & VANTETS, A., "The Space Group Determination from a Single-Crystal of a Member of the Adu Family on a Reciprocal Lattice Explorer". *J Nucl Mater*. **119**(1): 110, 1983.

163. LEROUX, S.D. & VANTETS, A., "The Space Group Determinations for 3 Single-Crystal Members of the Uo3-Nh3-H2o System on a Reciprocal Lattice Explorer". *Acta Crystallogr A*. **40**: C406, 1984.

164. LIEBERTZ, J. & STAHR, S., "Li2bap207 - Single-Crystal Growth, Metric and Space Group". *Z Kristallogr*. **162**(1-4): 313, 1983.

165. PASCHER, I.; SUNDELL, S.; EIBL, H. & HARLOS, K., "Interactions and Space Requirement of the Phosphate Head Group of Membrane-Lipids - the Single-Crystal Structures of a Triclinic and a Monoclinic Form of Hexadecyl-2-Deoxyglycerophosphoric Acid Monohydrate". *Chem Phys Lipids*. **35**(2): 103, 1984.

166. RAWN, C.J.; BIRNIE, D.P.; BRUCK, M.A.; ENEMARK, J.H. & ROTH, R.S., "Structural investigation of Ba(6-3x)Ln(8+2x)Ti(18)O(54) (x = 0.27, Ln = Sm) by single crystal x-ray diffraction in space group Pnma (No. 62)". *J Mater Res*. **13**(1): 187, 1998.

167. MASUNAGA, H.; SASAKI, S.; TASHIRO, K.; HANESAKA, M.; TAKATA, M.; INOUE, K.; OHTA, N. & YAGI, N., "Development of synchrotron DSC/WARD/SAXS simultaneous measurement system for polymeric materials at the BL40B2 in spring-8 and its application to the study of crystal phase transitions of fluorine polymers". *Polym J*. **39**(12): 1281, 2007.

168. BUCCI, R.; MAGRI, A.D. & MAGRI, A.L., "DSC in the Chemical Analysis of Drugs - Determination of diclofenac in pharmaceutical formulations". *J Therm Anal Calorim*. **61**(2): 369, 2000.

169. VANDOOREN, A.A. & MULLER, B.W., "Purity Determinations of Drugs with Differential Scanning Calorimetry (Dsc) - a Critical-Review". *Int J Pharm*. **20**(3): 217, 1984.

170. WESOLOWSKI, M.; SZYNKARUK, P. & MAKURAT, E., "DSC and IR as supporting tools for identification of methylxanthines in solid dosage forms of drugs". *J Therm Anal Calorim*. **109**(2): 807, 2012.

171. ULU, S.T. & ELMALI, F.T., "Highly sensitive spectrophotometric methods for the determination, validation and thermogravimetric analysis of antiulcer drugs, nizatidine and ranitidine in pure and pharmaceutical preparations". *J Anal Chem+*. **68**(6): 495, 2013.

172. THRELFALL, T.L., "Turning DSC Charts of Polymorphs into Phase Diagrams: A Tutorial Paper". *Org Process Res Dev*. **13**(6): 1224, 2009.

173. FLOYD, P.D.; VOGT, F.G.; GALOP, M.; KELLEY, W.P. & MULLER, F.X., "Quantitative determination of the disassociation of salts in the solid state from pharmaceutical formulations using NMR and TGA-MS.". *Abstr Pap Am Chem S*. **226**: U112, 2003.

ANNEX I

Table 1. Crystal data and structure refinement for shelx.

Identification code	shelx
Empirical formula	C17 H18 F2 N6 O6
Formula weight	440.37
Temperature	298(2) K
Wavelength	0.71073 Å
Crystal system	Monoclinic
Space group	P 21/n
Unit cell dimensions	a = 17.053(3) Å $\alpha = 90°$.
	b = 5.5995(10) Å $\beta = 105.418(4)°$.
	c = 21.154(3) Å $\gamma = 90°$.
Volume	1947.3(6) Å^3
Z	4
Density (calculated)	1.502 Mg/m^3
Absorption coefficient	0.128 mm^{-1}
F(000)	912
Crystal size	0.100 x 0.100 x 0.100 mm^3
Theta range for data collection	2.738 to 27.568°.
Index ranges	-21<=h<=21, -7<=k<=7, -26<=l<=27
Reflections collected	32870
Independent reflections	4492 [R(int) = 0.0781]
Completeness to theta = 25.242°	99.9 %
Refinement method	Full-matrix least-squares on F^2
Data / restraints / parameters	4492 / 0 / 298
Goodness-of-fit on F^2	1.030
Final R indices [I>2sigma(I)]	R1 = 0.0622, wR2 = 0.1218
R indices (all data)	R1 = 0.1347, wR2 = 0.1451
Extinction coefficient	n/a
Largest diff. peak and hole	0.212 and -0.205 e.Å^{-3}

Table 2. Atomic coordinates (x 10^4) and equivalent isotropic displacement parameters ($Å^2$x 10^3) for shelx. U(eq) is defined as one third of the trace of the orthogonalized U^{ij} tensor.

	x	y	z	U(eq)
F(1)	5068(1)	3634(3)	2185(1)	61(1)
F(2)	2317(1)	5413(5)	1392(1)	101(1)
O(1)	5430(1)	10072(3)	3269(1)	49(1)
N(1)	6885(1)	8280(4)	3011(1)	39(1)
N(2)	7401(2)	6417(4)	3223(1)	49(1)
N(3)	8009(1)	9910(4)	3570(1)	50(1)
N(4)	5128(11)	5630(40)	3938(13)	26(2)
N(5)	4334(4)	4588(12)	3768(4)	46(2)
N(6)	4308(9)	7144(17)	4596(7)	41(2)
C(1)	5426(2)	7769(4)	2998(1)	35(1)
C(2)	5650(2)	5911(5)	3554(1)	36(1)
C(8)	4593(2)	7210(4)	2541(1)	38(1)
C(3)	6065(2)	7848(5)	2605(1)	41(1)
C(9)	4446(2)	5160(5)	2169(1)	43(1)
C(5)	7259(2)	10321(5)	3222(1)	49(1)
C(4)	8062(2)	7505(6)	3554(2)	51(1)
C(6)	4948(16)	7630(40)	4397(13)	36(2)
C(7)	3950(6)	5340(15)	4191(5)	45(2)
C(10)	3698(2)	4519(6)	1774(1)	56(1)
C(11)	3071(2)	6031(7)	1770(2)	65(1)
C(12)	3157(2)	8067(7)	2123(2)	68(1)
C(13)	3926(2)	8671(6)	2507(2)	57(1)
O(2)	5742(1)	7827(4)	905(1)	62(1)
O(3)	5015(1)	4493(4)	752(1)	65(1)
O(4)	2993(1)	11142(4)	34(2)	80(1)
O(5)	2205(1)	7972(4)	-92(1)	62(1)
C(14)	5062(2)	6636(6)	724(1)	49(1)
C(15)	4344(2)	8266(6)	488(1)	50(1)
C(16)	2878(2)	8844(6)	62(2)	49(1)
C(17)	3622(2)	7395(6)	287(1)	53(1)
O(1W)	3369(1)	8531(4)	5364(1)	73(1)
N(41)	4944(11)	6040(40)	3888(13)	26(2)
N(51)	4604(4)	3601(12)	3842(4)	46(2)
N(61)	4186(8)	6321(18)	4472(7)	41(2)
C(61)	4831(16)	7070(30)	4283(12)	36(2)
C(71)	4087(6)	4172(13)	4187(5)	45(2)

Table 3.   Selected bond lengths [Å] and angles [°] for shelx.

_____

_____

Symmetry transformations used to generate equivalent atoms:

Table 4.   Bond lengths [Å] and angles [°] for shelx.

_____

BONDS					
F(1)-C(9)	1.354(3)	N(41)-N(51)	1.48(3)	N(6)-C(6)-H(6A)	124.8
F(2)-C(11)	1.365(4)	N(51)-C(71)	1.324(12)	N(4)-C(6)-H(6A)	123.3
O(1)-C(1)	1.411(3)	N(61)-C(61)	1.33(3)	N(5)-C(7)-N(6)	116.5(11)
O(1)-H(1)	0.8200	N(61)-C(71)	1.337(11)	N(5)-C(7)-H(7A)	122.0
N(1)-C(5)	1.327(3)	C(61)-C(71)	2.035(19)	N(6)-C(7)-H(7A)	121.3
N(1)-N(2)	1.361(3)	C(61)-H(6B)	0.9300	C(11)-C(10)-C(9)	116.2(3)
N(1)-C(3)	1.455(3)	C(71)-H(7B)	0.9300	C(11)-C(10)-H(10)	121.9
N(2)-C(4)	1.309(4)	**ANGLES**		C(9)-C(10)-H(10)	121.9
N(3)-C(5)	1.314(4)	C(1)-O(1)-H(1)	109.5	C(12)-C(11)-C(10)	123.5(3)
N(3)-C(4)	1.351(4)	C(5)-N(1)-N(2)	109.8(2)	C(12)-C(11)-F(2)	119.1(3)
N(4)-C(2)	1.37(3)	C(5)-N(1)-C(3)	130.0(2)	C(10)-C(11)-F(2)	117.5(3)
N(4)-N(5)	1.43(3)	N(2)-N(1)-C(3)	120.2(2)	C(11)-C(12)-C(13)	118.5(3)
N(4)-C(6)	1.57(3)	C(4)-N(2)-N(1)	102.0(2)	C(11)-C(12)-H(121)	120.7
N(5)-C(7)	1.310(13)	C(5)-N(3)-C(4)	102.9(3)	C(13)-C(12)-H(121)	120.7
N(6)-C(6)	1.30(3)	C(2)-N(4)-N(5)	128(2)	C(8)-C(13)-C(12)	121.4(3)
N(6)-C(7)	1.361(11)	C(2)-N(4)-C(6)	123(2)	C(8)-C(13)-H(13)	119.3
C(1)-C(8)	1.523(4)	N(5)-N(4)-C(6)	96.9(15)	C(12)-C(13)-H(13)	119.3
C(1)-C(3)	1.537(3)	C(7)-N(5)-N(4)	108.1(13)	C(14)-O(2)-H(2)	109.5
C(1)-C(2)	1.539(3)	C(6)-N(6)-C(7)	103.1(13)	C(16)-O(4)-H(4)	109.5
C(2)-H(2A)	0.9700	O(1)-C(1)-C(8)	110.4(2)	O(3)-C(14)-O(2)	124.1(3)
C(2)-H(2B)	0.9700	O(1)-C(1)-C(3)	105.4(2)	O(3)-C(14)-C(15)	124.3(3)
C(8)-C(9)	1.377(4)	C(8)-C(1)-C(3)	109.7(2)	O(2)-C(14)-C(15)	111.7(3)
C(8)-C(13)	1.388(4)	O(1)-C(1)-C(2)	109.6(2)	C(17)-C(15)-C(14)	120.2(3)
C(3)-H(3A)	0.9700	C(8)-C(1)-C(2)	110.21(19)	C(17)-C(15)-H(15)	119.9
C(3)-H(3B)	0.9700	C(3)-C(1)-C(2)	111.4(2)	C(14)-C(15)-H(15)	119.9
C(9)-C(10)	1.374(4)	N(4)-C(2)-C(1)	117.7(7)	O(5)-C(16)-O(4)	122.0(3)
C(5)-H(5)	0.9300	N(4)-C(2)-H(2A)	107.9	O(5)-C(16)-C(17)	122.6(3)
C(4)-H(4A)	0.9300	C(1)-C(2)-H(2A)	107.9	O(4)-C(16)-C(17)	115.4(3)
C(6)-H(6A)	0.9300	N(4)-C(2)-H(2B)	107.9	C(15)-C(17)-C(16)	124.4(3)
C(7)-H(7A)	0.9300	C(1)-C(2)-H(2B)	107.9	C(15)-C(17)-H(17)	117.8
C(10)-C(11)	1.363(5)	H(2A)-C(2)-H(2B)	107.2	C(16)-C(17)-H(17)	117.8
C(10)-H(10)	0.9300	C(9)-C(8)-C(13)	116.1(3)	H(1A)-O(1W)-H(1B)	103.5
C(11)-C(12)	1.348(5)	C(9)-C(8)-C(1)	122.1(2)	C(61)-N(41)-N(51)	114(2)
C(12)-C(13)	1.388(4)	C(13)-C(8)-C(1)	121.7(2)	C(71)-N(51)-N(41)	92.8(10)
C(12)-H(121)	0.9300	N(1)-C(3)-C(1)	113.2(2)	C(61)-N(61)-C(71)	99.4(12)
C(13)-H(13)	0.9300	N(1)-C(3)-H(3A)	108.9	N(41)-C(61)-N(61)	113.4(19)
O(2)-C(14)	1.304(3)	C(1)-C(3)-H(3A)	108.9	N(41)-C(61)-C(71)	74.4(17)
O(2)-H(2)	0.8200	N(1)-C(3)-H(3B)	108.9	N(61)-C(61)-C(71)	40.4(6)
O(3)-C(14)	1.205(4)	C(1)-C(3)-H(3B)	108.9	N(41)-C(61)-H(6B)	121.2
O(4)-C(16)	1.306(4)	H(3A)-C(3)-H(3B)	107.8	N(61)-C(61)-H(6B)	125.1
O(4)-H(4)	0.8200	F(1)-C(9)-C(10)	116.4(3)	C(71)-C(61)-H(6B)	163.7
O(5)-C(16)	1.209(3)	F(1)-C(9)-C(8)	119.3(2)	N(51)-C(71)-N(61)	116.3(10)
C(14)-C(15)	1.502(4)	C(10)-C(9)-C(8)	124.3(3)	N(51)-C(71)-C(61)	76.0(9)
C(15)-C(17)	1.288(4)	N(3)-C(5)-N(1)	110.3(3)	N(61)-C(71)-C(61)	40.2(10)
C(15)-H(15)	0.9300	N(3)-C(5)-H(5)	124.9	N(51)-C(71)-H(7B)	121.9
C(16)-C(17)	1.474(4)	N(1)-C(5)-H(5)	124.9	N(61)-C(71)-H(7B)	121.8
C(17)-H(17)	0.9300	N(2)-C(4)-N(3)	115.1(3)	C(61)-C(71)-H(7B)	162.0
O(1W)-H(1A)	0.8187	N(2)-C(4)-H(4A)	122.5		
O(1W)-H(1B)	0.9064	N(3)-C(4)-H(4A)	122.5		
N(41)-C(61)	1.07(3)	N(6)-C(6)-N(4)	111.7(14)		

Symmetry transformations used to generate equivalent atoms:

Table 5.   Anisotropic displacement parameters ($\text{Å}^2 \times 10^3$) for shelx. The anisotropic displacement factor exponent takes the form: $-2\pi^2[\, h^2 a^{*2} U^{11} + ... + 2\, h\, k\, a^*\, b^*\, U^{12}\,]$

	U^{11}	U^{22}	U^{33}	U^{23}	U^{13}	U^{12}
F(1)	74(1)	48(1)	53(1)	-12(1)	0(1)	14(1)
F(2)	59(1)	125(2)	100(2)	13(2)	-13(1)	-15(1)
O(1)	51(1)	30(1)	75(1)	-11(1)	30(1)	-6(1)
N(1)	43(1)	37(1)	45(1)	4(1)	23(1)	-2(1)
N(2)	49(2)	42(1)	62(2)	4(1)	24(1)	9(1)
N(3)	44(1)	50(2)	59(2)	-1(1)	18(1)	-3(1)
N(4)	13(7)	39(7)	26(3)	5(4)	2(5)	6(4)
N(5)	41(4)	56(5)	45(2)	-8(3)	18(3)	-18(3)
N(6)	39(4)	40(6)	45(5)	-3(4)	18(4)	-9(4)
C(1)	45(2)	23(1)	44(2)	-3(1)	21(1)	-3(1)
C(2)	44(2)	36(2)	34(1)	-3(1)	19(1)	-7(1)
C(8)	47(2)	30(1)	41(2)	9(1)	21(1)	0(1)
C(3)	47(2)	41(2)	40(2)	4(1)	20(1)	-2(1)
C(9)	52(2)	40(2)	34(2)	8(1)	7(1)	5(1)
C(5)	53(2)	36(2)	61(2)	5(1)	22(2)	-4(1)
C(4)	47(2)	53(2)	59(2)	6(2)	21(2)	10(2)
C(6)	45(6)	26(8)	40(7)	-9(5)	17(5)	-9(5)
C(7)	34(3)	54(6)	49(2)	5(5)	16(2)	-10(4)
C(10)	68(2)	53(2)	39(2)	7(1)	1(2)	-6(2)
C(11)	50(2)	80(3)	59(2)	15(2)	2(2)	-9(2)
C(12)	43(2)	68(2)	95(3)	12(2)	21(2)	7(2)
C(13)	50(2)	44(2)	86(2)	3(2)	32(2)	1(2)
O(2)	47(1)	58(1)	78(2)	3(1)	10(1)	4(1)
O(3)	60(1)	58(2)	77(2)	10(1)	18(1)	-1(1)
O(4)	45(1)	46(1)	154(2)	-3(2)	34(2)	-2(1)
O(5)	52(1)	47(1)	91(2)	0(1)	28(1)	-4(1)
C(14)	52(2)	58(2)	42(2)	3(2)	20(1)	2(2)
C(15)	52(2)	45(2)	57(2)	2(2)	22(2)	-2(2)
C(16)	51(2)	44(2)	62(2)	1(2)	29(2)	5(2)
C(17)	59(2)	46(2)	58(2)	1(2)	26(2)	-1(2)
O(1W)	64(1)	64(2)	106(2)	24(1)	51(1)	17(1)
N(41)	13(7)	39(7)	26(3)	5(4)	2(5)	6(4)
N(51)	41(4)	56(5)	45(2)	-8(3)	18(3)	-18(3)
N(61)	39(4)	40(6)	45(5)	-3(4)	18(4)	-9(4)
C(61)	45(6)	26(8)	40(7)	-9(5)	17(5)	-9(5)
C(71)	34(3)	54(6)	49(2)	5(5)	16(2)	-10(4)

Table 6.   Hydrogen coordinates (x 10^4) and isotropic displacement parameters (Å^2x 10^3)

for shelx.

_____

	x	y	z	U(eq)
H(1)	5066	10172	3454	74
H(2A)	5708	4376	3358	44
H(2B)	6179	6334	3837	44
H(3A)	6055	6343	2376	49
H(3B)	5920	9100	2278	49
H(5)	7025	11827	3136	58
H(4A)	8534	6684	3761	62
H(6A)	5286	8944	4531	43
H(7A)	3481	4595	4238	54
H(10)	3624	3130	1524	67
H(121)	2712	9045	2109	82
H(13)	3995	10084	2747	69
H(2)	6119	6898	1047	94
H(4)	2552	11818	-90	121
H(15)	4422	9910	487	60
H(17)	3566	5743	283	63
H(1A)	3624	8114	5105	109
H(1B)	3158	9964	5205	109
H(6B)	5137	8420	4442	43
H(7B)	3664	3161	4215	54

_____

Table 7. Selected torsion angles [°] for shelx.

_____

_____

Symmetry transformations used to generate equivalent atoms:

Table 8. Torsion angles [°] for shelx.

C(5)-N(1)-N(2)-C(4)	0.0(3)	C(5)-N(3)-C(4)-N(2)	-0.2(3)
C(3)-N(1)-N(2)-C(4)	178.9(2)	C(7)-N(6)-C(6)-N(4)	-14(2)
C(2)-N(4)-N(5)-C(7)	-159.9(14)	C(2)-N(4)-C(6)-N(6)	165.6(17)
C(6)-N(4)-N(5)-C(7)	-16.5(17)	N(5)-N(4)-C(6)-N(6)	20(2)
N(5)-N(4)-C(2)-C(1)	70(2)	N(4)-N(5)-C(7)-N(6)	10.8(16)
C(6)-N(4)-C(2)-C(1)	-64(2)	C(6)-N(6)-C(7)-N(5)	3(2)
O(1)-C(1)-C(2)-N(4)	64.6(14)	F(1)-C(9)-C(10)-C(11)	178.6(3)
C(8)-C(1)-C(2)-N(4)	-57.1(14)	C(8)-C(9)-C(10)-C(11)	-1.0(4)
C(3)-C(1)-C(2)-N(4)	-179.1(13)	C(9)-C(10)-C(11)-C(12)	0.6(5)
O(1)-C(1)-C(8)-C(9)	174.1(2)	C(9)-C(10)-C(11)-F(2)	-178.8(3)
C(3)-C(1)-C(8)-C(9)	58.4(3)	C(10)-C(11)-C(12)-C(13)	0.4(5)
C(2)-C(1)-C(8)-C(9)	-64.7(3)	F(2)-C(11)-C(12)-C(13)	179.8(3)
O(1)-C(1)-C(8)-C(13)	-9.9(3)	C(9)-C(8)-C(13)-C(12)	0.6(4)
C(3)-C(1)-C(8)-C(13)	-125.6(3)	C(1)-C(8)-C(13)-C(12)	-175.6(3)
C(2)-C(1)-C(8)-C(13)	111.3(3)	C(11)-C(12)-C(13)-C(8)	-1.1(5)
C(5)-N(1)-C(3)-C(1)	-84.8(3)	O(3)-C(14)-C(15)-C(17)	-1.3(5)
N(2)-N(1)-C(3)-C(1)	96.5(3)	O(2)-C(14)-C(15)-C(17)	179.7(3)
O(1)-C(1)-C(3)-N(1)	63.4(3)	C(14)-C(15)-C(17)-C(16)	178.3(3)
C(8)-C(1)-C(3)-N(1)	-177.7(2)	O(5)-C(16)-C(17)-C(15)	-176.1(3)
C(2)-C(1)-C(3)-N(1)	-55.3(3)	O(4)-C(16)-C(17)-C(15)	4.5(4)
C(13)-C(8)-C(9)-F(1)	-179.2(2)	C(61)-N(41)-N(51)-C(71)	20(2)
C(1)-C(8)-C(9)-F(1)	-3.0(4)	N(51)-N(41)-C(61)-N(61)	-24(3)
C(13)-C(8)-C(9)-C(10)	0.5(4)	N(51)-N(41)-C(61)-C(71)	-13.3(14)
C(1)-C(8)-C(9)-C(10)	176.7(2)	C(71)-N(61)-C(61)-N(41)	16(3)
C(4)-N(3)-C(5)-N(1)	0.2(3)	N(41)-N(51)-C(71)-N(61)	-9.2(13)
N(2)-N(1)-C(5)-N(3)	-0.1(3)	N(41)-N(51)-C(71)-C(61)	-9.8(11)
C(3)-N(1)-C(5)-N(3)	-178.9(2)	C(61)-N(61)-C(71)-N(51)	-1.0(17)
N(1)-N(2)-C(4)-N(3)	0.1(3)		

Table 9. Hydrogen bonds for shelx [Å and °].

_____

D-H...A	d(D-H)	d(H...A)	d(D...A)	<(DHA)

_____

ANNEX II

checkCIF/PLATON report

Structure factors have been supplied for datablock(s) shelx

THIS REPORT IS FOR GUIDANCE ONLY. IF USED AS PART OF A REVIEW PROCEDURE
FOR PUBLICATION, IT SHOULD NOT REPLACE THE EXPERTISE OF AN EXPERIENCED
CRYSTALLOGRAPHIC REFEREE.

No syntax errors found.   CIF dictionary   Interpreting this report

Datablock: shelx

```
Bond precision:   C-C = 0.0043 A           Wavelength=0.71073

Cell:          a=17.053(3)      b=5.5995(10)         c=21.154(3)
               alpha=90         beta=105.418(4)      gamma=90
Temperature:   298 K

                 Calculated                Reported
Volume         1947.3(6)                 1947.3(6)
Space group    P 21/n                    P 21/n
Hall group     -P 2yn                    -P 2yn
Moiety formula C13 H12 F2 N6 O, C4 H4 O4, C13 H12 F2 N6 O, C4 H4 O4,
               H2 O                      H2 O
Sum formula    C17 H18 F2 N6 O6          C17 H18 F2 N6 O6
Mr             440.37                    440.37
Dx,g cm-3      1.502                     1.502
Z              4                         4
Mu (mm-1)      0.128                     0.128
F000           912.0                     912.0
F000'          912.55
h,k,lmax       22,7,27                   21,7,27
Nref           4518                      4492
Tmin,Tmax      0.987,0.987
Tmin'          0.987

Correction method= Not given

Data completeness= 0.994          Theta(max)= 27.568

R(reflections)= 0.0622( 2444)     wR2(reflections)= 0.1451( 4492)

S = 1.030                  Npar= 298
```

The following ALERTS were generated. Each ALERT has the format
test-name_ALERT_alert-type_alert-level.
Click on the hyperlinks for more details of the test.

Alert level C

PLAT334_ALERT_2_C	Small Average Benzene C-C Dist. C8 -C13	1.37 Ang.
PLAT340_ALERT_3_C	Low Bond Precision on C-C Bonds	0.0043 Ang.
PLAT417_ALERT_2_C	Short Inter D-H..H-D H1A .. H4 ..	2.12 Ang.
PLAT417_ALERT_2_C	Short Inter D-H..H-D H1B .. H4 ..	2.11 Ang.
PLAT906_ALERT_3_C	Large K value in the Analysis of Variance	16.167 Check
PLAT906_ALERT_3_C	Large K value in the Analysis of Variance	2.382 Check
PLAT913_ALERT_3_C	Missing # of Very Strong Reflections in FCF	1 Note

Alert level G

PLAT007_ALERT_5_G	Number of Unrefined Donor-H Atoms	5 Report
PLAT171_ALERT_4_G	The CIF-Embedded .res File Contains EADP Records	5 Report
PLAT300_ALERT_4_G	Atom Site Occupancy of *N4 is Constrained at	0.500 Check
PLAT300_ALERT_4_G	Atom Site Occupancy of *N5 is Constrained at	0.500 Check
PLAT300_ALERT_4_G	Atom Site Occupancy of *N6 is Constrained at	0.500 Check
PLAT300_ALERT_4_G	Atom Site Occupancy of *N41 is Constrained at	0.500 Check
PLAT300_ALERT_4_G	Atom Site Occupancy of *N51 is Constrained at	0.500 Check
PLAT300_ALERT_4_G	Atom Site Occupancy of *N61 is Constrained at	0.500 Check
PLAT300_ALERT_4_G	Atom Site Occupancy of *C6 is Constrained at	0.500 Check
PLAT300_ALERT_4_G	Atom Site Occupancy of *C7 is Constrained at	0.500 Check
PLAT300_ALERT_4_G	Atom Site Occupancy of *C61 is Constrained at	0.500 Check
PLAT300_ALERT_4_G	Atom Site Occupancy of *C71 is Constrained at	0.500 Check
PLAT300_ALERT_4_G	Atom Site Occupancy of *H6A is Constrained at	0.500 Check
PLAT300_ALERT_4_G	Atom Site Occupancy of *H6B is Constrained at	0.500 Check
PLAT300_ALERT_4_G	Atom Site Occupancy of *H7A is Constrained at	0.500 Check
PLAT300_ALERT_4_G	Atom Site Occupancy of *H7B is Constrained at	0.500 Check
PLAT301_ALERT_3_G	Main Residue Disorder .... Percentage =	23 Note
PLAT773_ALERT_2_G	Check long C-C Bond in CIF: C61 -- C71 .	2.04 Ang.
PLAT779_ALERT_4_G	Suspect or Irrelevant (Bond) Angle in CIF .... #	80 Check
	N61 -C61 -C71 1.555 1.555 1.555	40.40 Deg.
PLAT779_ALERT_4_G	Suspect or Irrelevant (Bond) Angle in CIF .... #	86 Check
	N61 -C71 -C61 1.555 1.555 1.555	40.20 Deg.
PLAT793_ALERT_4_G	The Model has Chirality at C1 (Centro SPGR)	R Verify
PLAT910_ALERT_3_G	Missing # of FCF Reflection(s) Below Th(Min) ...	4 Report
PLAT912_ALERT_4_G	Missing # of FCF Reflections Above STh/L= 0.600	18 Note

---

  0 **ALERT level A** = Most likely a serious problem - resolve or explain
  0 **ALERT level B** = A potentially serious problem, consider carefully
  7 **ALERT level C** = Check. Ensure it is not caused by an omission or oversight
 23 **ALERT level G** = General information/check it is not something unexpected

  0 ALERT type 1 CIF construction/syntax error, inconsistent or missing data
  4 ALERT type 2 Indicator that the structure model may be wrong or deficient
  6 ALERT type 3 Indicator that the structure quality may be low
 19 ALERT type 4 Improvement, methodology, query or suggestion
  1 ALERT type 5 Informative message, check